

## Radiochemical Study on Photonuclear Reactions of Complex Nuclei at Intermediate Energies

Koh Sakamoto\*

Kanazawa Kids' Science Center, 16, San-Bancho, Nishi-cho, Kanazawa 920-0913, JAPAN

Received: November 11, 2003

A review is given on radiochemical study on photonuclear reactions on target nuclei ranging from  ${}^7\text{Li}$  to  ${}^{209}\text{Bi}$  at intermediate energies, i.e. bremsstrahlung end-point energies of 30–1200 MeV, by the author's group since 1980s. The study covers the yield measurements of photopion reactions, spallation, fragmentation and fission of preactinides,  ${}^{197}\text{Au}$  and  ${}^{209}\text{Bi}$ , systematically performed with respect to photon energy, target mass ( $A_t$ ) and/or target composition ( $N/Z_t$ ), and product mass ( $A$ ) and product composition ( $N/Z$ ). Such a thorough study has not existed in this field. Thousands of the yield data were compiled and found to be smoothly varying functions of these parameters. And the relevant empirical expressions for the reaction yields were derived. The data for the four reaction channels above 140 MeV indicate clear shapes of  $\Delta(1232)$ -resonance and strong effects of the nuclear medium on the cascade-evaporation process in nuclei with  $A_t$  higher than 110–130 or  $(N/Z)_t$  larger than 1.3–1.4. All of the results have been updatedly used to test Monte Carlo calculations based on the photon-induced intranuclear cascade and evaporation analysis (PICA) code and its improved versions, and the degrees of the validity of the codes have been demonstrated. New implications for nuclear structure and reaction mechanism have been discussed by referring to the nuclear models, on which the calculations are based. Kinematic information from additional experiments performed on several targets at the  $\Delta$ -resonance region has supported the findings from the yield measurements. The results of the yield measurements and the characteristic features of the four channels are explained separately, though these channels are competitive. Important consequences and perspectives of the accounted works are pointed out relevantly.

### 1. Introduction

It is now known that energetic photons are resonantly absorbed by nuclei, i.e. excitation to specific discrete levels of light- and medium-weight nuclei in an energy region of some keV–MeV, giant dipole resonance (GDR) around 20 MeV, and quasi-deuteron resonance (QDR) at 30 to 140 MeV. At energies above the pion threshold (140 MeV), the  $\Delta$  isobar is expected to be produced by the (3,3) resonance,  $P_{33}(1232)$ , interaction of an incident photon with a single nucleon inside the target nucleus, whereas the nonresonant Born terms have been reported to be responsible for the strong background for pion production, which varies with photon energy. The isobar decays immediately ( $10^{-24}$  s) into a stable nucleon and a pion, and either one or both particles produced in these initial processes would usually develop a cascade-evaporation process in the same nucleus, resulting in a multiple nucleon emission (spallation) and/or fission in case of heavy nuclei. The pion would give excitation energy of 140 MeV when its absorption occurs in the cascade process. Emissions of light nuclei with mass numbers of  $A < 40$  in high energy photonuclear reactions on medium- to heavy-weight targets have also been observed, but their formation mechanism during the cascade-evaporation process has not been well-understood as in high-energy hadron reactions. During the process in an early stage, one or both of the particles may escape from the nucleus. The probability of the escape may depend on the location of photoabsorption by a nucleon and nuclear transparency for the associated particles. If the pion were emitted in a forward direction at a small angle, the resulted nucleus would be left with an energy insufficient for developing the cascade-evaporation process. Especially, when photoabsorp-

tion occurs at the surface region of the target nucleus, the chance for an escape would be high and such simple reactions as  $(\gamma, n)$ ,  $(\gamma, p)$ , and  $(\gamma, \pi^\pm)$  could result.<sup>1,2</sup>

These simple reactions, especially on light nuclei, have received considerable attention since 1950s in order to gain valuable basic information concerning photonuclear interactions and nuclear structure.<sup>3</sup> Hughes and March<sup>4</sup> attempted for the first time to measure the residual nucleus of  ${}^{11}\text{B}(\gamma, \pi^-){}^{11}\text{C}$  by observing its positron activity of 20 min half life with use of the Glasgow 330 MeV electron synchrotron as early as in 1957. Good agreement with theoretical results of Laing and Moorehouse<sup>5</sup> was found if the surface production model was to be valid, and seemed to be consistent with pion observations performed since the first one by McMillan, Peterson and White in 1949.<sup>6</sup> One problem found in photopion measurements was irregularly varying  $(\pi^+/\pi^-)$  yield ratios from complex nuclei irrespective of their neutron-to-proton ratios.<sup>7</sup> Additional emissions of nucleon, mostly neutrons, will also occur if sufficient energy is left after the primary process. The neutron emission channels following pion emission, i.e.  $(\gamma, \pi^-n)$  reactions, had been studied far less extensively before the works by activation method by the present author's group, because of the overwhelming productions of other radionuclides due to spallation (see below) and of the experimental complexity regarding multiparticle coincidence in inclusive experiments. Most of the previous physical investigations were restricted to the inclusive measurements of one or two of the emitted particles from light nuclei. A series of double differential cross section measurements of pions and nucleons (2p and pn) from heavier targets was reported,<sup>8</sup> and the dependence of the energy-integrated differential cross sections on nuclear size ( $S_N$ ),  $S_N$  being the number of protons or neutrons in the target, was found to be described by  $d\sigma/d\Omega \propto S_N^\alpha$ , where the exponent  $\alpha$  is 0.6 for  $\pi^\pm$  and 1.15 for a proton. The authors explained the results of the cross sections as a consequence of a combina-

\*Corresponding author. E-mail: kohsakamoto@par.odn.ne.jp. FAX: +81-76-224-8253.

tion of volume production and pion reabsorption, although pure surface production could not be excluded from the pion data. These inclusive measurements do not distinguish the types of reactions responsible for the observed particles. Also, particle measurements were unavoidable from a certain restriction of the detection threshold ( $\sim 40$  MeV) of the particle spectrometers.

The activation method introduced by Hughes and March<sup>4</sup> was followed by a number of similar activity measurement that expected to allow studies of the cross sections for transitions to an isolated single final state or for transitions to several states which are stable against nucleon emission.<sup>3</sup> The activity method was also applied to many other heavier nuclei ranging from <sup>27</sup>Al to <sup>197</sup>Au, for which a theoretical analysis is quite difficult because of a large number of final states involved. For these reactions a Monte Carlo calculation combining elementary cross sections with a nuclear model gives some insight into pion and photon interaction with nuclei. Pioneer works for other types of competitive simple reactions, ( $\gamma$ , n) and ( $\gamma$ , p), light nuclear cluster emissions (fragmentation), photospallation and photofission were also numerous during 1950s to 1970s. All of these experiments were performed by irradiation of bremsstrahlung beams of continuous spectra ranging from 0 to their end-point energies ( $E_0$ ) of 100 to 1000 MeV with use of betatrons, electron linear accelerators (Electron Linacs) and electron synchrotrons (ES). Some were above 1000 MeV with use of the 2.5 GeV ES at the University of Bonn, the 7.4 GeV ES at the Deutsches Electron Synchrotron (DESY), and the 5 GeV ES at the Yerevan Physics Institute, Armenia (see References in 3.1. and 4.1. for electron accelerators).

In these studies, the radioactivity measurements of the irradiated targets were performed nondestructively with a few exceptions. In an irradiation of medium-heavy and heavy nuclei, a huge variety of radionuclides mostly produced through spallation make an accurate measurement difficult, and the reported results by different authors were often discrepant. With the advent of high intensity and high energy electron accelerators together with tagging systems and high-resolution particle spectrometers for inclusive measurements during the late 1970s, photonuclear reaction study with bremsstrahlung of continuous energy spectrum has faded out.

For the activation method a bremsstrahlung beam has still been a unique tool due to the absence of high energy monochromatic photon source with sufficiently high intensity. It has been expected to reveal the variation of the cross sections as a function of photon energy ( $k$ ), when the irradiations are carried out at small steps of  $E_0$  to be sufficient enough for unfolding of the yield variations into the cross sections as stated by Jonsson and Persson in their paper on <sup>127</sup>I-photospallation in 1970.<sup>9</sup> The activation method is useful for identifying individual reactions unambiguously. With bremsstrahlung of high  $E_0$ , simple reactions are always accompanied by dominant reactions of single and multiple nucleon emissions, spallation, and fission in case of heavy targets due to GDR and QDR mechanisms caused by low energy photons up to  $k = 100$  MeV, as well as that due to a cascade-evaporation process initiated by  $\Delta$ -decay. Many radioisotopes decay to their isobaric daughter nuclei, which are observed as a sum of the primary product and its decay products. Radiochemical methods can evaluate the respective contributions of the isobaric yields by changing the time of irradiation or that of chemical isolation.

The information obtained from the activation method is integral with respect to the energy and angle, and forgoes a detailed theoretical analysis of the final states involved.<sup>3</sup> However the complete picture concerning competitive reaction paths opened especially by  $\Delta$ -resonance such as photopion reactions ( $\gamma$ ,  $\pi^{\pm}xn$ ) different in the number of neutrons emitted  $x$ , and the individual reactions leading to photospallation, photofragmentation, and photofission can be clarified.

Under these situations by 1970s, we started to try the yield measurements of photonuclear reactions on a variety of targets ranging from <sup>7</sup>Li to <sup>209</sup>Bi at  $E_0 = 30$ –1200 MeV in small  $E_0$  steps with the aid of intensive chemical separations to systematize all types of residual nuclides produced by photopion reaction,<sup>10–13</sup> spallation,<sup>14–23</sup> fragmentation<sup>24, 25</sup> and fission of preactinides, <sup>197</sup>Au and <sup>209</sup>Bi.<sup>26–28</sup> Empirical expressions for the reaction yields as well as for the parameters included in the expressions have been derived. A simple nuclear recoil experiment using the thick-target thick-catcher method has been performed, in addition to the yield measurements, on 167 radionuclides formed in the photonuclear reactions of <sup>27</sup>Al, <sup>nat</sup>V, <sup>nat</sup>Cu, <sup>93</sup>Nb, <sup>nat</sup>Ag, <sup>nat</sup>Ta, and <sup>197</sup>Au to obtain kinematic information and to deepen our understanding on reaction mechanism.<sup>20–23, 26–28</sup> An account on this subject has recently been made in this journal by Haba.<sup>29</sup> All of the results have been discussed in conjunction with a theoretical calculation based on the photon-induced intranuclear cascade analysis code (PICA) by Gabriel et al.<sup>30, 31</sup> and its improved versions by Fu<sup>32</sup> and Sato et al.<sup>33, 34</sup>

In the following, we describe our experimental methods and the results of photopion reactions, spallation, fragmentation and fission separately, though all these processes are competitive. Simple photoreactions such as ( $\gamma$ , n), ( $\gamma$ , p), ( $\gamma$ ,  $\alpha$ ), and others on the light and medium-weight nuclei have been the subject of a number of investigators since 1950s, but are not treated here except for ( $\gamma$ , xn) reactions in 4.3. We try to emphasize why and how we have made the measurements of those reaction yields and what we have discovered from the investigations of photonuclear reaction processes.

## 2. Experimental Procedures

Irradiations were performed using stacked targets with natural isotopic abundances (nat.) in suitable chemical forms and sizes comprising of duplicated target disks and beam monitors. Electron-free collimated bremsstrahlung beams of  $E_0 = 250$  to 1200 MeV were supplied in air from the 1.3 GeV ES of the Institute for Nuclear Study (INS), the University of Tokyo (later The High Energy Accelerator Research Organization, KEK, at Tanashi). Uncollimated beams of  $E_0 = 30$  to 250 MeV were delivered from the 300 MeV Electron Linac of the Laboratory of Nuclear Science (LNS), Tohoku University. A series of irradiation of  $E_0 = 100$ –250 MeV was performed in a water-cooled target holder with an electron beam being passed through an energy-compressing system to confine the electron energy to  $\pm 1\%$  at full width at half maximum. Irradiation of CsCl at 305 MeV was tested in air with use of the 600 MeV Electron Linac at the Electrotechnical Laboratory (ETL). Bremsstrahlung was produced in a 0.5 mm-thick Pt converter both at LNS and ETL and in a 0.05 mm-thick Pt plate at INS. The size of the bremsstrahlung beam was about 10 mm in diameter at the target position both at INS and ETL and about 5 mm in diameter at LNS, and the beam intensity was monitored with a Wilson type thick chamber quantimeter at INS, though the photon intensity used in the yield calculation for  $E_0 \geq 100$  MeV was obtained from the monitor reaction <sup>27</sup>Al( $\gamma$ , 2pn)<sup>24</sup>Na (Ref. 35) and those for  $E_0 = 30$ –75 MeV was from <sup>197</sup>Au( $\gamma$ , n)<sup>196</sup>Au (Refs. 36 and 37) in aluminum and gold monitor foils, respectively, irradiated together with the targets. The yield data of the monitor reactions were experimentally examined by ourselves<sup>37</sup> by referring to the reported values. The average intensities in the series of irradiation were  $10^9$ – $10^{10}$  equivalent quanta (eq.q.) per second from INS-ES and  $10^{12}$ – $10^{13}$  eq.q. per second from LNS linac.

After irradiation, chemical separation procedures of almost 200 recipes were applied to target disks with use of proper carriers for  $\gamma$ -ray spectrometry and accelerator mass spectrom-

etry, AMS, for  $^{10}\text{Be}$ , and without carrier for  $\alpha$ -spectrometry for polonium isotopes from  $^{209}\text{Bi}$  and for  $\gamma$ -ray spectrometry for mercury isotopes from  $^{197}\text{Au}$  and for noble-gas isotopes from  $^{41}\text{K}$ ,  $^{87}\text{Rb}$ ,  $^{127}\text{I}$ ,  $^{133}\text{Cs}$ , and  $^{139}\text{La}$ . The chemical procedures have been described in the relevant publications quoted below, but not all. The remaining irradiated targets were subjected to measurements for characteristic  $\gamma$ -rays from the reaction products nondestructively. Only the nondestructive measurements were carried out for very short-lived products from light- and medium-weight targets. Special low-level counting technique was applied to the low-yield and long-lived nuclide,  $^{22}\text{Na}$ . Radioactivity measurements were continued for more than one month in general to confirm the half-lives and no contribution from interferences. For the  $\gamma$ -ray measurements, several calibrated HPGe detectors of 1.6–1.7 keV resolution at 1331 keV coupled each with a 4k PHA were used. The characteristic photopeaks<sup>38–40</sup> were evaluated with an automatic peak-search program by Komura,<sup>41</sup> and later with its up-dated version, “SPEC anal 98” by Hamajima.<sup>42</sup>

### 3. Photopion Nuclear Reactions

**3.1. Background.** Among simple types of photopion reaction studied experimentally and theoretically before 1970s, the reaction yields of  $^{11}\text{B}(\gamma, \pi^-)^{11}\text{C}$ ,  $^{27}\text{Al}(\gamma, \pi^+)^{27}\text{Mg}$ ,  $^{51}\text{V}(\gamma, \pi^-x\text{n})^{51-x}\text{Cr}$  for  $x = 0$  and 2, and  $^{51}\text{V}(\gamma, \pi^+)^{51}\text{Ti}$  had been reported many times by different authors who used the University of Glasgow 330 MeV ES,<sup>4</sup> the University of Illinois 340 MeV Betatron,<sup>43–45</sup> the INS-720 MeV ES,<sup>46</sup> the University of Lund 1.2 GeV ES,<sup>47–50</sup> the University of Bonn 2.5 GeV ES,<sup>51</sup> the 0.36 and 2 GeV Electron Linac of Physico-technical Institute of the Ukrainian Academy of Sciences, Ukraine,<sup>52</sup> DESY-7.4 GeV ES,<sup>53</sup> the 170 MeV Bates Linac of the Massachusetts Institute of Technology (MIT),<sup>54</sup> DESY-580 MeV Linac,<sup>55, 56</sup> and the Frascati-1.0 GeV ES of the Frascati National Laboratory.<sup>57</sup>

A common problem in activation methods is the presence of non-mesic interactions; secondary protons and neutrons lead to the same products of  $(\gamma, \pi^-x\text{n})$  and  $(\gamma, \pi^+)$  reactions through  $(p, x'n)$  and  $(n, p)$  reactions, respectively. This secondary contribution had been noticed in the earlier studies, but not well studied with respect to the yield variation of the secondaries before our findings for the disentangling. The secondary neutrons were considered to be generated in the machine, and the contribution was estimated from off-beam samples.<sup>47, 48</sup> We first examined the same procedure and also the depth profiles of the yield by using a stack of target plates, and found that these were not sufficient for the proper correction.<sup>11</sup> The emphasis in our works was placed on runs below and above the thresholds for pion production to assess the contribution of the interfering reactions,<sup>10–13</sup> that could be performed by calculations of the secondary reaction yields with the relevant excitation functions measured and/or calculated by the ALICE code<sup>58, 59</sup> for the proton and neutron reactions and the secondary photoproton<sup>60–62</sup> and photoneutron spectra.<sup>63, 64</sup> The magnitude was obtained by fitting the calculations to the experimental values below the photopion threshold. The detailed description of the correction method and its empirical expression for the secondary contributions as a function of the target mass number ( $A_t$ ) and the number of neutrons emitted ( $x$ ) were given in Reference 65. It is noted that  $(\gamma, \pi^+x\text{n})$  reactions for  $x \geq 1$  are not able to be studied by activation methods, because the concomitant  $(\gamma, px'n)$  reactions lead the same residual nuclides.

**3.2. Revisit to Photopion Reactions on  $^{51}\text{V}$ .** We started our study of photopion reactions with a revisit to the measurement of chromium and titanium isotopes produced in photoreactions of  $^{51}\text{V}$  with an aid of chemical technique in the mid 1980s.<sup>10</sup> The observed yields for the respective nuclides as a function of  $E_0$  for 30–1050 MeV showed smooth curves hav-

ing one step around the photopion threshold (Figure 1 for  $^{49}\text{Cr}$  yields); below the step the nuclide production is purely due to the secondary reaction but the secondary reaction is superimposed by the photopion reaction above its threshold. The secondary-corrected yields increase rapidly from the threshold with an increase of  $E_0$  and attain a plateau at around 300–500 MeV, suggesting that photons responsible for production of these nuclides are mostly of energies lower than 400 MeV. Our results for the secondary-corrected yields of  $^{51}\text{V}(\gamma, \pi^-2\text{n})^{49}\text{Cr}$  were more close to the ones by Blomqvist et al.<sup>55</sup> than the other previous data, while those for  $^{51}\text{V}(\gamma, \pi^-)^{51}\text{Cr}$  and  $^{51}\text{V}(\gamma, \pi^+)^{51}\text{Ti}$  agreed only around the thresholds and the high energy regions showing the discrepant shapes of the yield curves as a function of  $E_0$ . The reasons for the discrepancies might be due to insufficient or inaccurate secondary corrections and to differences in beam monitors. For  $^{51}\text{Cr}(\gamma, \pi^-3\text{n})^{48}\text{Cr}$ , our yield values were lower by a factor of 50 than those reported for  $E_0 = 300$  to 1000 MeV by di Napoli et al.<sup>57</sup> that were not consistent with the systematic variations with respect to  $x$ , as will be shown below (3.3. and 3.6.).

The yields,  $Y(E_0)$ , are expressed as

$$Y(E_0) = E_0 \int_0^{E_0} \sigma(k) \cdot N(E_0, k) dk / \int_0^{E_0} k \cdot N(E_0, k) dk, \quad (1)$$

and can be unfolded into cross section  $\sigma(k)$  per photon of energy  $k$ . We employed the method of Tesch<sup>66</sup> with aid of the LOUHI-82 code<sup>67</sup> by assuming the Schiff spectrum<sup>68</sup> to approxi-

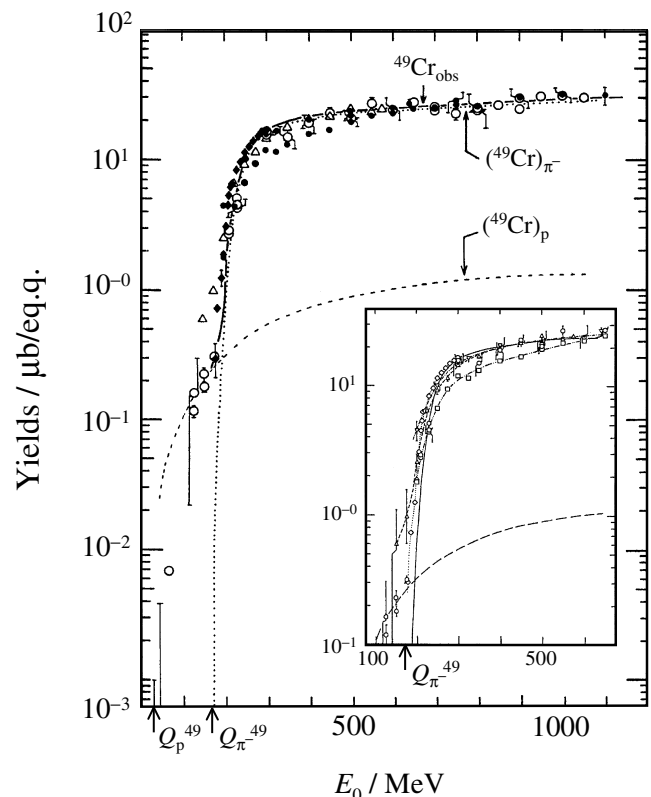


**Figure 1.** The yields in units of  $\mu\text{b}/\text{eq.q.}$  as a function of bremsstrahlung end-point energy  $E_0$ . The observed yields in the authors' work,  $^{49}\text{Cr}_{\text{obs}}$ , are shown by open circles connected with a solid line. The dashed line indicate the yields from the secondary  $(^{49}\text{Cr})_p$ . The net yields obtained from subtraction of  $(^{49}\text{Cr})_p$  from the observed yields  $^{49}\text{Cr}_{\text{obs}}$  are for  $^{51}\text{V}(\gamma, \pi^-2\text{n})^{49}\text{Cr}$  and shown by a dotted curve noted with  $(^{49}\text{Cr})_{\pi^-}$ . Comparisons are made with the reported ones: closed diamonds,<sup>44</sup> closed circles,<sup>47, 50, 57</sup> and triangles.<sup>55</sup> An inset is an expanded one in  $100 \leq E_0 \leq 650$  MeV for a detailed comparison with the literature data for  $(^{49}\text{Cr})_{\pi^-}$ . Diamonds connected with dotted curve are from Meyer and Hummel,<sup>44</sup> squares with two dot-broken curve from Nydahl and Forkman,<sup>47</sup> triangles with broken curve from Blomqvist et al.,<sup>55</sup> and reversed triangles and closed circles both with one dot-broken curve from Bülow et al.,<sup>50</sup> and di Napoli et al.<sup>57</sup> Arrows on  $E_0$  axis show the  $Q$ -values for  $^{51}\text{V}(p, 3\text{n})^{49}\text{Cr}$  and  $^{51}\text{V}(\gamma, \pi^-2\text{n})^{49}\text{Cr}$ . (Reprinted from Reference 10 with permission from the Elsevier Ltd.)

mate the bremsstrahlung production cross section.

It was shown that the four excitation curves  $\sigma(k)$  for productions of  $^{51}\text{Cr}$ ,  $^{49}\text{Cr}$ , and  $^{48}\text{Cr}$  from  $^{51}\text{V}(\gamma, \pi^-x\text{n})$  for  $x = 0, 2$  and  $3$ , respectively, and  $^{51}\text{Ti}$  from  $^{51}\text{V}(\gamma, \pi^+)$  reactions are of similar shape with the full width at half maximum (FWHM) of  $(70 \pm 5)$  MeV for  $^{51-x}\text{Cr}$  and about 80 MeV for  $^{51}\text{Ti}$  (Figure 4(a) below). The peak energy for  $^{51-x}\text{Cr}$  increases rather regularly from 210 to 245 MeV with an increase of  $x$  from 0 to 3. The peak for  $^{51}\text{Ti}$  locates at  $k = 235$  MeV which is higher than that ( $k = 210$  MeV) for  $^{51}\text{Cr}$ .

The unfolded results of cross sections  $\sigma(k)$  for production of  $^{49}\text{Cr}$  from  $^{51}\text{V}(\gamma, \pi^-2\text{n})$ , as an example, are illustrated by a thick line together with the previously reported ones and theoretical calculations in Figure 2. The theoretical calculations were reported for  $^{51}\text{Ti}$  and  $^{49}\text{Cr}$  as well as for  $^{27}\text{Al}(\gamma, \pi^+)^{27}\text{Mg}$  on the basis of a valence nucleon model (surface production model) by Nydahl and Forkman<sup>47</sup> and of distorted-wave impulse approximation (DWIA) with and without final-state interaction of the outgoing pion through optical potentials by Blomqvist et al.,<sup>56</sup> the latter of which was for  $^{51}\text{Ti}$  not shown in Figure 2 but see Figure 3 of Reference 10. Nydahl and Forkman<sup>47</sup> also made a calculation for  $^{49}\text{Cr}$  by considering that the primary photon interacts with neutrons located both in valence states and inner shells (volume production), and their results (II) is shown together with those of the valence nucleon model (I) in Figure 2. It was then concluded that all the magnitudes, peak energies and the shapes of the calculations are in disagreement with the experiment. Booth quoted in his review work<sup>69</sup> a statement by Blomqvist et al.<sup>56</sup> that the blame is placed on the optical potential which gives too weak an s-wave repulsion and too strong a p-wave absorption. A considerable improvement was reported for the total cross sections  $^{27}\text{Al}(\gamma, \pi^+)^{27}\text{Mg}$  (Ref. 70) by investigating that of  $^{51}\text{V}(\gamma, \pi^+)^{51}\text{Ti}$  (Ref. 71) using pion optical potentials having different analytic forms within the frame work of the DWIA, but the calculation for those for  $^{51}\text{V}(\gamma, \pi^-x\text{n})^{51-x}\text{Cr}$  have not been given.

We then performed a Monte Carlo intranuclear cascade-evaporation calculation by using the PICA code by Gabriel et al.<sup>30,31</sup> which had not been well tested for  $\sigma(k)$  for the production of residual nuclei from (3,3) resonance (see 3.5. for the PICA code). The incident particle histories of  $(0.4-1.0) \times 10^6$  were followed with the parameter values given by the original

authors in the calculation. The calculated results are compared with our experiment in Figure 3. It is shown that the PICA code could reproduce the gross feature of our  $\sigma(k)$ , provided that all the calculated results were shifted higher on the  $k$  axis by 30 MeV for  $^{51-x}\text{Cr}$  and by 60 MeV for  $^{51}\text{Ti}$ . Also the calculated peak cross sections of  $^{50}\text{Cr}$  from  $^{51}\text{V}(\gamma, \pi^-n)$ ,  $^{49}\text{Cr}$  from  $^{51}\text{V}(\gamma, \pi^-2\text{n})$ , and  $^{51}\text{Ti}$  from  $^{51}\text{V}(\gamma, \pi^+)$  reactions are fairly good in the reproduction, but those of  $^{51}\text{Cr}$  from  $^{51}\text{V}(\gamma, \pi^-)$  and  $^{48}\text{Cr}$  from  $^{51}\text{V}(\gamma, \pi^-3\text{n})$  reactions give a lower value for the former and a higher one for the latter both by a factor of more than 2 compared with the experimental values, provided the energy shifts mentioned above is disregarded. It was shown that there is a strong even-odd effect in the PICA calculation.

It was found that the  $(\gamma, \pi^-x\text{n})$  channel amounts only to about 0.6% of the total absorption deduced from the observed average of the total hadronic cross sections or from our measurement of the yield values of photospallation of  $^{51}\text{V}$  that will be described in section 4 (see Figure 5 of Reference 10 and Figure 7 and Table 1 of Reference 19). Though the relative contributions are slightly energy- and  $A_i$ -dependent, the reaction channel for  $(\gamma, \pi^-x\text{n})$  is actually one of the simplest decay parts of the (3,3) resonance absorption among others, being opened at the lowest excitation of the resonance absorption. It was suggested that the photoreaction samples the entire nuclear volume, but the mechanism is not so simple as those described by the old model of surface production nor volume production.

### 3.3. Photopion Reactions on Medium- and Heavy-Nuclei.

We extended the same type of the experiment to other targets to investigate the effects of  $A_i$  and/or target composition  $(N/Z)_i$  on the yield profiles: the nuclear surface is proportional to  $A_i^{2/3}$  and the volume to  $A_i$ . The first example of our extension was to  $^{133}\text{Cs}$ .<sup>11</sup> It was surprising to find that the mass yields,  $Y(E_0)$ , of  $^{133-x}\text{Ba}$  from  $^{133}\text{Cs}(\gamma, \pi^-x\text{n})$  reaction for  $x = 0-9$  as a function of  $x$  showed a broad maximum around  $x = 3$  for the relevant energies, indicating that the excitation energy remaining in the target nucleus after  $\pi^-$  emission is sufficiently high to evaporate 7 to 9 neutrons with appreciable probabilities, quite different from that of  $^{51}\text{V}(\gamma, \pi^-x\text{n})$ , in which the yields decrease rapidly with an increase of  $x$  from 0 to 3 (see Figure 6 below). The  $(\gamma, \pi^-)$  yields from  $^{51}\text{V}$  and  $^{133}\text{Cs}$  seemed to be equal and higher by a factor of 5-6 than the  $(\gamma, \pi^+)$  yields in the  $\Delta$ -reso-

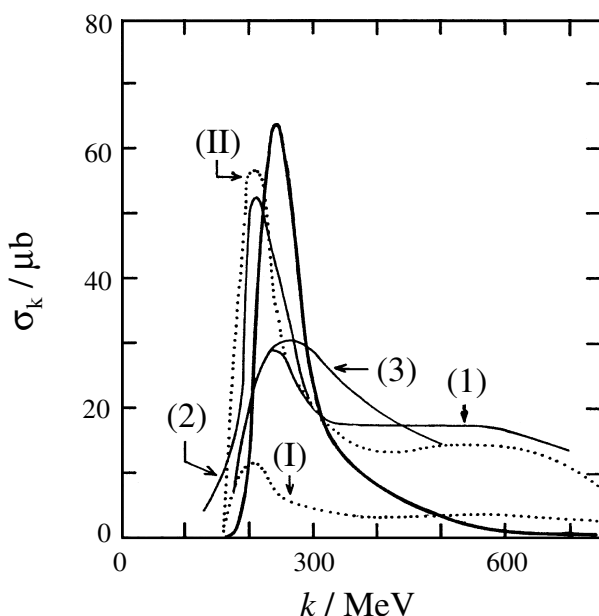


**Figure 2.** Comparison of the present  $\sigma_k$  (thick line) with the reported results (thin lines) and theoretical predictions (dotted curves) for the cross sections of  $^{51}\text{V}(\gamma, \pi^-2\text{n})^{49}\text{Cr}$ . Experimental results: thin line (1),<sup>47</sup> thin line (2),<sup>44</sup> and thin line (3).<sup>55</sup> Theory: curve (I)<sup>47</sup> based on surface production, and curve (II)<sup>47</sup> on volume production model. (Reprinted from Reference 10 with permission from the Elsevier Ltd.)

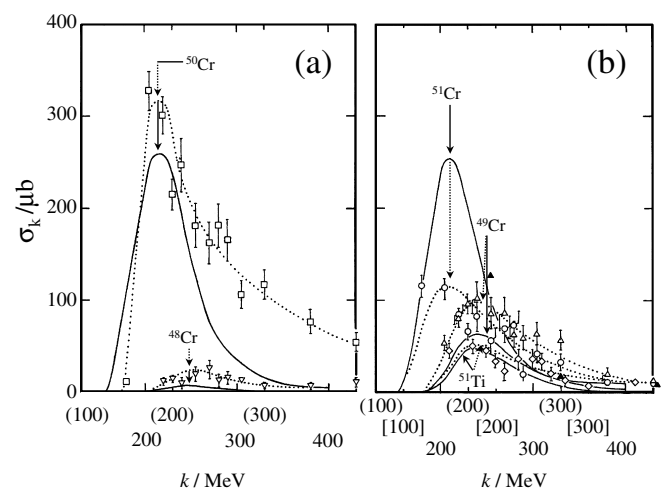


**Figure 3.** Comparison of the present results with the PICA code calculation. The calculated results are shown by symbols with statistical error bars for even mass products; squares for  $^{50}\text{Cr}$  and reversed triangles for  $^{48}\text{Cr}$ , and (b) for odd mass products, circles for  $^{51}\text{Cr}$ , triangles for  $^{49}\text{Cr}$  and diamonds for  $^{51}\text{Ti}$ . The closed triangles in (b) are those calculated with the same code by Bülow et al.<sup>50</sup> The energy scale for all the calculated points is shown by numbers in parentheses except for  $^{51}\text{Ti}$  by those in square brackets. The dotted curves are drawn to guide the eye and the solid ones are the present experimental results. (Reprinted from Reference 10 with permission from the Elsevier Ltd.)

nance region. The excitation functions  $\sigma(k)$ , in unit of  $\mu\text{b}$  per photon, as a function of photon energy  $k$  are illustrated in Figure 4: (a) is for  $^{51}\text{V}$  target<sup>10</sup> and (b) is for  $^{133}\text{Cs}$  target.<sup>11</sup> The dashed curves show  $\sigma(k)$  estimated by interpolation. The uncertainty in  $\sigma(k)$  was estimated to be at most about (30–50)% at peak from the range of scattering of the observed yield values measured at  $E_0 = 30\text{--}1050$  MeV in steps of 50 MeV or less and from ambiguity inherited from unfolding process. The shape of the excitation curves, peak cross section, peak energy and width for  $^{133-x}\text{Ba}$ , was found to be a smooth function of  $x$  and to be consistent with the shape for  $^{51-x}\text{Cr}$  from  $^{51}\text{V}$  target, as seen in Figure 4(a) and (b). It was difficult in the present data to extract the nonresonant absorption of photon due to the Born terms and the high mass resonant contributions of  $D_{13}$  (1520) and  $F_{15}$  (1680) as observed in hydrogen and deuterium targets.<sup>2,3</sup> A search for radioactivities in lanthanum fractions separated from  $^{133}\text{Cs}$  irradiated at  $E_0 = 600\text{--}1000$  MeV indicated no detectable effect of the double pion emission.

The PICA calculation for  $^{133}\text{Cs}(\gamma, \pi^- \text{xn})$  cross sections could reproduce the gross feature of the observed excitation curves, though a strong even-odd effect and energy shifts were evident as in the case of  $^{51}\text{V}$  target; the reproduction of the peak cross sections is excellent for the even-mass but not for the odd-mass products, though the peak energy of the calculated curves should be shifted higher by 30 MeV to fit the experiment for  $(\gamma, \pi^- \text{xn})$  reactions (see Figure 6 of Reference 11).

In this work, the yield measurement of  $^{133}\text{Xe}$  from  $^{133}\text{Cs}(\gamma, \pi^+)$  reaction was preliminary, so a series of photoreactions producing

noble gas isotopes, not only on  $^{133}\text{Cs}$  but also  $^{41}\text{K}(\gamma, \pi^+)^{41}\text{Ar}$ ,  $^{87}\text{Rb}(\gamma, \pi^+)^{87}\text{Kr}$ , and  $^{127}\text{I}(\gamma, \pi^- \text{xn})^{127-x}\text{Xe}$  ( $x = 0, 2, 4, 5$ , and  $6$ ) was studied together with photospallations of  $^{133}\text{Cs}(\gamma, \text{pxn})^{132-x}\text{Xe}$  ( $x = 1, 3, 5, 7, 9, 10$ , and  $11$ ) and  $^{139}\text{La}(\gamma, 3\text{pxn})^{136-x}\text{Xe}$  ( $x = 7, 9, 11, 13, 14$ , and  $15$ ) by constructing a simple glass vacuum system for extraction and collection of noble gases.<sup>12</sup> Here  $^{127}\text{I}$  was chosen to compare with the  $^{133}\text{Cs}$  results, and the  $(\gamma, \pi^+)$  reactions were also to compare with the  $^{51}\text{V}$  result. The characteristic features of  $A_i$  dependence for the energy ( $k$ )–integrated cross sections,  $\int_0^{E_0} \sigma(k) dk$ , were found in the above-mentioned works to be the same as those of  $Y(E_0)$ , because of the resonance nature of the photonuclear interactions. Therefore, we present and discuss only the values of  $Y(E_0)$  for some selected  $E_0$  hereafter.

The important findings in this work were as follows: (1) The  $(\gamma, \pi^- \text{xn})$  yields as a function of  $x$  (mass yield distributions) appear a smooth function of  $A_i$  and  $E_0$ , and the  $^{127-x}\text{Xe}$  yields with  $x = 0\text{--}6$  are close to the  $^{133-x}\text{Ba}$  yields with  $x = 0\text{--}9$  at the same  $E_0$ . (2) The  $(\gamma, \pi^-)$  and  $(\gamma, \pi^+)$  yields are  $A_i$ -independent, and the yield values for the former are  $92 \pm 13$ ,  $80 \pm 13$ , and  $50 \pm 8$   $\mu\text{b}/\text{eq. q.}$  at  $E_0 = 800, 400$ , and  $250$  MeV, respectively, as obtained by averaging over the yields of  $^{51}\text{Cr}$  from  $^{51}\text{V}$ ,  $^{127}\text{Xe}$  from  $^{127}\text{I}$  and  $^{139}\text{Ce}$  from  $^{139}\text{La}$  (Ref. 72) and those for the latter are  $19.6 \pm 1.4$ ,  $17.0 \pm 1.5$ , and  $8.40 \pm 1.14$   $\mu\text{b}/\text{eq. q.}$  at  $E_0 = 800, 400$ , and  $250$  MeV, respectively, by averaging over the yields of  $^{41}\text{Ar}$  from  $^{41}\text{K}$ ,  $^{51}\text{Ti}$  from  $^{51}\text{V}$ ,  $^{65}\text{Ni}$  from  $^{65}\text{Cu}$  (Ref. 48),  $^{87}\text{Kr}$  from  $^{87}\text{Rb}$ ,  $^{133}\text{Xe}$  from  $^{133}\text{Cs}$ ,  $^{138}\text{Cs}$  from  $^{138}\text{Ba}$  (Ref. 73),  $^{139}\text{Ba}$  from  $^{139}\text{La}$  (Ref. 72) and  $^{181}\text{Hf}$  from  $^{181}\text{Ta}$  (Ref. 72). The PICA calculation at  $E_0 = 400$  and  $250$  MeV also gave the  $A_i$ -independence of the  $(\gamma, \pi^-)$  and  $(\gamma, \pi^+)$  yields, but a lower value ( $56 \pm 8$   $\mu\text{b}/\text{eq. q.}$ ) for the former and a higher one ( $30.7 \pm 3.7$   $\mu\text{b}/\text{eq. q.}$ ) for the latter at  $E_0 = 400$  MeV, for an example.

**3.4.  $A_i$ - and  $E_0$ -dependence of  $(\gamma, \pi^\pm)$  Yields.** Further experiments on many additional targets were performed to confirm those findings. The yield values for  $(\gamma, \pi^-)$  and  $(\gamma, \pi^+)$  reactions at  $E_0 = 800, 400$ , and  $250$  MeV are plotted in Figures 5(a)–5(c) as a function of  $A_i$ . Closed circles represent the yields for  $(\gamma, \pi^-)$  reactions on the targets indicated on the upper horizontal axis of Figure 5(b). The large symbols show the values for  $(\gamma, \pi^-)$  reactions obtained by our group including those mentioned above. Literature data indicated by small symbols are on  $^7\text{Li}$  (Refs. 74 and 75),  $^{11}\text{B}$  (Refs. 4, 48, and 52),  $^{12}\text{C}$  (Refs. 75 and 76),  $^{14}\text{N}$  (Ref. 77),  $^{51}\text{V}$  (Ref. 56),  $^{60}\text{Ni}$  (Ref. 78), and  $^{197}\text{Au}$  (Ref. 79). The  $Y(E_0)$  values for  $(\gamma, \pi^+)$  reactions are plotted as open squares for the targets indicated on the lower horizontal axis of Figure 5(b). The large symbols are for our values and the smaller ones for literature data for  $^9\text{Be}$  (Ref. 80),  $^{27}\text{Al}$  (Refs. 46, 48, 52, and 56),  $^{41}\text{K}$  (Ref. 48),  $^{51}\text{V}$  (Ref. 56),  $^{65}\text{Cu}$  (Ref. 48),  $^{88}\text{Sr}$  (Ref. 48), and  $^{138}\text{Ba}$  (Ref. 48). Our values for the  $^{14}\text{O}$ ,  $^{75}\text{Ge}$ , and  $^{109}\text{Pd}$  yields from  $^{14}\text{N}$ ,  $^{75}\text{As}$ , and  $^{109}\text{Ag}$ , respectively, are upper limits, i.e. no corrections for the secondaries (about 10% or less for the latter two) were performed. The solid lines are the weighted means of the measured values discussed below. Dotted lines are the weighted means of the values calculated for the particle histories of  $(1\text{--}4) \times 10^6$  by the PICA code for the mentioned reactions. The calculational model employed was only applicable to the reactions over the energy range of  $30\text{--}400$  MeV for both monoenergetic photons and thin-target bremsstrahlungs of Schiff spectra and over a range of  $A_i \geq 12$ ,<sup>30,31</sup> so the calculation at  $E_0 = 800$  MeV was not possible.

While some of the yield values are associated with large uncertainties, especially at  $E_0 = 250$  MeV where the yields increase very rapidly, both the  $(\gamma, \pi^\pm)$  yields are actually  $A_i$ -independent except for light targets, irrespective of  $E_0$ . The yields for  $(\gamma, \pi^-)$  reactions on lighter targets such as  $^7\text{Li}$  (Refs. 74 and 75),  $^{11}\text{B}$  (Refs. 4, 48, and 52),  $^{12}\text{C}$  (Refs. 75 and 76),  $^{14}\text{N}$  (Ref. 77) are anomalously small compared with those for the heavier targets. The low values for the  $^7\text{Be}$  and  $^{14}\text{O}$  yields up

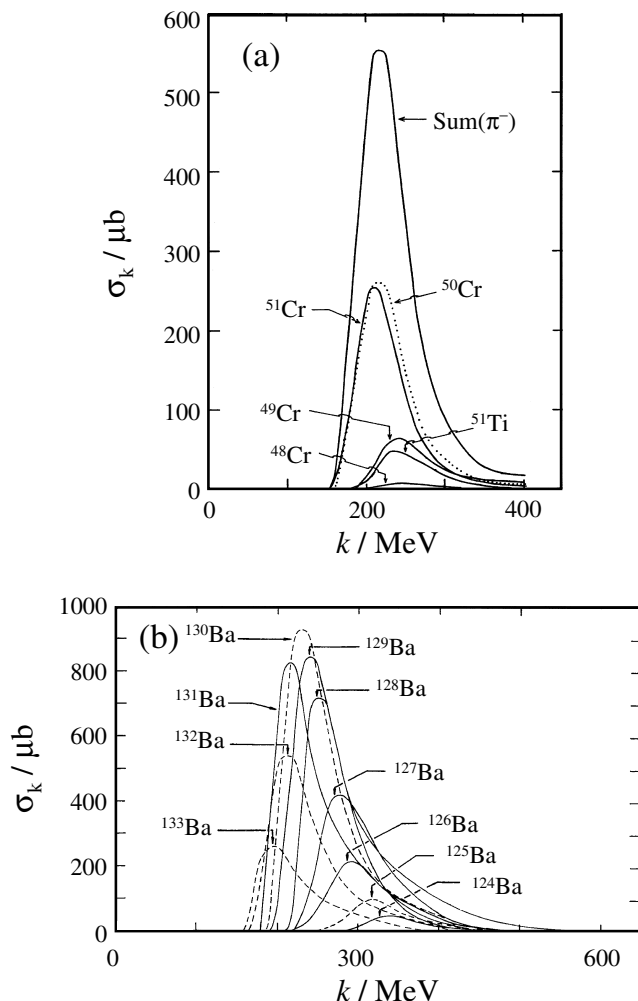


**Figure 4.** Cross sections  $\sigma_k$  in units of  $\mu\text{b}$  as a function of photon energy  $k$ , for (a)  $^{51}\text{V}(\gamma, \pi^- \text{xn})^{51-x}\text{Cr}$  ( $x = 0\text{--}3$ ) and  $^{51}\text{V}(\gamma, \pi^+)^{51}\text{Ti}$  and for (b)  $^{133}\text{Cs}(\gamma, \pi^- \text{xn})^{133-x}\text{Ba}$  ( $x = 0\text{--}9$ ), obtained by unfolding of the yield curves. ((a) Reprinted from Reference 10 and (b) from Reference 11 with permissions from the Elsevier Ltd. and the American Physical Society)

to  $E_0 = 1200$  MeV were confirmed in our work,<sup>81</sup> and the low yields are explained as due to small numbers of particle stable states (two in  ${}^7\text{Be}$ , ten in  ${}^{11}\text{C}$ , one in  ${}^{12}\text{N}$  and  ${}^{14}\text{O}$ ). It is now clearly shown by our experiments that the irregular  $\pi^+/\pi^-$  variations with respect to  $A_t$  found in the earlier days<sup>7</sup> were in error. On the other hand, many bound states leading to  $(\gamma, \pi^\pm)$  reactions exist in the heavy nuclei. This manifests the  $A_t$ -independence in the heavy target region; the weighted means of the yields values of  $(\gamma, \pi^-)$  reactions on targets having  $A_t \geq 44$  are  $91 \pm 6$ ,  $78 \pm 6$ , and  $51 \pm 5$   $\mu\text{b}/\text{eq. q.}$  for  $E_0 = 800$ , 400, and 250 MeV, respectively (lower horizontal solid lines in Figure 5). The PICA calculations for the corresponding reactions on these heavy targets at  $E_0 = 400$  and 250 MeV are smaller than the measured values by 35% on average. The calculations also indicate  $A_t$ -independence (upper dotted line in Figure 5). The  $(\gamma, \pi^\pm)$  reaction yields are also  $A_t$ -independent for  $A_t \geq 27$ , and their weighted means are  $18 \pm 2$ ,  $14 \pm 2$ , and  $7.3 \pm 1.1$   $\mu\text{b}/\text{eq. q.}$  for  $E_0 = 800$ , 400, and 250 MeV, respectively (lower horizontal lines in Figure 5). As noted above, a number of yield measurements for  ${}^{27}\text{Mg}$  from  ${}^{27}\text{Al}(\gamma, \pi^+)$  reactions have been reported, but the results are quite different among the different reports. Our values fall in between those of Masaike<sup>46</sup> and of Blomqvist et al.<sup>48</sup> The values of Noga et al.<sup>52</sup> and ours seemed

to be consistent with the mean values obtained from the heavier targets. Although both the  $(\gamma, \pi^-)$  and  $(\gamma, \pi^+)$  reactions on the light nuclei have been of interest from theoretical point of view,<sup>3</sup> they were not included in our discussion. The PICA calculation for  $(\gamma, \pi^+)$  reactions in the heavy target region reproduces the  $A_t$ -independence, but the average values (lower horizontal dotted lines in Figure 5) are two times larger than those of the measured ones. The measured yields in the  $A_t$ -independent region at  $E_0 = 400$ –800 MeV give a yield ratio of  $Y(\gamma, \pi^-)/Y(\gamma, \pi^+) = 5.6 \pm 1$ , while the corresponding PICA value at  $E_0 = 400$  MeV is  $1.8 \pm 0.3$ , confirming the previous findings described in 3.3.

### 3.5. Implications of $A_t$ -independence of $(\gamma, \pi^\pm)$ Yields.

The high observed yield ratios compared with the calculation may imply new nuclear structure effects that are not taken into consideration in theoretical ground in the PICA code. The nuclear model used in the theoretical calculations is exactly the same as the one used in the Bertini calculations.<sup>82</sup> The continuous charge density distribution inside the nucleus obtained by electron scattering data<sup>83</sup> was approximated by dividing the nucleus into three concentric spheres: a central and two surrounding spherical annuli having the uniform densities of 0.9, 0.2, and 0.01 of  $\rho(0)$  at the center of the nucleus. The neutron to proton density ratios of the spheres were assumed to be equal to that of the entire nucleus. Cross sections for the photoabsorption by a nucleon in the (3,3) resonance region were taken from those for elementary processes for free nucleon-photon interactions, by assuming  $\sigma(\gamma p \rightarrow \pi^+) = \sigma(\gamma n \rightarrow \pi^-)$  from charge-symmetry considerations. The intranuclear cascade calculation of Bertini<sup>82</sup> was then used to account for the secondary effect of nucleon- and pion-interactions with the remaining nucleus following the initial photon interaction. Pion absorption was assumed to occur via two-nucleon mechanism with a cross section for the absorption of a charged pion by a nucleon with isobaric spin projection of the opposite sign (i.e. a pair of nucleons must contain at least one proton to absorb a negative pion and at least one neutron to absorb a positive pion).

The higher yields of the  $(\gamma, \pi^-)$  reactions and the lower ones of the  $(\gamma, \pi^+)$  reactions relative to those expected from the PICA calculation, found in our series of studies, could possibly be understood if the neutron density in nuclear surface region is higher than the inner density of the nucleus. An initial production of negative pions by way of  $\gamma+n \rightarrow \Delta^0 \rightarrow p+\pi^-$  would be more probable than those of positive pions by way of  $\gamma+p \rightarrow \Delta^+ \rightarrow n+\pi^+$ , and the secondary absorption of negative pion by way of  $\pi^-+pp$  or  $\pi^-+pn$  would be less than those of positive pions by way of  $\pi^++np$  or  $\pi^++nn$  in the neutron-rich surface region.

These processes which lead to  $(\gamma, \pi^-)$  and  $(\gamma, \pi^+)$  reactions were, therefore, considered here to occur in the surface region of the nucleus, but the experimental observations showed that the cross sections are not proportional to  $A_t^{2/3}$  but  $A_t$ -independent. This  $A_t$ -independence may be explained as due to a compensation of the increase in pion production with increasing nuclear size (surface) by the competitive increase of neutron emissivity associated with pion emission (see below for discussions of  $(\gamma, \pi^\pm xn)$  reactions). The available final transitions are, therefore, limited to a certain number of levels below the particle separation energy which was set equal to 7 MeV in PICA. While the number of the bound states and the transition strength to these states are unknown, they must be statistically significant, as the  $A_t$ -independence from the PICA calculation also suggests. There has been no evidence for the density difference between protons and neutrons in the stable nucleus, but neutron skin and neutron halo structures have been discovered in very neutron-rich light nuclei near the drip line.<sup>84, 85</sup> Further study of structural changes in nuclei closer to the  $\beta$ -stability line is required. Our work suggests that photonuclear processes may cause such effects.

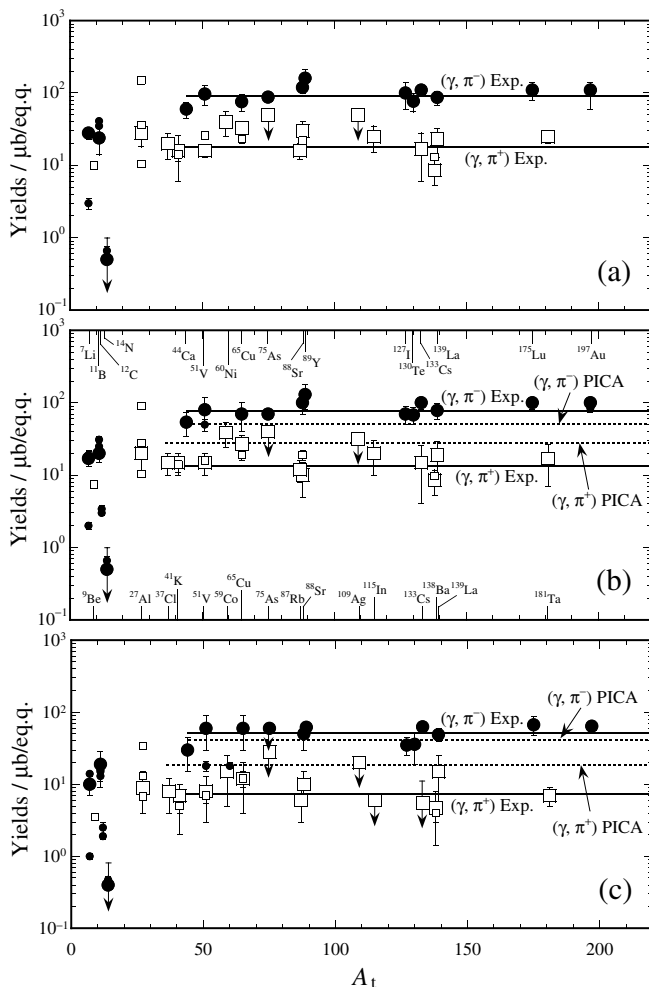


**Figure 5.** Target mass dependence of the  $(\gamma, \pi^\pm)$  yields in unit of  $\mu\text{b}/\text{eq. q.}$  at  $E_0 = 800$  MeV (a),  $E_0 = 400$  MeV (b), and  $E_0 = 250$  MeV (c). Closed circles represent the  $(\gamma, \pi^-)$  yields and open squares the  $(\gamma, \pi^+)$  yields. The large symbols show the values obtained by the author's group and the small ones from the literature (see text), as measured for the targets indicated along the upper axis for the  $(\gamma, \pi^-)$  reactions and the lower axis for the  $(\gamma, \pi^+)$  reactions in (b). The arrow symbols show measured values not corrected for secondary contributions. The solid lines are the weighted means of  $Y(E_0)$  for  $(\gamma, \pi^-)$  reactions on targets with  $A_t \geq 44$  and for  $(\gamma, \pi^+)$  reactions on  $A_t \geq 27$ . The dotted lines in (b) and (c) show the average PICA results calculated for the same reactions. (Reprinted from Reference 13 with permission from the American Physical Society)

**3.6. Characteristic Features of  $(\gamma, \pi^n xn)$  Yields.** The  $E_0$ -dependence of the  $(\gamma, \pi^n xn)$  yields is shown in Figure 6, where the measured yield values at  $E_0 = 800, 400,$  and  $250$  MeV from  $^{51}\text{V}, ^{59}\text{Co}, ^{75}\text{As}, ^{89}\text{Y}, ^{109}\text{Ag}, ^{115}\text{In}, ^{127}\text{I}, ^{133}\text{Cs}, ^{139}\text{La}, ^{175}\text{Lu}, ^{197}\text{Au},$  and  $^{209}\text{Bi}$  targets<sup>13</sup> are plotted as a function of the number of neutrons emitted ( $x$ ), i.e. isotopic mass yield curves. Arrows on the symbols indicate the observed values which are not corrected for secondary contributions (less than 10%). The solid, broken and dotted curves are drawn through the data points for  $E_0 = 800, 400,$  and  $250$  MeV, respectively.

The mass yield curves at  $E_0 = 800$  and  $400$  MeV are almost the same and higher than those at  $250$  MeV, reflecting characteristics of the  $\Delta$ -resonance. The difference between the yield patterns for  $250$  MeV and  $400$  (and  $800$ ) MeV increases with the increasing  $A_t$ , and it becomes more prominent at larger  $x$  in the  $A_t$  region from  $127$  to  $209$ . As noted above (Figure 5), the yields for  $(\gamma, \pi^-)$  reactions ( $x = 0$ ) are almost the same for all of the studied medium to heavy targets at  $E_0 = 800, 400,$  and  $250$  MeV. It is now clearly shown that the reactions of high neutron multiplicities become progressively more possible as  $A_t$  increases, and the reaction probabilities for  $x = 2-7$  (and even more) at  $E_0 \geq 400$  MeV are nearly comparable for a heavy target such as  $^{175}\text{Lu}, ^{197}\text{Au},$  and  $^{209}\text{Bi}$ , though not at  $E_0 = 250$  MeV. On the other hand, the reactions with such high neutron multiplicities are not possible for lighter targets with  $A_t \leq 100$ . The neutron multiplicity reflects primarily the excitation energy left after pion emission, while the energy spectrum of neutrons is to be known.

In order to understand the yield variations quantitatively, the widths of the mass yield curves at  $E_0 = 400$  and  $250$  MeV were defined as the  $x$  values of the  $(\gamma, \pi^n xn)$  reaction, for which the yield is equal to that of the  $(\gamma, \pi^-)$  reaction,  $78 \mu\text{b}/\text{eq.q.}$  for  $E_0 =$

$400$  MeV and  $51 \mu\text{b}/\text{eq.q.}$  for  $E_0 = 250$  MeV by reading from the fit curves in Figure 6, and plotted as a function of the neutron-to-proton ratio of the target,  $(N/Z)_t$ , in Figure 7. The target-dependent variation of the yields from the  $(\gamma, \pi^n xn)$  reaction for  $x \geq 1$  could not be parameterized by target mass  $A_t$  nor by the number of target neutrons  $N_t$ , because the  $(\gamma, \pi^- 2n)$  and  $(\gamma, \pi^- 3n)$  yields from  $^{51}\text{V}$  were found to be higher by a factor of 3 than those from  $^{59}\text{Co}$ , as seen in the upper left corner of Figure 6. As noted above, the range of neutron multiplicity is larger for heavier targets. However, the degree of the increase of the width at  $E_0 = 400$  MeV is not monotonic, but changes largely at  $(N/Z)_t = 1.32-1.40$  ( $^{109}\text{Ag}-^{127}\text{I}$ ), and the rate of increase becomes smaller at  $(N/Z)_t = 1.32-1.35$  ( $^{109}\text{Ag}-^{115}\text{In}$ ) and  $1.49-1.52$  ( $^{197}\text{Au}-^{209}\text{Bi}$ ). The change of the width at  $E_0 = 250$  MeV is small, but the rate of increase changes also at  $(N/Z)_t \approx 1.35$ . The peak positions also increase with an increase of  $(N/Z)_t$  in a manner similar to the widths.

In order to reveal further the target-dependent change of the  $(\gamma, \pi^n xn)$  yields for each  $x$  of  $x \geq 0$ , the yield values at  $E_0 = 400$  MeV (closed squares) are plotted against  $(N/Z)_t$  in Figure 8(a) and 8(b). Solid lines representing  $x = 0-9$  are drawn through the observed points with the aid of the smoothed mass yield curves in Figure 6. Open circles in Figure 8(a) are the calculated values by the PICA code<sup>31</sup> based on particle histories of  $(1-4) \times 10^6$  and those in Figure 8(b) by the PICA 3/GEM code by Sato et al.<sup>34</sup> based on particle histories of  $7 \times 10^7$ .

The PICA 98/EVAP code by Sato et al.<sup>33</sup> was able to reproduce almost exactly our yield data on  $(\gamma, \pi^n xn)$  reactions except for  $x = 0$  (not shown in Figure 8(b)). The PICA 98 is a modification of PICA 95 by Fu<sup>32</sup> who extended the original PICA code by Gabriel et al.<sup>30, 31</sup> to be applicable to  $E_0 \leq 3.5$  GeV by including multiple-pion (up to five pions) production channels. In the PICA 98, the calculational method for cross sections of GDR and QDR was changed and the nuclear medium effect on the N-N scattering cross section was considered. Also the mass formula and the level density parameters used in the calculation of evaporation process were updated. The PICA 3/GEM code is a further improvement of PICA 95 by adopting the total photopion production cross section per nucleon calculated after the method by Bianchi et al.<sup>86</sup> In this improved code, PICA 3, the fitting parameters in the equations were determined by taking the nuclear medium effect by Bianchi et al.<sup>86</sup> and the nuclear shadowing effect by Piller et al.,<sup>87</sup> which is effective above the  $\Delta$ -resonance region, into consideration. Then the preequilibrium was taken into account and followed by a replace of the evaporation part with the generalized evaporation model and fission model GEM by Furihata.<sup>88</sup>

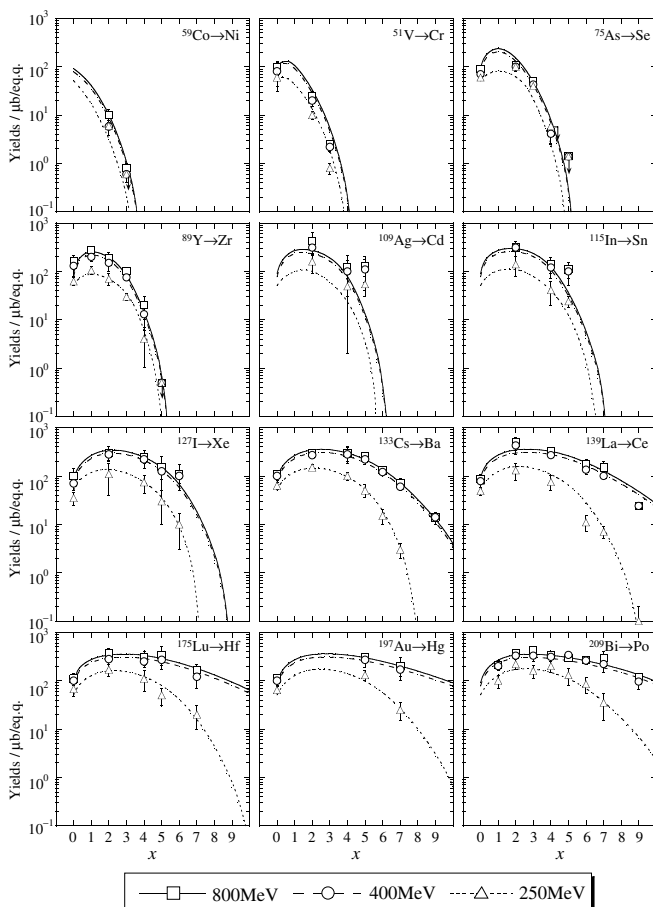


**Figure 6.** Variations for  $(\gamma, \pi^n xn)$  reaction yields in unit of  $\mu\text{b}/\text{eq.q.}$  as a function of number of emitted neutrons,  $x$ , at  $E_0 = 800$  MeV (squares connected by solid curves),  $400$  MeV (circles connected by broken curves), and  $250$  MeV (triangles connected by dotted curves). (Reprinted from Reference 13 with permission from the American Physical Society)

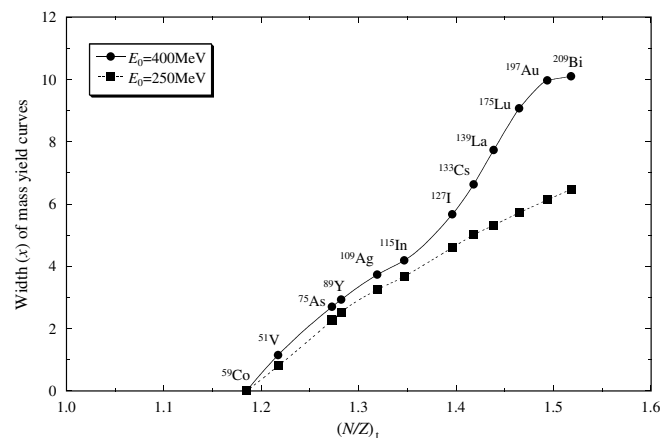


**Figure 7.** Widths of the isotopic mass yield curves as a function of the neutron-to-proton ratio of the target,  $(N/Z)_t$  at  $E_0 = 400$  and  $250$  MeV. The width is defined as the  $x$  value of the  $(\gamma, \pi^n xn)$  reaction for which the yield is equal to that of the  $(\gamma, \pi^-)$  reaction,  $78 \mu\text{b}/\text{eq.q.}$  for  $E_0 = 400$  MeV and  $51 \mu\text{b}/\text{eq.q.}$  for  $E_0 = 250$  MeV. (Reprinted from Reference 13 with permission from the American Physical Society)

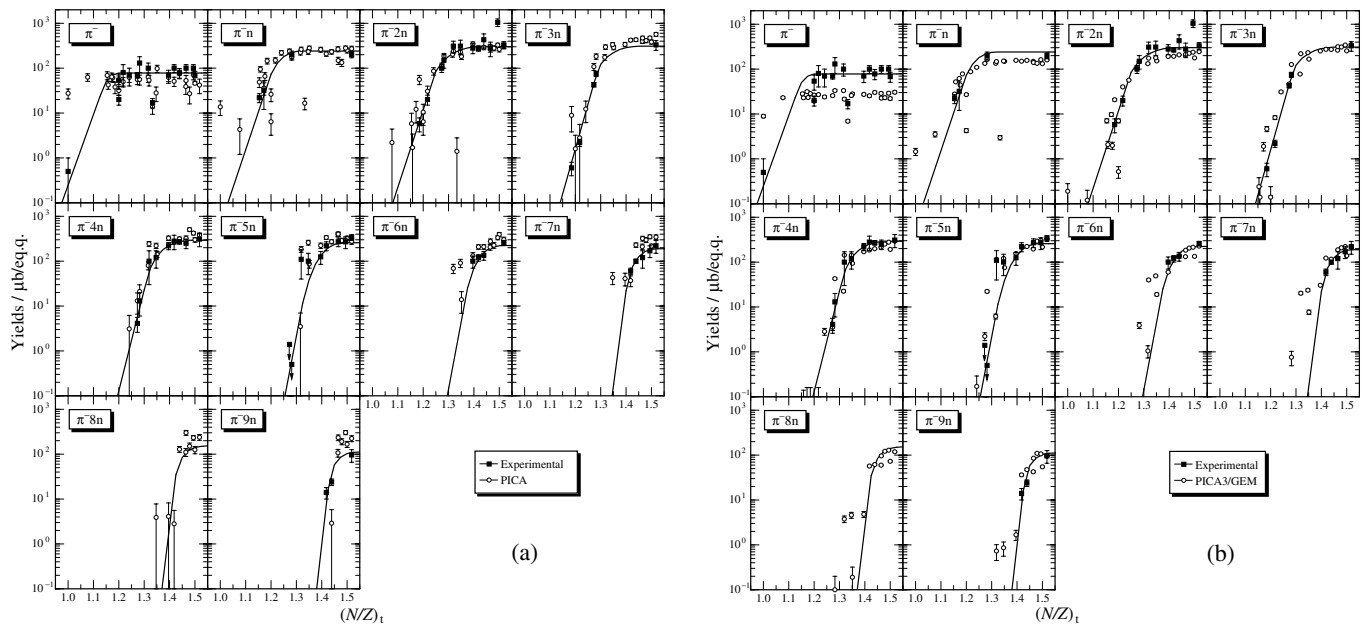


**Figure 8.** Variations in the  $(\gamma, \pi^-xn)$  reaction yields in unit of  $\mu\text{b}/\text{eq.q.}$  for  $x = 0-9$  as a function of the proton-to-neutron ratio of target,  $(N/Z)_t$ , at  $E_0 = 400$  MeV: (a) comparison of PICA calculation and (b) comparison of PICA 3/GEM calculation, both shown as open circles, with experimental values are shown as closed squares. ((a) Reprinted from Reference 13 with permission from the American Physical Society)

The yield values change systematically with respect to  $x$  and  $(N/Z)_t$ . Both the observed and the calculated values for the individual reactions begin at a certain  $(N/Z)_t$ , increase rapidly with increasing  $(N/Z)_t$ , and reach a plateau at  $E_0 = 400$  MeV. The PICA 3/GEM is the most updated modified PICA code. The PICA code reproduces well the experimental  $(\gamma, \pi^-xn)$  yields for  $x = 1$  and 2 on the whole, but discrepant for larger  $x$  and at  $(N/Z)_t = 1.18$  ( $^{59}\text{Co}$ ), 1.32 ( $^{109}\text{Ag}$ ), and 1.35 ( $^{115}\text{In}$ ). On the other hand, the PICA3/GEM code underestimates the  $(\gamma, \pi^-xn)$  yields for  $x = 0-2$ , though it gives a good agreement with the  $(\gamma, \pi^-xn)$  yields for  $x \geq 3$ . The PICA 98 calculations reproduce the observed profiles for the  $(\gamma, \pi^-xn)$  yields for  $x \geq 1$  much better than PICA-3/GEM. The calculated values for the  $(\gamma, \pi^\pm)$  yields by all the revised codes remain essentially the same as those by the PICA code, as stated above.

The sums of the  $(\gamma, \pi^-xn)$  yields at  $E_0 = 400$  and 250 MeV are shown in Figure 9(a) and 9(b), respectively. In the figures, the sums of the measured yields of the reactions of  $x = 0$  to 1, 2, ..., 9, and the maximum possible  $x(\text{max})$ ,  $\sum_{i=0}^{\text{max}} Y_i(N/Z)_t$ , are shown by solid lines, and to fall in the region between the two dotted curves from the PICA 3/GEM calculation. In the original paper,<sup>13</sup> the PICA results were also compared with the experiment, and exhibited a large deviation in the high  $(N/Z)_t$  region. The fact that the variations in the observed reaction yields are well parameterized with  $(N/Z)_t$ , but not with  $A_t$  nor  $N_t$ , suggests that photopion reactions are initiated by competitive photoabsorptions by neutrons and protons in the entire nucleus. Also, the rapid but sigmoidal increase of the total (final) yields with increasing  $(N/Z)_t$  does not conflict with the nuclear model of neutron-rich surface proposed above. The richer the concentration of neutron in the outer region of the nuclei, the smaller the amount of negative-pion reabsorption and also the more probable the occurrence of multiple-neutron emission. For  $(\gamma, \pi^-xn)$  reactions with  $x \geq 1$ , pions may carry small amounts of kinetic energy which allow emission of multiple neutrons during both the cascade process and the evaporation process from the excited cascade residue. The latter would be dominant in  $(\gamma, \pi^-xn)$  reactions of large  $x$  which is possible in target nuclei of larger  $(N/Z)_t$ . The energies of the emitted particles may be too low to be detected by current particle spectrometers, and this difference in the target dependence from particle measurements could be explained by the differences from the radiochemical observations as described in the Introduction.

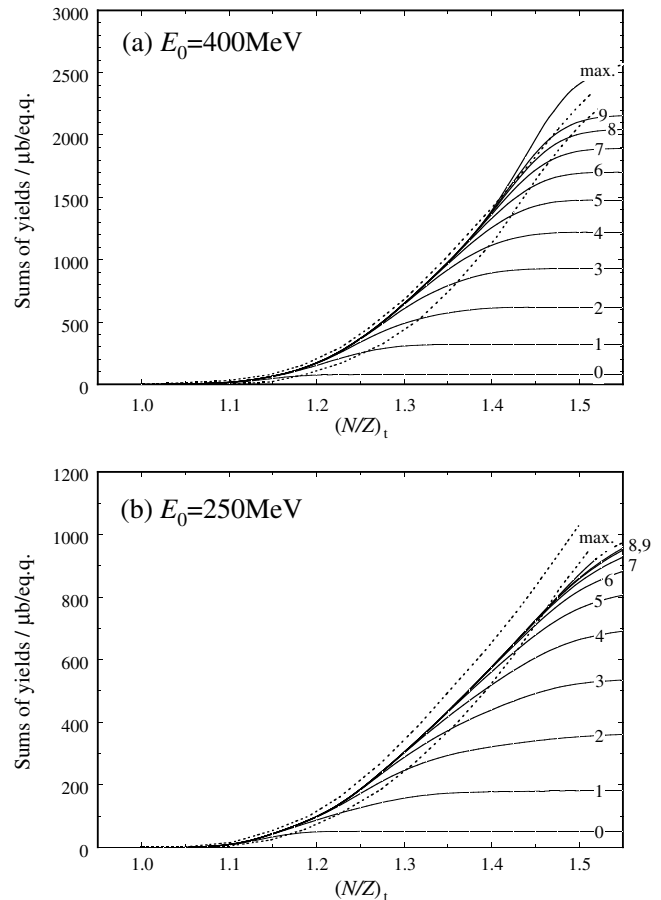


**Figure 9.** The sum of the  $(\gamma, \pi^-xn)$  yields,  $\sum_{i=0}^{\text{max}} Y_i(N/Z)_t$ , in unit of  $\mu\text{b}/\text{eq.q.}$  Solid lines are the sums of the measured yields,  $Y_i(N/Z)_t$  from Figure 7 for  $x = 0$  to  $x = 1, 2, \dots$ , maximum possible  $x(\text{max})$ . Dotted curves show the range of the total yields obtained from the PICA3/GEM calculations. (a) for  $E_0 = 400$  MeV and (b) for  $E_0 = 250$  MeV. (Reprinted from Reference 13 with permission from the American Physical Society, but the PICA results are replaced with those of the PICA3/GEM)

The features of  $Y(E_0)$  vs  $(N/Z)_t$  were characterized more quantitatively by evaluating the "target thresholds,  $(N/Z)_{\text{th}}$ ", the slopes of the rising portions of the curves and the values at the plateau as a function of  $x$  (Figure 6 of Reference 13). The

“target threshold” was defined as the  $(N/Z)_t$  for which each  $(\gamma, \pi^-xn)$  reaction starts to occur with a certain probability, say 1  $\mu\text{b}/\text{eq.q.}$  It was found that  $(N/Z)_{\text{th}}$  increases linearly with increasing  $x$  from 0 to 5, which can be expressed as

$$(N/Z)_{\text{th}} = 1.040 + 0.050x \quad \text{for } E_0 = 400\text{--}800 \text{ MeV} \quad (2)$$

and as

$$(N/Z)_{\text{th}} = 1.100 + 0.046x \quad \text{for } E_0 = 250 \text{ MeV}. \quad (3)$$

Some deviations from the linear relationship occur at  $x > 5$  for the 1  $\mu\text{b}/\text{eq.q.}$  threshold, suggesting that there may be some change in the reaction process in the heavy target region of  $(N/Z)_t$  corresponding to  $(N/Z)_{\text{th}} \geq 1.3\text{--}1.4$ , where reactions involving high neutron multiplicities can occur. The slopes for the rapidly rising yield section for individual reactions with respect to  $(N/Z)_t$  are almost the same for  $x = 0\text{--}2$ , but then increase especially for  $x > 5$ . The maximum yields decrease very slowly with increasing  $x$  from 300  $\mu\text{b}/\text{eq.q.}$  at  $x = 3$  to 100  $\mu\text{b}/\text{eq.q.}$  at  $x = 9$ . The existence of plateaus in the yields for  $(\gamma, \pi^-xn)$  reactions of individual  $x$  might be due to the increase of multineutron emission of larger  $x$  being compensated by an increase in nuclear size.

All of the evidences point to changes in the widths of the isotopic mass yield curves, the “target thresholds,  $(N/Z)_{\text{th}}$ ”, the slopes in the sections of increasing yields with respect to  $(N/Z)_t$ , and the maximum yields at  $(N/Z)_t = 1.3\text{--}1.4$ , above which the occurrence for  $(\gamma, \pi^-xn)$  reactions of  $x \geq 5$  becomes pronounced. It is now clear that the changes in the yield profiles for the targets heavier than  $A_t = 100$  are associated with pronounced nuclear medium effects giving rise to more excessive excitation as compared with medium-heavy targets of  $A_t \leq 100$ . It is noted that the original PICA code overestimates the plateau values of the  $(\gamma, \pi^-xn)$  reactions for  $x \geq 3$  by a factor of about 2, but the PICA-98 and PICA-3/GEM reproduces them very well. The latter codes consider the medium effect on the N-N scattering cross section as noted above.

## 4. Photospallation

**4.1. Background.** Multiple nucleon emissions expressed as  $(\gamma, xny_p)$ ,  $x$  and  $y$  being the numbers of neutrons and protons emitted, i.e. spallation, in high energy nuclear reactions on medium to heavy nuclei are the most dominant competitive channel among others, and a broad spectrum of spallation residues is produced.

In general, the mechanism of spallation reactions has been explained by the cascade-evaporation model by Serber.<sup>89</sup> The incident projectile initiates a knock-on cascade by the interaction with a nucleon inside the target nucleus, and a number of particles are ejected from the nucleus during the cascade. The residual nucleus is deexcited by the evaporation of nucleons or nuclear clusters, and then the final product is formed. Systematic studies of spallation of complex nuclei by high energy photons seemed to be rather scanty in comparison with those by protons in the mid-1980s. The observed mass yield distribution of photospallation products appears very similar, in some of the chief features, to the yield pattern in the bombardment of high energy hadrons, in spite of the difference in their initial interactions; photospallation is initiated by purely electromagnetic interaction occurring deep inside the nucleus, while the hadron reaction is strong interaction induced by hadron incidence from the outside of the nucleus. The similarity between the yield patterns was first observed by the group of MIT<sup>90–92</sup> in the photoreactions on medium-weight targets by use of 320 MeV bremsstrahlung from the MIT synchrotron in 1954. The authors paid their attention to the yields of nuclides which are more than a few mass unit lighter than the targets, and examined the effect of evaporation of the

last few particles on the regularly changing form of the observed patterns with increasing distances from the targets and from the center of the stability valley. Simple reactions, in which only a few nucleons are ejected, such as  $(\gamma, n)$ ,  $(\gamma, 2n)$ , and  $(\gamma, pn)$  reactions, were attributed to the low energy part of bremsstrahlung, i.e. GDR. It was of interest for us to confirm why the yield distributions are not affected by the difference of the initial interactions between photons and hadrons incident on the same target nucleus, though some of the earlier authors stated that the highly excited nucleus has lost its memory of formation.<sup>93</sup>

A number of the previously reported results have been analysed with a five-parameter formula by Rudstam<sup>94</sup> who empirically derived it on the basis of the proton- and heavy ion-induced spallation data in a wide range of energy and mass. The proposed formula for charge distribution (CD) and mass yield distribution (MD) is

$$\sigma(Z, A) = \frac{\hat{\sigma}PR^{2/3}\exp[PA-R|Z-SA+TA^2|^{3/2}]}{1.79\{\exp(PA_t) - 1\}}, \quad (4)$$

where  $\sigma(Z, A)$  is a formation cross section of a nuclide  $(Z, A)$  produced from a target  $(Z, A_t)$ , and  $P, \hat{\sigma}, R, S,$  and  $T$  are free parameters. The parameter  $P$  defines the slope of the mass yield curve,  $\hat{\sigma}$  the total inelastic cross section,  $R$  the width, and  $S$  and  $T$  the location of CD through the most probable charge  $Z_p = SA - TA^2$ . Therefore, the parameters  $P$  and  $\hat{\sigma}$  define the shape of MD, the former the slope and the latter the magnitude, and depend on both  $E_0$  and  $A_t$ . The parameter  $R$  is independent of the kind and energy of the projectiles and depends on the product mass  $A$  and charge  $Z$ ;  $R = d'A^{-e'}$ ,  $d'$  and  $e'$  being constant. For the same reason as in the case of  $R$ , the peak position  $Z_p$  of CD depends on the proton and neutron separation energies and on the Coulomb barrier and  $S$  and  $T$  can then be constant.

Sato<sup>95</sup> tried to find the physical implications of the parameters in the formula by unifying them with the  $Q_{\text{gg}}$  rule<sup>96</sup> and the Serber model.<sup>89</sup> A three-parameter formula was derived from the statistical consideration of the spallation process by Gupta et al.<sup>97</sup> A slight modification of this formula was proposed and the degree of performance of these formulae was examined for hadron spallation by Foschina et al.<sup>98</sup> More recently Foschina et al.<sup>99</sup> extended their four-parameter formula to electron- and photon-induced spallation, and shown that the formula can be used to estimate the unknown cross sections of the spallation process more accurately (within a factor of 2) and easily than theoretical calculations such as cascade-evaporation calculation. However, these formulae were limited to the products not close to the targets of medium-weights.

Owing to its success in the approximation of hadron-induced spallation with fairly good accuracy, Jonsson and Persson<sup>9</sup> measured the yields of photospallation of  $^{127}\text{I}$  at  $E_0 = 250\text{--}900$  MeV at steps of 100–200 MeV with use of chemical separations of Te, (Ag), Sb, Sn, and In from the irradiated iodine and tried to fit their data to the Rudstam formula in terms of the mean cross sections, i.e. the slope of linear array in  $Y(E_0)$  vs  $\ln E_0$  plots under the assumption of  $1/E_0$  variation for bremsstrahlung spectra. The significance of the different parameters were discussed by referring to those by the Rudstam's for particle-induced spallation. Kumbartzki et al.<sup>51,93</sup> extended the nondestructive yield measurements to the targets of  $^{27}\text{Al}$ ,  $^{51}\text{V}$ ,  $^{55}\text{Mn}$ ,  $^{56}\text{Fe}$ ,  $^{59}\text{Co}$ , and  $^{75}\text{As}$  with bremsstrahlung of  $E_0 = 0.8\text{--}2.1$  GeV from the 2.5 GeV ES at University of Bonn and also found that the photospallation yields can be represented by the Rudstam formula. About the same time, the groups who used the 5 GeV Cambridge Electron Accelerator in Massachusetts and the Linear Accelerator (16 GeV) Center at Stanford, USA,<sup>100,101</sup> the 7.4 GeV ES and 0.6 GeV Linac at DESY, Germany,<sup>53,55</sup> the 4 GeV ES at the Daresbury Nuclear Physics Laboratory, England,<sup>102</sup>

the 1.2 GeV ES at the University of Lund, Sweden,<sup>9, 50</sup> the 2.5 GeV ES at University of Bonn, Germany,<sup>51, 93, 103</sup> the 5 GeV ES at the Yerevan Physics Institute,<sup>104, 105</sup> and the Frascati 1.0 GeV ES, Italy<sup>57, 106</sup> started series of photospallation studies on <sup>nat</sup>Fe at  $E_0 = 1.5, 3, 5,$  and  $16$  GeV-electrons,<sup>101</sup> on <sup>127</sup>I and <sup>197</sup>Au at  $E_0 = 1-7.4$  GeV,<sup>53</sup> on <sup>59</sup>Co, <sup>127</sup>I, and <sup>181</sup>Ta by 4 GeV-electron,<sup>102</sup> on <sup>45</sup>Sc and <sup>nat</sup>Cu at  $E_0 = 2$  GeV,<sup>103</sup> on <sup>51</sup>V by both electrons and photons at  $E_0 = 130-580$  MeV,<sup>55</sup> on <sup>51</sup>V, <sup>55</sup>Mn, and <sup>nat</sup>Cu at  $E_0 = 2, 3, 4,$  and  $5$  GeV,<sup>104, 105</sup> on <sup>51</sup>V, <sup>55</sup>Mn, <sup>nat</sup>Fe, and <sup>59</sup>Co at  $E_0 = 300-1000$  MeV<sup>57</sup> and analyzed the yield data with the Rudstam formula<sup>50, 51, 57, 93, 103, 105, 107</sup> and/or the Monte Carlo calculation (PICA).<sup>50, 55, 107</sup> It may be noteworthy here that both bremsstrahlung- and electron-induced nuclear reactions are regarded as photonuclear reactions: use of virtual photon concept has been made for the latter. The reaction yield ratios of bremsstrahlung- to electron-reaction,  $Y_Q/Y_{e^-}$ , are as high as several tens to 100 times and vary with target  $Z$  and  $E_0$  (see References 55 and 102 and references therein).

In the meantime, Jonsson and Lindgren<sup>108</sup> compiled and analysed the then available photo- and electro-spallation data with the five-parameter formula in terms of charge and mass distributions (CDMD-formula) in 1973, and updated the systematics in 1977.<sup>109</sup> They showed the capability of the CDMD-formula in predicting the yields and cross sections within a factor of about 2 with some exceptions of factors of up to 5, in a broad energy and target mass region with a set of the new parameter values. However, it was obvious that more precise parameters could not be obtained without more systematic measurements with respect to  $A, E_0,$  and  $A$ .

Monte Carlo calculations on intranuclear cascades made by Metropolis et al.<sup>110</sup> in 1958 combined with the analytical treatment of the evaporation step given by Rudstam for high-energy protons<sup>111</sup> were utilized for calculations for photoreactions in the early days.<sup>9</sup> After 1970, the PICA code was occasionally tested also in terms of photospallation,<sup>50, 55, 107</sup> too. A similar treatment was also proposed by Barashenkov et al.<sup>112</sup> in 1974 for  $A \geq 27$  in photon energies of 50 MeV–1.3 GeV, which gives higher mean excitation energy above  $k = 200$  MeV (see Reference 107 and References therein).

**4.2. Similarity and Dissimilarity between Photospallation and Hadron Spallation.** Paying our attentions to these historical developments in photospallation study, we first tried to observe the isotopic, isobaric and charge distributions by ourselves with an extensive measurement of spallation from two mass regions: one of <sup>133</sup>Cs and <sup>139</sup>La (Ref. 14), the other of

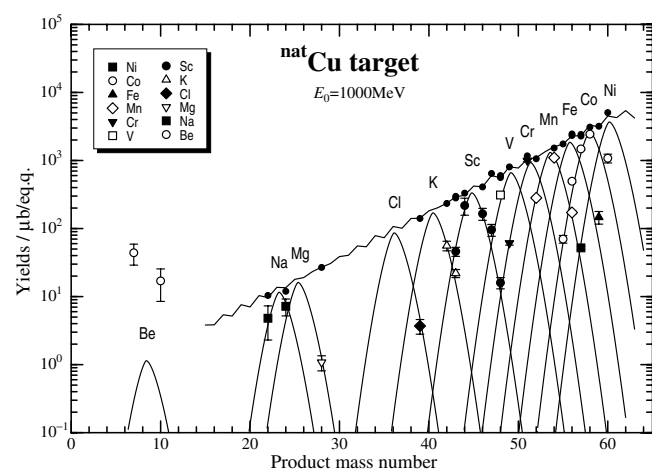


**Figure 10.** Yield distributions for products from <sup>nat</sup>Cu( $\gamma$ , spallation) reactions at  $E_0 = 1000$  MeV. Large symbols denote the measured yields obtained in our works.<sup>16</sup> Solid curves were obtained by the parameters estimated by a nonlinear least-squares fit to the yield data. Small closed circles indicate the mass yields estimated by the Rudstam's formula (eq 5 in 4.3.). (Reprinted from Reference 16 with permission from the American Physical Society, but revised to include the latest data.<sup>123-125</sup>)

<sup>nat</sup>Rb, <sup>nat</sup>Sr, and <sup>89</sup>Y (Ref. 15) at  $E_0 = 100$  and  $200$  MeV at LNS. Chemical separations of Cs, Xe, I, Te, and Sb from irradiated CsCl and of La, Ba, Cs, Xe, I, Te, and Sb from irradiated La<sub>2</sub>O<sub>3</sub> were performed together with iterative separations of <sup>120g</sup>I, <sup>121</sup>I, <sup>123</sup>I, and <sup>121g</sup>Te for the former and <sup>129</sup>Cs and <sup>121g</sup>Te for the latter to increase the numbers of the independent yields. Chemical separations of Sr, Rb, Kr, Br, Se, and As from the irradiated Y<sub>2</sub>O<sub>3</sub>, SrCl<sub>2</sub>, and RbCl were also performed. Comparison was made of the yields from different durations of irradiation. The mass and charge distributions of the yields at  $E_0 = 100$  and  $200$  MeV and also the differences of the yields at  $E_0 = 200$  and  $100$  MeV were then examined with use of the Rudstam CDMD formula, and it was found that the spallation yields are governed by nuclear stability and the characteristics of the yield features previously reported are essentially correct. It is noted that the contributions of secondary reactions are not important in photospallation yields discussed here.

The logarithmic slope of the mass yield curve,  $P$ , decreases linearly with an increase of the kinetic energy of proton and heavy ions (<sup>14</sup>N, <sup>12</sup>C, and <sup>40</sup>Ar) up to  $\sim 2$  GeV and approaches a constant value in the higher energy region, the limiting regime, irrespective of particles,<sup>113-115</sup> and the smaller slope has been suggested to be an indirect measure for higher average deposition energy. On the other hand, the results of photospallations of <sup>51</sup>V (Ref. 50) and <sup>127</sup>I (Ref. 9) showed that the  $P$  values decrease with the increase of  $E_0$  up to  $600$  MeV and show a limiting above  $E_0 \geq 600$  MeV.<sup>109</sup> This trend was confirmed also by us,<sup>15</sup> and was considered to be apparently different from those observed in the hadron spallation. From this point of view, the yields of 24 nuclides from photospallation of Cu were studied by nondestructive measurements with bremsstrahlung beams of  $E_0 = 100-1000$  MeV in steps of 5 to 100 MeV in order to compare directly with the results of proton and heavy-ion spallation of Cu by Cumming et al.<sup>113-115</sup> and also to confirm the above-mentioned trend further.<sup>16</sup> Figure 10 is the yield distributions for products from Cu ( $\gamma$ , spallation) reactions at  $E_0 = 1000$  MeV. The data points obtained in later years are included in this Figure, which is described in 4.5. The comparison of the  $P$  values for Cu is reproduced in Figure 11, indicating that the  $P$  values of photospallation approach a constant value above  $600$  MeV, while those of hadron spallation attain the limiting regime at about  $2$  GeV as stated above,

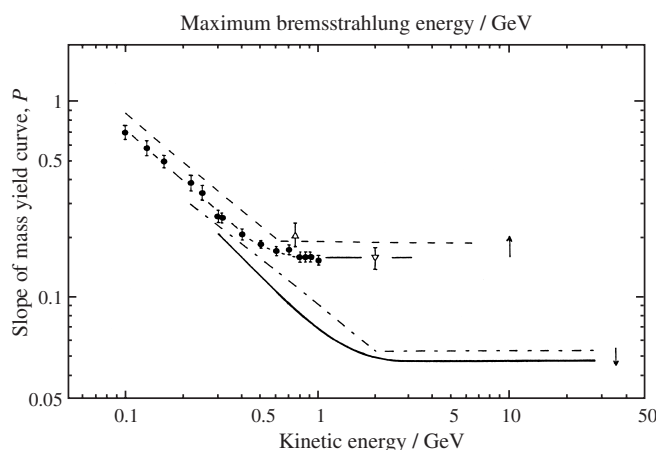


**Figure 11.** Logarithmic slope of the mass yield curve ( $P$ ) as a function maximum bremsstrahlung energy or kinetic energy of nuclear projectiles. Solid circle denotes our work,<sup>16</sup> open triangle denotes the value from Reference 9, open inverted triangle denotes the value from Reference 103. The thin solid curve is to guide the eye for the solid circles. The dashed line was estimated for Cu target from the relations (3) in Reference 109. The thick solid curve is for the slopes obtained by Cumming et al.<sup>113-115</sup> for Cu spallation induced by protons and heavy ions (<sup>14</sup>N, <sup>12</sup>C, and <sup>40</sup>Ar). Results for  $\alpha$ -induced spallation of Cu by Karol<sup>121</sup> are also included in this curve. The dash-dotted line is for  $P$  values obtained by Rudstam.<sup>94</sup> (Reprinted from Reference 16 with permission from the American Physical Society)

and that the slope values of photospallation are larger than those of hadron spallation. The yield values were converted to the mean cross sections,  $\bar{\sigma}(E) = dY(E_0)/d(\ln E_0)$ , in the energy region of 300–1000 MeV according to Jonsson and Persson,<sup>9</sup> and the parameter values obtained for these mean cross sections were found to be almost identical with those of  $Y(E_0)$  at  $E_0 = 600$  and 700 MeV. The limiting of the  $P$  values for Cu reached around 600 MeV or less, because the mean energy of the interacting photons is less than  $E_0$ . The comparison with the  $P$  values from hadron spallation showed that the limiting excitation energy is higher in hadron spallation than in photon spallation in this incident energy region. It seemed plausible that these differences would partly be caused by the difference of the initial interaction between photon and hadron spallation because the threshold energy of pion production in photon-nucleon interaction is lower than that in nucleon-nucleon interaction.

Another support for this discussion was obtained by taking the ratios of production yields (mb/eq.q.) for photospallation at  $E_0 = 850$  MeV to cross sections (mb) for proton spallation at  $E_p = 3.9$  GeV<sup>113</sup> as a function of product mass number  $A$ , which showed a linear relationship decreasing from 0.1 at  $A \geq 60$  with increase of  $\Delta A (= A_t - A)$  (Figure 5 of Reference 16). The average excitation energy of cascade residues estimated from the  $P$  values was found to be in the order  $\gamma < p = \alpha = \text{heavy ion} \approx \pi^-$  for the several hundred MeV to several GeV energy region.

The width of the charge dispersion of the Cu photospallation was also found to be slightly narrower than that of proton spallation. Furthermore, the neutron-to-proton ratio of the most probable products,  $(N/Z)_p$ , in photospallations of Cu was estimated by  $Z_p = SA_m - TA_m^2$ , where the medium mass  $A_m = A_t - 1/P$  and  $1/P$  gives the average number of nucleons emitted,<sup>94</sup> and was found to be constant ( $1.148 \pm 0.003$  on average) in the  $E_0$  region of 100 MeV–1 GeV. The  $(N/Z)_p$  values of then unpublished Y, I, Cs, and Au (Ref. 116) were also obtained. The results of  $(N/Z)_p$  showed a linear relation-

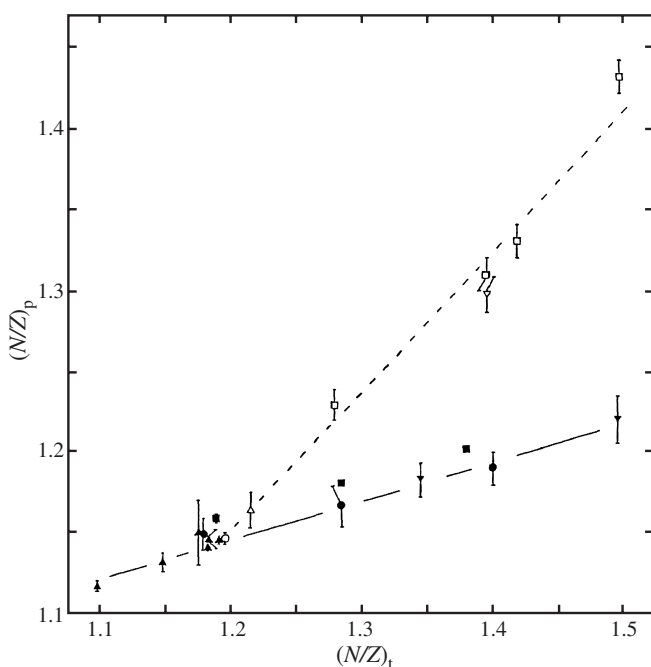


**Figure 12.** Most probable product  $(N/Z)_p$  as a function of target  $(N/Z)_t$ . Open symbols represent photon results and solid symbols proton and  $\alpha$  results. Open circle denotes our work,<sup>16</sup> open triangle<sup>109</sup> (V target), open inverted triangle (I),<sup>9</sup> open square (Y, I, Cs, and Au),<sup>116</sup> solid circle (<sup>96</sup>Zr, <sup>96</sup>Mo, and <sup>96</sup>Ru),<sup>118</sup> solid triangle (Ti, Fe, Co, Ni, Cu, and Zn),<sup>119</sup> solid inverted triangle (In and Au),<sup>117</sup> solid square (<sup>92</sup>Mo, <sup>96</sup>Mo, and <sup>100</sup>Mo).<sup>120</sup> The solid and dashed lines are to guide the eye. A portion of the results for proton and  $\alpha$  spallation was reproduced from Reference 120. (Reprinted from Reference 16 with permission from the American Physical Society)

ship with target  $(N/Z)_t$  as shown in Figure 12, but the slope of which was quite larger than that from  $E_p = 1.8$ ,<sup>117</sup> 2.9,<sup>118</sup> and 12 GeV<sup>119</sup> proton and 720 MeV  $\alpha$  spallation<sup>121</sup> of targets with various values of  $(N/Z)_t$ . For the larger  $(N/Z)_t$ , the most probable product  $(N/Z)_p$  is shifted to the more neutron rich side in photospallation than in proton- and  $\alpha$ -spallation. Solid and dashed lines in the figure, which are to guide the eye, cross around  $(N/Z)_t = 1.2$ , i.e. the value of Cu. This phenomenon is related to the average excitation energy of cascade residues produced by spallation. At the end of the cascade process, the  $(N/Z)$  ratio of the cascade residues is approximately equal to  $(N/Z)_t$ . As the cascade residues are deexcited by evaporation, the Coulomb barrier tends to suppress the emission of charged particles. The average excitation energy of the cascade residues in photospallation is lower than that in hadron spallation, as evidenced by the difference of the parameter  $P$ , and the emission of nucleon is relatively limited. Therefore, the most probable  $(N/Z)_p$  is higher in photospallation compared with hadron spallation. This phenomenon would be observed easily in neutron-rich target nuclei, though difficult to observe in medium-weight nuclei such as Cu,  $(N/Z)_t$  of which is close to unity.

**4.3. Systematics in Photospallation.** A further extensive accumulation of the yield data of photospallation of a wide range of targets, including some reinvestigations of the reported ones, was performed at  $E_0 = 30$ –1000 MeV in steps of 100 MeV or less with the aid of suitable radiochemical separation to derive more accurate systematics and to deepen our understanding of the reaction mechanism.<sup>17</sup> The chosen targets were <sup>51</sup>V<sub>28</sub>, <sup>59</sup>Co<sub>32</sub>, <sup>89</sup>Y<sub>50</sub>, <sup>127</sup>I<sub>74</sub>, <sup>133</sup>Cs<sub>78</sub>, <sup>139</sup>La<sub>82</sub>, and <sup>197</sup>Au<sub>118</sub>, as these are naturally monoisotopic or essentially monoisotopic. Among these targets the near-by three targets, <sup>127</sup>I, <sup>133</sup>Cs, and <sup>139</sup>La, were received special attention, since <sup>139</sup>La is  $N = 82$  magic and <sup>133</sup>Cs and <sup>127</sup>I are  $4n$  and  $8n$ , respectively, off from  $N = 82$  magic. These targets are separated by two units of atomic number and produce many common radionuclides by spallation. This provides us some advantages in the yield measurements; employed chemistry specific to the products, especially in chemical purifications, and radioactivity assays are common in many of radionuclides, and possible problems such as gamma-ray data would confidently be clarified, as intended before.<sup>14, 15</sup> The chemical procedures for La, Ba, Cs, Xe, I, Te, Sb, Sn, In, Cd, and Ag were essentially the same as in References 14 and 15. Chemical separations of Pt, Ir, Os, Re, and W from Au were also performed. There exist the same advantages of radioassay in the choice of lighter targets (<sup>51</sup>V and <sup>59</sup>Co), in addition to <sup>nat</sup>Cu described above, though the yield measurements for these targets were performed non-destructively. The <sup>59</sup>Co and <sup>nat</sup>Cu targets are one unit of atomic number off from the proton magic  $Z = 28$ . Another neutron-magic target, <sup>89</sup>Y<sub>50</sub>, was added to fill the gap between the  $A_t$  ranges of 51–63 and 127–139. The <sup>197</sup>Au target was chosen as a representative of the heavy one in the periodic table. The yield values, totaling 22 nuclides from <sup>51</sup>V, 29 from <sup>59</sup>Co, 31 from <sup>89</sup>Y, 28 from <sup>127</sup>I, 44 from <sup>133</sup>Cs, 52 from <sup>139</sup>La, and 40 from <sup>197</sup>Au were identified as either independent or cumulative. For most of the cumulative yields, corrections for the precursor-decays were performed by using the precursor yields obtained from the iterative least-squares fit of the Rudstam CDMD formula, the method of which was devised and reported in the part II of this series of works.<sup>18</sup>

The individual yield data obtained were carefully examined from the view points of self-consistency in the yield curves as a function of  $E_0$  and in the isotopic MD and CD with the aid of the Rudstam CDMD formula. A detailed comparison with the previously reported results were made in the form of the yield curves. Then the expressions for the parameters reported by Jonsson and Lindgren<sup>108, 109</sup> were revised;

$$\begin{aligned}
 P &= (134.8 \pm 27.1) A_t^{(-0.229 \pm 0.024)} E_0^{(-0.916 \pm 0.031)} \\
 &\quad \text{at } 100 \leq E_0 \leq 600 \text{ MeV,} \\
 P &= (0.419 \pm 0.045) A_t^{(-0.229 \pm 0.024)} \quad \text{at } E_0 \geq 600 \text{ MeV,} \\
 \hat{\sigma} &= [(-0.87 \pm 0.11) + (0.23 \pm 0.02) \ln E_0] A_t^{(1.03 \pm 0.03)} \\
 &\quad \text{mb/eq.q.,} \quad (5) \\
 R &= (96.5 \pm 9.5) A^{- (0.95 \pm 0.05)}, \\
 S &= 0.53 \pm 0.02, \text{ and } T = (6.5 \pm 3.5) \times 10^{-4} \text{ to give } Z_p = SA - TA^2.
 \end{aligned}$$

It should be noted that these parameter values were derived from the data on  $51 \leq A_t \leq 133$  and the products of  $(\gamma, xn)$  and  $(\gamma, pxn)$  reactions of  $x \geq 3-7$ . The derived  $P$  and  $\hat{\sigma}$  values for  $A_t \geq 139$  ( $^{139}\text{La}$ ,  $^{175}\text{Lu}$ , and  $^{197}\text{Au}$ ) appeared somewhat anomalous compared to the characteristics for the lighter  $A_t$ . In the derivations of the expression (5), the data on  $A_t \geq 139$  were excluded, and the possible magic effects were not obvious beyond the experimental uncertainties.

Although the parameter values obtained were improved compared with those by Jonsson and Lindgren,<sup>108,109</sup> the degree of the fits were not yet satisfactory: 70–85% of the data were within the quoted uncertainty and the remainings were within  $3\sigma$  at  $E_0 = 1000$  MeV. Measurements of the yields of more wide range of the products, especially from heavier targets of  $A_t \geq 150$  at the whole range of  $E_0$  and the lighter ones of  $A_t \leq 50$  at  $E_0 \leq 300$  MeV seemed to be required for further refinements. (Note: our later measurements of the products with larger  $\Delta A$  from these heavies targets have revealed that the values in the expression (5) are valid. See 4.5.)

An empirical formula for the  $(\gamma, xn)$  yields of near-by products to targets were derived by analyzing isotopic distributions from  $^{51}\text{V}$ ,  $^{59}\text{Co}$ ,  $^{89}\text{Y}$ ,  $^{127}\text{I}$ ,  $^{133}\text{Cs}$ , and  $^{197}\text{Au}$  for  $E_0 = 300-1000$  MeV:

$$\ln \sigma(Z_t, A) = ax + b \quad (6)$$

with  $a = (1.01 \pm 0.13) A_t^{-(6.61 \pm 0.64)}$  and  $b = 6.78 \pm 0.21$ .

The slope  $a$  is independent of  $E_0$  of 300–1000 MeV, suggesting the contribution from low-energy photons responsible for GDR and QDR.<sup>18</sup>

In the part 1 of this work,<sup>17</sup> isomeric yield ratios for 38 pairs were also studied in some details in terms of  $E_0$ ,  $A_t$ , and spin-dependence. It was found that the ratios are almost independent of  $E_0$ . The  $A_t$ -dependence was not clear but the sensitivity of the isomer ratios on reaction complexity (large  $\Delta A$ ) looked weak in contrast to the conclusion by Eriksson and Jonsson<sup>122</sup> and Bachschi et al.<sup>103</sup> that the isomer ratios of  $^{44}\text{Sc}$  increase with increase of  $\Delta A$  due to build-up of angular momenta during the cascade and evaporation. The products having spin closer to the target spin were found to be favored in our work.

**4.4. Cascade-Evaporation Calculation (PICA) for Photospallation.** In section 3, the Monte Carlo intranuclear cascade-evaporation calculation code (PICA) by Gabriel and Alsmiller was described to be able to reproduce the gross feature of the photopion reaction yields, though some problems remained for further modifications. The reproducibility of the code for photospallation was then examined by referring to our experimental data quoted in 4.3. above.<sup>17</sup> The calculation was performed with the same parameter values as for photopion reactions, except for some alternative sets of cutoff energies for emitted particles which did not exhibit any notable difference in the results.<sup>19</sup> The incident particle histories of  $(0.4-1.0) \times 10^6$  were traced in each of 2–4  $E_0$ 's from 200 to 400 MeV for each target. The calculated yield values showed a zig-zag pattern in the isotope distribution; the yield values were high for even- $N$  products and low for odd- $N$  products in both the even- $Z$  and odd- $Z$  elements. In the case of  $^{133}\text{Cs}(\gamma, \pi^- xn)^{133-x}\text{Ba}$  reactions

described in 3.3., the calculated peak values for even- $N$  products were in good agreement with the experiment in contrast to those for odd- $N$  products.

The comparison of the PICA results with the experiment was made by regarding the zig-zag change, in addition to statistical errors, as the range of uncertainty in the PICA. It was stated that the PICA code reproduces almost all the observed values for  $^{51}\text{V}$ ,  $^{59}\text{Co}$ , and  $^{89}\text{Y}$  within their error bands, as far as the comparison was concerned with the results at  $E_0 = 200-400$  MeV, though the PICA on  $^{51}\text{V}$  and  $^{89}\text{Y}$  overestimates the corresponding yields of the products very close to and far from the targets, i.e.  $(\gamma, 0-1pxn)$  and  $(\gamma, 5-8 \text{ or } 9pxn)$  reaction products, respectively. The discrepancy becomes more apparent for heavier targets of  $^{127}\text{I}$ ,  $^{133}\text{Cs}$ , and  $^{139}\text{La}$  (Figure 2 of Reference 19). For these heavier targets, the PICA results show the broader and more asymmetric distributions at  $(\gamma, 0-4 \text{ or } 5pxn)$  reactions with high values at the products closer to the targets and are also larger than the measured values. It was interesting that the PICA results for  $^{127}\text{I}-^{139}\text{La}$  at  $E_0 = 400$  MeV were comparable in magnitude to the ones obtained at  $E_0 = 700-1000$  MeV. The reproducibility of the PICA code for photospallation were the same as that for photopion reaction: the most important conclusion was the need of inclusion of the nuclear medium effect in PICA.

The problem in the heavier targets encountered also in the systematic analysis with use of the Rudstam formula as described in 4.3. remained open at this stage. It was then concluded that the PICA code can be used for an approximate estimation of the photospallation yields even at  $E_0 = 400-1000$  MeV, but a better prediction was available from the empirical findings (see 4.5.).

**4.5. Further Developments in Photospallation Study.** We have further extended our measurements of photospallation yields of the products with larger  $\Delta A$  for the previously studied targets, in addition to new ones from  $^{27}\text{Al}$  to  $^{197}\text{Au}$  at  $E_0 = 60-1200$  MeV.<sup>23,123-125</sup> A list of the targets are included in Figure 4 for our photopion study. The studied ranges of  $\Delta A$  were, for examples, 190 (61) for  $^{197}\text{Au}$ , (62) for  $^{\text{nat}}\text{Ag}$ , and 82 (50) for  $^{89}\text{Y}$ . The numbers in brackets are for spallation origin. The empirical expressions (5) and (6) for the yields of both  $(\gamma, xnyp)$  reactions and  $(\gamma, xn)$  reactions, respectively, described in 4.3. were proved to reproduce the observed values within 20%.

The reproducibility of the PICA 3/GEM code, obtained from calculations of particle histories of  $7 \times 10^7$ , was found to have been improved greatly for photospallation, though not completely satisfied. Figure 13 shows typical examples of MD (see also Figures 10 and 18). The PICA 3/GEM code for photospallation of both  $(\gamma, xn)$  and  $(\gamma, xnyp)$  types and also the yields of the light nuclei (section 5), gives a good agreement with the experiment, though the smaller values for the  $(\gamma, xnyp)$  yields for  $\Delta A \geq 40$  for  $^{59}\text{Co}$ ,  $\Delta A \geq 50$  for  $^{89}\text{Y}$ , and  $\Delta A \geq 55$  for  $^{197}\text{Au}$  at  $E_0 = 400$  MeV appear, for examples. The latter discrepancies become smaller for heavier targets at higher  $E_0$ . These results suggest that the code requires to be improved for the contribution more from deep spallation. Our systematic recoil experiments<sup>23</sup> have also indicated that the code reproduces well the kinematic properties for  $^{51}\text{V}$ ,  $^{\text{nat}}\text{Cu}$ ,  $^{93}\text{Nb}$ , and  $^{\text{nat}}\text{Ag}$ , but underestimates the kinetic energies  $T$  of the residual nucleus in the heavy target region of  $^{181}\text{Ta}$  and  $^{197}\text{Au}$ . It is now possible to trace how the particle emissions occur and which stages in the cascade-evaporation are responsible for productions of the final products, by analyzing the calculational steps in the improved PICA 3/GEM, and some efforts are under way in our group.

## 5. Photofragmentation

**5.1. Background.** Formation of light nuclei such as  $^{7,10}\text{Be}$  and  $^{22,24}\text{Na}$  in high energy nuclear reactions on medium- to heavy-weight targets has been an old but still new open prob-

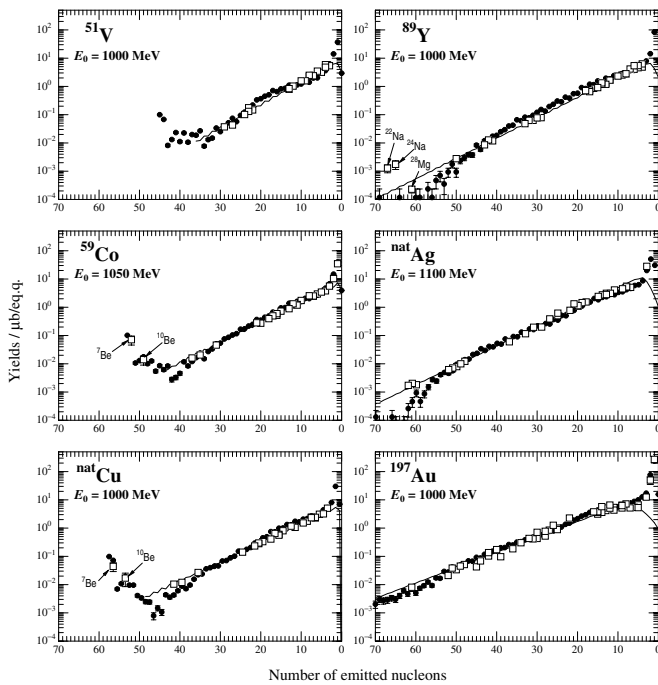


**Figure 13.** Mass yields of  $^{51}\text{V}$ ,  $^{59}\text{Co}$ ,  $^{\text{nat}}\text{Cu}$ ,  $^{89}\text{Y}$ ,  $^{\text{nat}}\text{Ag}$ , and  $^{197}\text{Au}$  targets around the energy of  $E_0 = 1000$  MeV together with those from PICA3/GEM code.<sup>34</sup> Open squares denote the mass yields obtained by adding unknown isobaric yield estimated by the Rudstam formula (eq 5 in 4.3.) to our experimental yields in References 16, 17, 123–125. Solid lines indicate the mass yields estimated by the Rudstam formula, (eq 5 in 4.3.). Closed circles indicate the yields calculated by PICA3/GEM.<sup>34</sup> (Constructed from References 16, 17, 123, and 125 with permissions from the American Physical Society and the Oldenbourg Wissenschaftsverlag)

lem regarding to reaction mechanisms. During 1950s, measurements of radionuclide yields from the interaction of GeV-protons revealed large deviations in the region of  $15 < A < 35$  from the expected spallation patterns<sup>126</sup> which have not been explained by the cascade-evaporation model.<sup>127</sup> The term “fragmentation” has been coined for the formation process for these light nuclei in which the split-off of such a large piece of nuclear fragments from an excited nucleus during a nucleonic cascade is somehow supposed.

Since then, extensive works have been continued by studying radiochemically the formation cross sections and/or yields especially of  $^7\text{Be}$ ,  $^{11}\text{C}$ ,  $^{18}\text{F}$ ,  $^{24}\text{Na}$ ,  $^{28}\text{Mg}$ , and other light radionuclides from proton-, neutron- and photon-induced nuclear reactions on a variety of targets, recently down to the thresholds around several tens of MeV.<sup>128</sup> An approximate feature of the cross sections, mostly derived from proton reactions of energies ( $E_p$ ) of 0.1-several GeV, with respect to  $A_t$  and/or target asymmetry,  $[(N-Z)/A]_t$ , has been obtained.<sup>129–131</sup> The cross sections of the light nuclide formation decrease exponentially with an increase of  $A_t$  up to 50–100. Above  $A_t = 50$ –100, the cross sections seemed to decrease gradually at lower incident energies but increase at higher energies (see Figure 17 below in 5.5.).

In photonuclear reactions, the apparent deviations of the yields of the light nuclei from the spallation systematics have been reported during the late 1960s to 1970s (see Figures 10, 13, and 18 for the concerned regions, as examples). Fulmer et al.<sup>100, 101</sup> ascribed the comparable and very high  $^{24}\text{Na}$  and  $^{32}\text{P}$  yields, by a factor of  $10^3$  compared with the expected spallation yields, from iron targets irradiated with 3, 5, and 16 GeV-electrons to “photofission”. No  $^7\text{Be}$  was detected in their search in a Be fraction chemically separated from the irradiated iron foils. The relatively high yields of  $^{15}\text{O}$  and  $^{11}\text{C}$  from a 16 GeV irradiation of Al were regarded as possible evidence of “photofission” of Al, but the high relative yield of  $^7\text{Be}$  was considered to be suggestive of “fragmentation”. Butement et

al.<sup>102</sup> also ascribed the high relative yields of  $^{24}\text{Na}$  and  $^{32}\text{P}$  from 4 GeV irradiations of Co, I, and Ta to “presumed fragmentation”. The large yields of  $^7\text{Be}$  from  $^{27}\text{Al}$  and of  $^{11}\text{C}$  and  $^7\text{Be}$  from  $^{32}\text{S}$  at  $E_0 = 1$  GeV were also explained by “fragmentation” in a fast process as the only mechanism for the production by Di Napoli et al.<sup>106</sup> Di Napoli et al. continued measurements of the yields of light nuclei ( $^{22}\text{Na}$ ,  $^{18}\text{F}$ ,  $^{11}\text{C}$ , and  $^7\text{Be}$ ) from  $(\gamma, 2p3n)$  reactions on  $^{27}\text{Al}$ ,  $^{23}\text{Na}$ ,  $^{16}\text{O}$ , and  $^{12}\text{C}$ , respectively,<sup>132</sup> of  $^{18}\text{F}$ ,  $^{22}\text{Na}$ , and  $^{24}\text{Na}$  from  $^{23}\text{Na}$ ,  $^{27}\text{Al}$ ,  $^{28}\text{Si}$ ,  $^{31}\text{P}$ ,  $^{32}\text{S}$ ,  $^{35,37}\text{Cl}$ ,  $^{39}\text{K}$ , and  $^{40}\text{Ca}$ ,<sup>133</sup> and  $^{11}\text{C}$  and  $^7\text{Be}$  from  $^{40}\text{Ca}$ ,<sup>134</sup> all at  $E_0 = 0.3$ –1 GeV, and the “fragmentation-like” process was concluded to explain the large deviations from the spallation pattern:  $^7\text{Be}$  from  $^{12}\text{C}$  by  $(\gamma, \alpha n)$  reaction could be explained by an ejection of a  $^4\text{He}$  fragment in the fast step and the evaporation of a neutron in the second step leading to  $^7\text{Be}$ .<sup>134</sup> Emission of light fragments such as  $^8\text{Li}$ ,  $^7\text{Be}$ ,  $^{11}\text{C}$ , and others would justify the large yields of  $^{18}\text{F}$  from  $^{31}\text{P}$  and  $^{32}\text{S}$  and of  $^{22}\text{Na}$  from targets heavier than  $^{32}\text{S}$ . On the other hand, energetics suggested a large contribution of “fission” in producing some nuclides far enough from the targets such as  $^{18}\text{F}$  from  $^{35,37}\text{Cl}$  and  $^{40}\text{Ca}$  and  $^{22}\text{Na}$  from  $^{40}\text{Ca}$ ,<sup>133</sup> though the authors emphasized later that the large yields of  $^{11}\text{C}$  and  $^7\text{Be}$  from  $^{40}\text{Ca}$  had to be attributed to a “fragmentation-like” process, neither spallation nor fission.<sup>134</sup> In a later work, a “fission-like” process was not excluded for the  $^{11}\text{C}$  productions from targets with  $27 \leq A_t \leq 40$ .<sup>57, 135</sup>

Jonsson and Persson<sup>9</sup> stated that the  $^{24}\text{Na}$  from  $^{127}\text{I}$  is not probably a fission product and the emission of  $^{24}\text{Na}$  might be possible by local heating due to reabsorption of pions, as suggested by Wolfgang et al. in proton reaction.<sup>136</sup> The explanation of the high yields of  $^{24}\text{Na}$  by a “binary fission” process was made in a series of works by Järund et al., who measured  $^{24}\text{Na}$  yields from the 11 targets ranging from Al to Cu at  $E_0 = 100$ –1000 MeV,<sup>137</sup> from the 9 targets ranging from Br to U at  $E_0 = 400$ –1000 MeV,<sup>138</sup> and from  $^{159}\text{Tb}$  at  $E_0 = 400$ –800 MeV.<sup>139</sup> Also Kumbartzki and Kim<sup>51</sup> obtained the high yields relative to spallation in the mass range of  $20 < A < 30$  from 1.5 GeV irradiations of  $^{27}\text{Al}$ ,  $^{51}\text{V}$ ,  $^{55}\text{Mn}$ ,  $^{56}\text{Fe}$ ,  $^{59}\text{Co}$ , and  $^{75}\text{As}$  and 1.0–2.0 GeV irradiations of  $^{51}\text{V}$ , and the “fission-like breakup” of the iron nucleus was considered to be responsible for the  $^{24}\text{Na}$  (and  $^{27}\text{Mg}$ ) yields based on energetics of  $^{24}\text{Na}$  inferred from catcher foil technique. In the lighter targets closer to the products mass, spallation process would dominates, in which the light clusters are left as one of the cascade residues.

The distinctions of the fragmentation and/or fission contributions from the total yields had to be clarified before those complicated discussions. Our success in measurements of formation cross sections of  $^{10}\text{Be}$  ( $T_{1/2} = 1.5 \times 10^6$  y,  $\beta^-$  emitter) and  $^{26}\text{Al}$  ( $T_{1/2} = 7.2 \times 10^5$  y,  $\beta^+ - \gamma$  emitter) from Al, Fe, Co, Ni, Cu, Zn, Ag, and Au irradiated with 12 GeV-protons at KEK with use of accelerator mass spectrometry (AMS) at the Micro Analysis Laboratory, Tandem Accelerator (MALT) of the University of Tokyo,<sup>131</sup> prompted us to measure  $^7\text{Be}$  and  $^{10}\text{Be}$  produced by photoreactions on a wide range of  $A_t$ , by  $\gamma$ -ray assay for  $^7\text{Be}$  and AMS for  $^{10}\text{Be}$  in order to clarify the “fragmentation” problem described above.

**5.2.  $^7\text{Be}$  and  $^{10}\text{Be}$  produced by Photoreactions and Proton Reactions.** We first chose O, Al, Cl, Co, Cu, Y, Ag, and Au of natural abundance as targets and measured the  $^7\text{Be}$  and  $^{10}\text{Be}$  yields at  $E_0 = 250$ –1050 MeV at small  $E_0$  steps.<sup>24</sup> The aim of this work was at first to search for a possible effect on the yields caused by the difference of the initial interactions between photoreaction and proton reaction at the respective limiting regions observed at  $E_0 > 600$  MeV and  $E_0 > 2$  GeV as investigated before (see 4.2.). Unfortunately, only upper limits for formation yields of  $^7\text{Be}$  and  $^{10}\text{Be}$  from the heavier targets of  $^{\text{nat}}\text{Ag}$  and  $^{197}\text{Au}$  were available. However, an important finding was obtained in this work, i.e. appreciable yields were observable below the  $Q$  values for productions of  $^7\text{Be}$  and  $^{10}\text{Be}$  by  $(\gamma, xnyp)$  reactions on  $^{59}\text{Co}$ ,  $^{\text{nat}}\text{Cu}$ , and  $^{89}\text{Y}$  and no change in

increasing rate of the yields due to spallation appeared above the  $Q$ -values, suggesting appreciable contribution of fragmentation process to the formation of these nuclides. It was also suggested that the production of a nuclide in fragmentation process is closely related to the proton-to-neutron ratios of targets. A comparison of the ratios of the derived mean cross sections,  $^{10}\text{Be}/^{7}\text{Be}$ , at  $E_0 = 0.4\text{--}1$  GeV with those from proton reactions at  $E_p = 0.8, 1.2, 2.6,$  and  $12$  GeV indicated that the average energy deposition to the cascade residue in photoreaction is smaller than that in the proton reaction in the concerned energy region, which is consistent with the conclusion from the comparison of photon- and proton-spallation described in 4.2.

### 5.3. Systematic Study of Light Fragment Productions

*a. Overview.* A series of the measurements of the isotopic pairs of  $^{7,10}\text{Be}$  and  $^{22,24}\text{Na}$  up to  $E_0 = 1200$  MeV have then been performed on 23 targets ranging from  $^{\text{nat}}\text{B}$  to  $^{197}\text{Au}$ , including the same ones as studied above, with the aids of AMS for  $^{10}\text{Be}$  and of a low-level counting technique for  $^{22}\text{Na}$  to confirm the above-mentioned findings from the  $^{7,10}\text{Be}$  measurements.<sup>25</sup> The  $^{22}\text{Na}$  counting was performed at the Ogoya Underground Facility of the Low Level Radioactivity Laboratory (LLRL) of Kanazawa University.<sup>140</sup> In addition, the photoreaction yields of  $^{28}\text{Mg}$ ,  $^{39}\text{Cl}$ ,  $^{43,44\text{m},44\text{g},46,47,48}\text{Sc}$ ,  $^{59}\text{Fe}$ , and  $^{56,57,58,60}\text{Co}$  from the heavier targets were measured radiochemically to survey the contribution of fragmentation relative to spallation and/or fission in the mass yield distributions. The measured results were investigated in terms of  $E_0$ - and  $A_t$ -dependence of the yields and compared with those results of proton reactions reported in the literature. A quantitative evaluation of the contribution of

the fragmentation yields to the measured yields was obtained and a strong and clear effect of target properties on the fragmentation formation was confirmed.

*b.  $E_0$ -dependence of Light Fragment Yields.* Figure 14 shows some typical examples of the yield variation as a function of  $E_0$  together with the literature data.<sup>57, 133, 135, 137, 138</sup> The arrows on the  $E_0$  axis indicate the  $Q$  values for the products as spallation residues left after multiple nucleon emission. The superscript and subscript of  $Q$  indicate the  $A_t$  and the numbers of the emitted neutron and proton in  $(\gamma, xnyp)$  reaction, respectively. Some of the literature values (closed symbols) are in good agreement with ours, but the yield values of  $^7\text{Be}$  from  $^{\text{nat}}\text{O}$  and  $^{22}\text{Na}$  from  $^{\text{nat}}\text{Cl}$  are not. It is noted that the yield increase is steep after the threshold and attains a plateau at  $E_0 = 400\text{--}500$  MeV for reactions with a small  $\Delta A$ , which is a typical feature of the (3,3) resonance (Figures on left). In the reactions with larger  $\Delta A$ , i.e., the reactions on heavier targets, the yields increase slowly and reach a plateau at  $E_0 \geq 800$  MeV (Figures on right). Those characteristics in the  $E_0$ -dependence of the yields have also been observed in photospallation yields.<sup>17</sup> The yield increase at  $E_0 \geq 600$  MeV appears to be ascribable to the medium effect in nuclei; broadening of excitation function.<sup>10, 11</sup>

The reaction thresholds for  $^{7,10}\text{Be}$ ,  $^{22,24}\text{Na}$ , and  $^{28}\text{Mg}$  formations from the light targets are not so different from the  $Q$ -values for spallation, but the difference increases with an increase of  $\Delta A$ . This discrepancy is attributed to contribution from fragmentation process associated with the direct emission of these light nuclei from an excited target, the threshold of

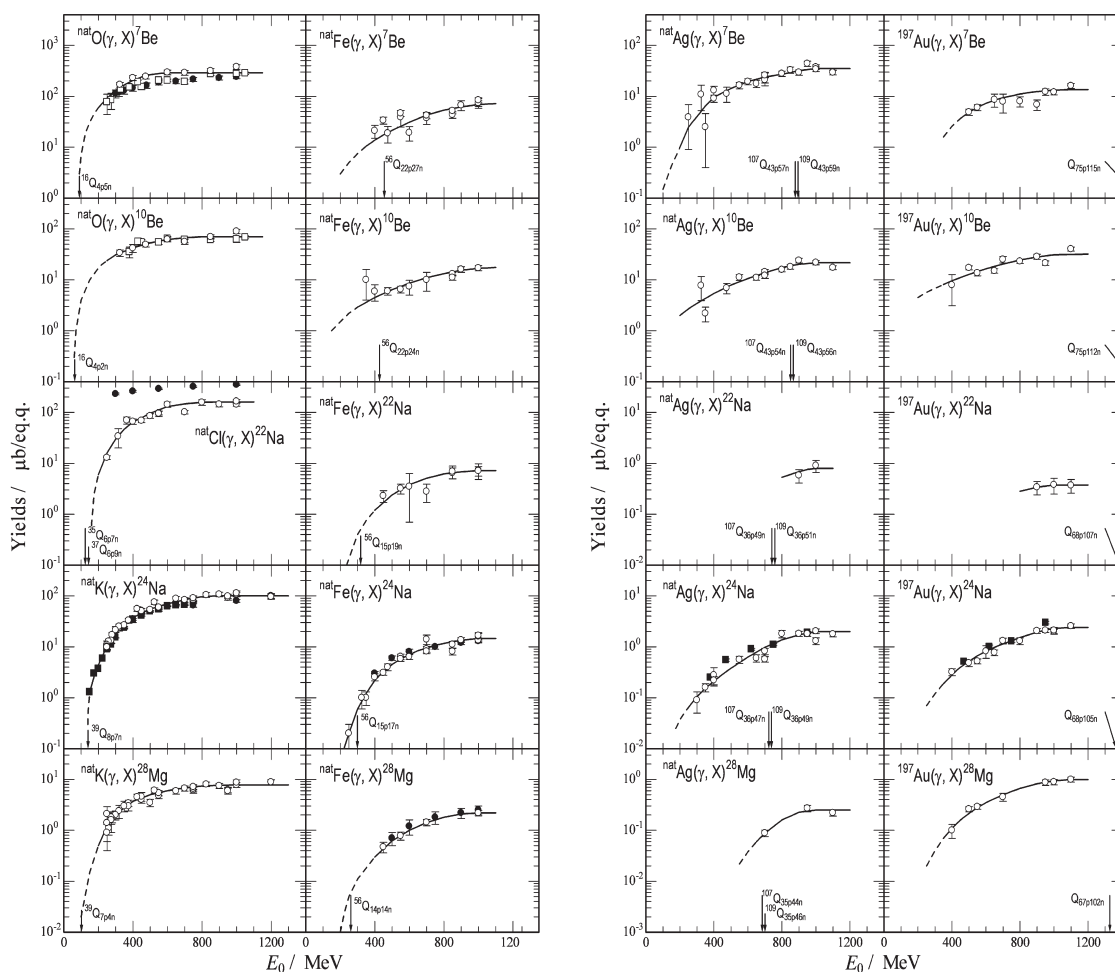


**Figure 14.** Typical examples of the measured yields of  $^7\text{Be}$ ,  $^{10}\text{Be}$ ,  $^{22}\text{Na}$ ,  $^{24}\text{Na}$ , and  $^{28}\text{Mg}$  for the reactions on  $^{\text{nat}}\text{O}$ ,  $^{\text{nat}}\text{Cl}$ ,  $^{\text{nat}}\text{K}$ ,  $^{\text{nat}}\text{Fe}$ ,  $^{\text{nat}}\text{Ag}$ , and  $^{197}\text{Au}$  as a function of the bremsstrahlung end-point energies,  $E_0$ . Open circles<sup>25</sup> and open squares<sup>24</sup> denote the values obtained in our works. Closed circles and closed squares represent the data from References 57, 133, and 135 and References 137 and 138, respectively. Solid lines are drawn through the points to guide the eye. The arrows on the horizontal axis show the  $Q$ -values for the products as a spallation residue left after multiple nucleon emission. The superscript and subscript of  $Q$  indicate the mass number of the target and the number of the emitted nucleons in  $(\gamma, xnyp)$  reaction, respectively, used for  $Q$ -value calculation. (Reprinted from Reference 25 with permission from the Oldenbourg Wissenschaftsverlag)

which are lower than the respective  $Q$ -values for spallation, as found in the previous work.<sup>24</sup>

**5.4.  $A_t$ -dependence of Light Fragment Yields.** There exist two components in the  $A_t$ -dependence of the yields of  ${}^7\text{Be}$ ,  ${}^{10}\text{Be}$ ,  ${}^{22}\text{Na}$ ,  ${}^{24}\text{Na}$ , and  ${}^{28}\text{Mg}$  as shown for  $E_0 = 1000$  MeV in Figure 15. The first component is a steep exponential decrease with an increase of  $A_t$  up to 40–80 for all of the five products, and the second is a slower exponential decrease of the  ${}^7\text{Be}$  and  ${}^{22}\text{Na}$  yields and a gradual increase of the  ${}^{10}\text{Be}$ ,  ${}^{24}\text{Na}$ , and  ${}^{28}\text{Mg}$  yields at  $A_t \geq 40$ –80. This feature of the  $A_t$ -dependence was the first finding in photoreaction.

As described in section 4, the photospallation systematics shows that the isobaric yields decrease exponentially with an increase of  $\Delta A$  as seen in Figures 10, 13, and 18, which is concordant with the first component at  $A_t \leq 40$ –80. The high  ${}^{7,10}\text{Be}$  yields relative to the expected spallation yields were confirmed in the medium-weight targets such as  ${}^{51}\text{V}$ ,  ${}^{59}\text{Co}$ , and  ${}^{\text{nat}}\text{Cu}$ , and the high  ${}^{22,24}\text{Na}$  and  ${}^{28}\text{Mg}$  yields together with the high  ${}^{7,10}\text{Be}$  yields were found only in the targets heavier than  $A_t \approx 80$ . It was then concluded that the first component is ascribed to spallation and the second to fragmentation. The slopes of the  ${}^7\text{Be}$  and  ${}^{10}\text{Be}$  yields for  $A_t$  up to 20–30 are smaller than those of the  ${}^{22}\text{Na}$ ,  ${}^{24}\text{Na}$ , and  ${}^{28}\text{Mg}$  yields. This fact suggests that the contribution of fragmentation for the production from these target nuclides is more significant in the  ${}^7\text{Be}$  and  ${}^{10}\text{Be}$  yields than in the  ${}^{22}\text{Na}$ ,  ${}^{24}\text{Na}$ , and  ${}^{28}\text{Mg}$  yields in the light targets examined.

An extraction of a pure fragmentation component has then become possible: the yields,  $Y(A_t)$ , in unit of  $\mu\text{b}/\text{eq. q.}$  of  ${}^7\text{Be}$ ,  ${}^{10}\text{Be}$ ,  ${}^{22}\text{Na}$ ,  ${}^{24}\text{Na}$ , and  ${}^{28}\text{Mg}$  can be expressed as

$$Y(A_t) = a \exp(bA_t) + c \exp(dA_t) \quad (7)$$

The first term corresponds to spallation component and the second one to the fragmentation. The parameters,  $a$ ,  $b$ ,  $c$ , and  $d$  were calculated by the least squares fit to the present yield data as shown by the broken lines in Figure 15 for  $E_0 = 1000$  MeV and given in Table 3 of Reference 25. The first component reasonably agrees with the values calculated by the Rudstam formula for photospallation (eq 5 in 4.3.) as marked by crosses in Figure 15.

The pure fragmentation yields of  ${}^7\text{Be}$  ( $N/Z = 0.75$ ) and  ${}^{22}\text{Na}$  ( $N/Z = 1.00$ ), which are deficient in neutron with respect to the

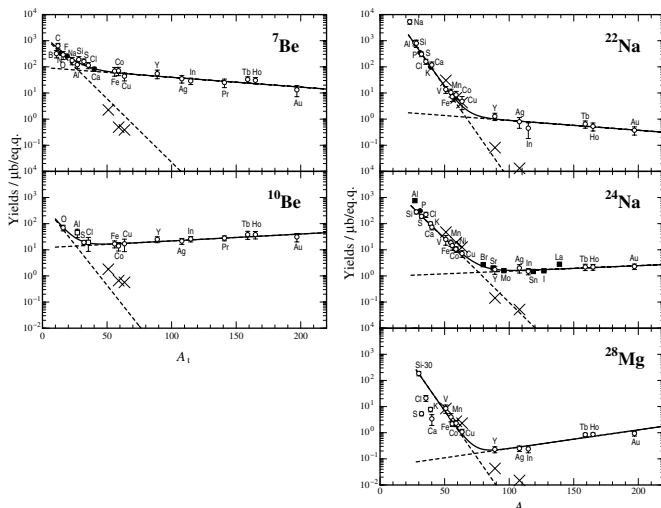


**Figure 15.** Yield variations of  ${}^7\text{Be}$ ,  ${}^{10}\text{Be}$ ,  ${}^{22}\text{Na}$ ,  ${}^{24}\text{Na}$ , and  ${}^{28}\text{Mg}$  at  $E_0 = 1000$  MeV as a function of the target mass number,  $A_t$ . Open circles<sup>25</sup> and open squares<sup>26</sup> denote the values obtained in our works. Closed circles represent the data from References 133, 134, and 135. The quoted data shown by closed squares are from References 137 and 138. Crosses indicate the values from the Rudstam formula (eq 5 in 4.3.) for spallation. See Reference 25 for details. (Reprinted from Reference 25 with permission from the Oldenbourg Wissenschaftsverlag)

$\beta$ -stability valley, decrease exponentially with an increase of  $A_t$ , while the yields of the neutron-rich  ${}^{10}\text{Be}$  ( $N/Z = 1.50$ ),  ${}^{24}\text{Na}$  ( $N/Z = 1.18$ ), and  ${}^{28}\text{Mg}$  ( $N/Z = 1.33$ ) increase, indicating that the fragment production is largely dependent on target properties: the neutron-rich fragments are more probable from heavier target nuclei with higher  $(N/Z)_t$  (see Figure 6 of Reference 25). This feature was studied more quantitatively by looking at the relationship of the yield ratios of  ${}^{10}\text{Be}/{}^7\text{Be}$ ,  ${}^{24}\text{Na}/{}^{22}\text{Na}$ ,  ${}^{28}\text{Mg}/{}^{22}\text{Na}$ , and  ${}^{28}\text{Mg}/{}^{24}\text{Na}$  and the target composition,  $(N/Z)_t$ . Figure 16 shows these ratios plotted as a function of  $(N/Z)_t$  at  $E_0 = 1000$  MeV. For the  ${}^{28}\text{Mg}$  yield, the  ${}^{24}\text{Na}$  or  ${}^{22}\text{Na}$  yield is used as the denominator and both the yield ratios are shown in Figure 16. All of the yield ratios of the isotopic pairs increase exponentially with an increase of  $(N/Z)_t$ . This fact implies that the fragments of high  $(N/Z)$  are preferably formed from the targets of high  $(N/Z)_t$  in fragmentation process. The preformation of nuclear clusters in excited nuclei leading to fragmentation would reflect the composition of the excited nuclei, though the penetrability affects the emissivity and composition of the clusters. It is shown that the  $(N/Z)_t$  values at which the production ratios exceed unity (the horizontal broken lines in Figure 16) are closer to the  $(N/Z)$  values of  ${}^{10}\text{Be}$ ,  ${}^{24}\text{Na}$ , and  ${}^{28}\text{Mg}$ , respectively. The overwhelming productions of  ${}^7\text{Be}$  and  ${}^{22}\text{Na}$  from the targets with the  $(N/Z)_t$  larger than the  $(N/Z)$  of these nuclides suggest the production of these two nuclides after some neutron emissions from the excited targets. Further measurements of other light nuclides such as  ${}^{11,14}\text{C}$ ,  ${}^{26}\text{Al}$ ,  ${}^{31,32}\text{Si}$ , and  ${}^{36,38,39}\text{Cl}$  would help to elucidate the trend.

**5.5. Comparison with Proton Reaction.** The profiles of  $A_t$ -dependence of proton reaction cross sections for formation of the light nuclei vary with the incident proton energy as noted in 5.1., and those at  $E_p = 600$  MeV are similar in shape to those of photoreaction yields at  $E_0 = 1000$  MeV, as seen in a compilation shown Figure 17 (References for the proton data are given in Reference 25). This is consistent with the fact that the effective photon energies in bremsstrahlung of  $E_0 = 1000$  MeV are 140–800 MeV for formation of these light nuclei. It

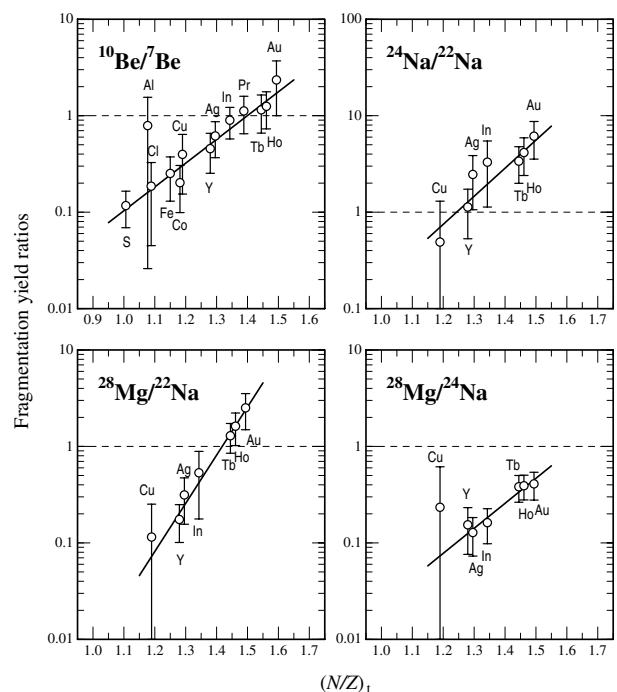


**Figure 16.** Fragmentation yield ratios of  ${}^{10}\text{Be}/{}^7\text{Be}$ ,  ${}^{24}\text{Na}/{}^{22}\text{Na}$ ,  ${}^{28}\text{Mg}/{}^{22}\text{Na}$ , and  ${}^{28}\text{Mg}/{}^{24}\text{Na}$  at  $E_0 = 1000$  MeV obtained in our work<sup>25</sup> as a function of the neutron-to-proton ratios of the target nucleus,  $(N/Z)_t$ . The solid lines are the least-squares fits to the plotted points. The neutron-to-proton ratios,  $N/Z$ , of  ${}^7\text{Be}$ ,  ${}^{10}\text{Be}$ ,  ${}^{22}\text{Na}$ ,  ${}^{24}\text{Na}$ , and  ${}^{28}\text{Mg}$  are 0.75, 1.50, 1.00, 1.18, and 1.33, respectively. (Reprinted from Reference 25 with permission from the Oldenbourg Wissenschaftsverlag)

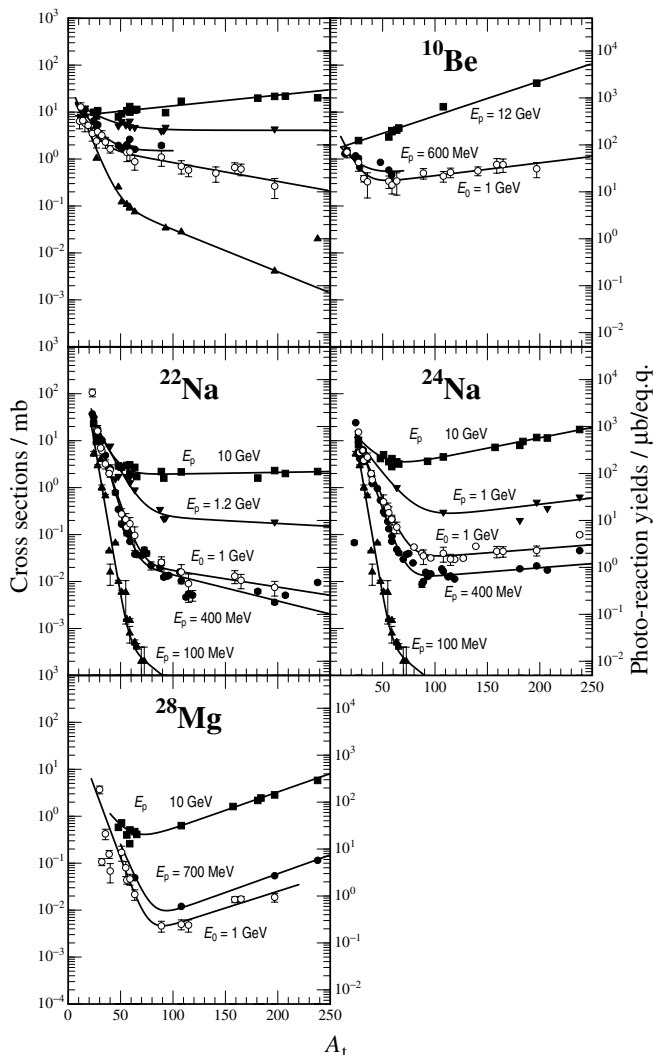


**Figure 17.** Photoreaction yields at  $E_0 = 1000$  MeV (open circles; right ordinate) and the literature data (Reference 25 and references therein) on cross sections obtained in proton irradiations (closed symbols; left ordinate) as a function of  $A_t$ . (Reprinted from Reference 25 with permission from the Oldenbourg Wissenschaftsverlag)

is noted that the cross sections for proton reactions become constant at  $E_p \geq 10$  GeV, and combined together in Figure 17. The proton data were then decomposed into two components, spallation and fragmentation, in the same way as for photoreactions, and the fragmentation cross section ratios for the pairs of  $^{10}\text{Be}/^7\text{Be}$ ,  $^{24}\text{Na}/^{22}\text{Na}$ ,  $^{28}\text{Mg}/^{22}\text{Na}$ , and  $^{28}\text{Mg}/^{24}\text{Na}$  were investigated in terms of the variations with  $(N/Z)_t$ . Although the cross section data on proton reactions, especially for  $^{10}\text{Be}$  and  $^{28}\text{Mg}$ , are not sufficient for such comparison, the ratios appear to be somewhat less dependent on  $(N/Z)_t$  compared with photoreactions (Figure 9 of Reference 25). However, any effects in the fragmentation yields of these nuclides due to the difference of the initial interaction between photo and proton reactions were not clear. Further systematic measurements on the formation of these light nuclei especially  $^{10}\text{Be}$  and  $^{22}\text{Na}$  in proton reactions on heavier targets at varied energies, at least as comparable to our photoreaction measurements, are required for more detailed discussion.

**5.6. Perspectives of Fragmentation Study.** In our recent works,<sup>124</sup> the PICA 3/GEM code has indicated that the reproducibility of the fragmentation yields for  $^{7,10}\text{Be}$  is excellent as well as that of photospallation, as illustrated in Figures 13 and 18. But the reproduction of the code is still poor for the  $^{22,24}\text{Na}$  and  $^{28}\text{Mg}$  yields from target nuclei with  $A_t \geq 30$ . Further examinations of the code are under way to reveal the detailed cascade-evaporation steps effective of fragment emission, as described in 4.5. An increase of the sensitivity of the MALT-

AMS in Tokyo has been now allowing to measure both  $^{10}\text{Be}$  and  $^7\text{Be}$ , and the results have already been obtained for  $^{\text{nat}}\text{Cu}$ ,  $^{\text{nat}}\text{Ag}$ , and  $^{197}\text{Au}$  targets at  $E_0 = 200$  MeV.<sup>141</sup> Further experiments at low  $E_0$  are of interest to investigate the different contributions of  $\Delta$ -resonance and QDR mechanisms.

One of the breakthrough discoveries in the study on nuclear stability during the last decades was the spontaneous emission of  $^{14}\text{C}$  from  $^{223}\text{Ra}$  in 1984,<sup>142</sup> which has led an extensive development of cluster radioactivities both experimentally and theoretically.<sup>143, 144</sup> This cold subbarrier phenomenon has been tried to be understood by connecting to other phenomena such as  $\alpha$  radioactivity and spontaneous fission. A unified framework to account for all these nuclear break-up phenomena that may differ in a time sequence of the intranuclear process both in subbarrier cold and highly excited hot regions of energy is expected from further detailed clarifications of their individual aspects. Our efforts is believed to have given an important observational constraint to such developments.

## 6. Photofission

**6.1. Background.** It has been a natural consequence of photospallation and fragmentation study for us to pay our attention to the yields of the reaction (fission) products with mass range of  $A = 40$ – $140$  from  $^{197}\text{Au}$  and  $^{209}\text{Bi}$ ; the outsidies of the range are fragmentation and spallation products already described above. So we have been careful in the yield measurements of nuclides around these boundaries. The total photofission yields or cross sections of  $^{197}\text{Au}$  and  $^{209}\text{Bi}$  as well as other preactinides and actinides at intermediate and high energies have extensively been measured with ionization chambers and solid-state detectors since 1950s (see references quoted in References 26, 28 and references quoted below). Works measuring CD and MD, which are further essential for understanding fission mechanisms, were not many in the past.

Komar et al.<sup>145</sup> reported the symmetric MD with  $\text{FWHM}_{\text{MD}} = 40$  mass units (m.u.) for  $^{197}\text{Au}$  and 44 m.u. for  $^{209}\text{Bi}$  by coincident energy measurements of fission fragment pairs at  $E_0 = 1000$  MeV, assuming the fissioning nucleus to be  $A_f = 194$  for the former and  $A_f = 205$  for the latter. Schröder et al.<sup>146</sup> measured the relative fission yields for 9 mass chains of  $A = 85$ – $112$  from  $^{209}\text{Bi}$  at  $E_0 = 700$  MeV using a catcher foil technique, and reported a symmetric MD with the most probable mass  $A_p = 102.5$  m.u. and  $\text{FWHM}_{\text{MD}} = 22$  m.u. Di Napoli et al.<sup>147</sup> also measured the yields of 11 fission products with  $A = 90$ – $112$  from  $^{209}\text{Bi}$  at  $E_0 = 1000$  MeV radiochemically, and reported the MD with  $A_p = 101$  m.u. and  $\text{FWHM}_{\text{MD}} = 19$  m.u. On the other hand, Areskoug et al. measured the relative yields of 29 radionuclides from  $^{197}\text{Au}$  (Ref. 148) and 43 radionuclides from  $^{209}\text{Bi}$  (Ref. 149) at  $E_0 = 600$  MeV using the catcher foil technique. They analyzed the yields by a six-parameter CD and MD formula and reported a Gaussian MD with  $A_p = 92.6 \pm 0.6$  m.u. and  $\text{FWHM}_{\text{MD}} = 30.9 \pm 1.7$  m.u. for  $^{197}\text{Au}$  and  $A_p = 96.3 \pm 0.5$  m.u. and  $\text{FWHM}_{\text{MD}} = 34.8 \pm 0.7$  m.u. for  $^{209}\text{Bi}$ . They concluded that the larger widths of MD for  $^{197}\text{Au}$  and  $^{209}\text{Bi}$  reported by Komar et al.<sup>145</sup> were attributed to the higher photon energy investigated and that the values for  $A_p$  and  $\text{FWHM}_{\text{MD}}$  deduced by Schröder et al.<sup>146</sup> and di Napoli et al.<sup>147</sup> were not reliable due to the narrow mass ranges investigated.

**6.2. Systematic Investigation of Photofission of  $^{197}\text{Au}$  and  $^{209}\text{Bi}$ .** The mass yield curves of the photofission of  $^{197}\text{Au}$  and  $^{209}\text{Bi}$  obtained by us at  $E_0 = 1000$  MeV<sup>26, 28</sup> are shown in Figure 18 along with photopion reactions, photospallation and fragmentation yields for  $^{197}\text{Au}$ . Here the reaction yields of 58 radionuclides as the fission products with the mass number  $A = 42$ – $131$  from  $^{197}\text{Au}$  were measured at 13  $E_0$ 's in the range from  $E_0 = 300$  to 1100 MeV in steps of 50 or 100 MeV using the catcher foil technique with the aid of intensive chemical separations. Thirty-six nuclides in the mass range of  $A = 46$ – $131$

were identified both in the forward and backward catcher foils and 50 nuclides in the range of  $A = 42-131$  were in the Au foils nondestructively and/or radiochemically. The recoil properties of the 37 product nuclei in the mass range of  $24 \leq A \leq 131$  were also investigated along with photospallation results and compared with the literature data on the proton reactions.<sup>27</sup> For the  $^{209}\text{Bi}$  fission,<sup>28</sup> the reaction yields of 63 radionuclides with  $A = 56-135$  were measured at six  $E_0$ 's in the range of  $E_0 = 450-1100$  MeV by the same technique as for the  $^{197}\text{Au}$  fission study.

The charge distributions and mass yield distributions were then constructed and their characteristics were investigated. The summary of the investigations has been given in the recent paper by Haba.<sup>29</sup> Also the reproducibility of the PICA3/GEM code for photofissions of  $^{197}\text{Au}$  and  $^{209}\text{Bi}$  was studied and discussed. The calculations were performed with particle histories of  $1 \times 10^9$  events for  $^{197}\text{Au}$  and  $5 \times 10^9$  events for  $^{209}\text{Bi}$  at  $E_0 = 100-1000$  MeV in steps of 100 MeV, and the results are included to compare with our experiments in Figure 18. It was noted that the code reproduces the approximate features of the CD and MD for  $^{197}\text{Au}$ , but the  $\text{FWHM}_{\text{CD}}$  for  $^{209}\text{Bi}$  is higher by about 0.5 charge unit and the parameters  $R$  and  $S$  in the expression for the most probable charge,  $Z_p = RA + S$ , are discrepant from the experimental one for  $^{209}\text{Bi}$ . The  $S$  value for  $^{197}\text{Au}$  is also higher by a factor of more than two compared with the experiment. The  $R$  value of  $(0.424 \pm 0.001)$  deduced for  $^{197}\text{Au}$  leads the number of prefission neutrons,  $\nu_{\text{pre}}$ , to be  $(11 \pm 1)$  through  $R = Z_f/(A_f - \nu_{\text{pre}})$  under the assumption of the unchanged charge distribution (UCD) hypothesis. The parameter  $S$  is a measure of the number of average post fission neutrons,  $\nu_{\text{post}}$  as  $S = Z_f - \nu_{\text{post}}/(A_f - \nu_{\text{pre}})$ . The  $S$  value of  $(0.7 \pm 0.1)$  deduced for  $^{197}\text{Au}$  implies the average  $\nu_{\text{post}}$  of  $(1.7 \pm 0.3)$ . The values of  $\nu_{\text{pre}}$  and  $\nu_{\text{post}}$  for  $^{209}\text{Bi}$  are  $(12 \pm 1)$  and  $(1.4 \pm 0.3)$ , respectively, which are comparable with those for  $^{197}\text{Au}$ .

Then the mass numbers of the fissioning nucleus  $A_f$  were estimated to be 186 for  $^{197}\text{Au}$  and 197 for  $^{209}\text{Bi}$ . The most probable mass  $A_p$  of  $(92 \pm 1)$  m.u. is 4 m.u. smaller than that for  $^{209}\text{Bi}$  ( $96 \pm 1$  m.u.), and the  $\text{FWHM}_{\text{MD}}$  of  $(39 \pm 1)$  m.u. is larger by 6 m.u. than that of  $^{209}\text{Bi}$  ( $33 \pm 3$  m.u.). The reported  $A_p$  and  $\text{FWHM}_{\text{MD}}$  by Komar et al.,<sup>145</sup> Schröder et al.,<sup>146</sup> and di Napoli et al.<sup>147</sup> are not consistent with ours, as noted by Areskou et al.<sup>149</sup> whose  $A_p$  and  $\text{FWHM}_{\text{MD}}$  values are very close to ours except for the narrow  $\text{FWHM}_{\text{MD}}$  by 8 m.u. for  $^{197}\text{Au}$ . The charge distribution parameters  $\text{FWHM}_{\text{CD}}$ ,  $R$  and  $S$  for  $^{197}\text{Au}$  at  $E_0 = 600$  MeV reported by Areskou et al.<sup>148</sup> are almost consistent with ours.

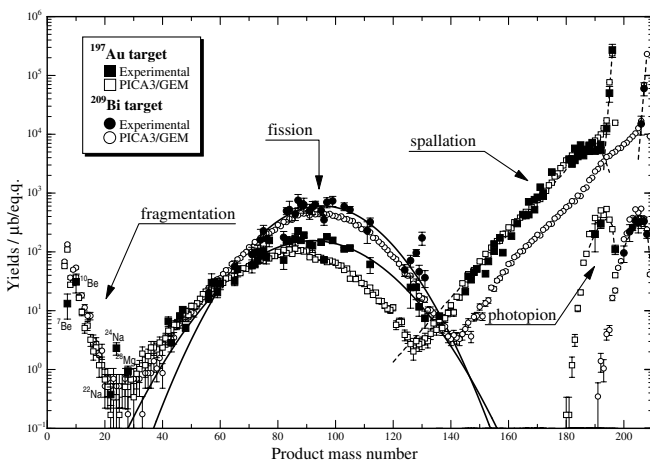


**Figure 18.** Experimental and calculated mass or isotopic yields of photonuclear reactions of  $^{197}\text{Au}$  and  $^{209}\text{Bi}$  at  $E_0 = 1000$  MeV. The experimental yields by fission on  $^{197}\text{Au}$  and  $^{209}\text{Bi}$  were taken from References 26 and 28. Those by photopion on  $^{197}\text{Au}$  and  $^{209}\text{Bi}$  were taken from Reference 13. Those by spallation on  $^{197}\text{Au}$  were taken from References 17 and 123. Those by fragmentation on  $^{197}\text{Au}$  were taken from Reference 25. The results of the PICA3/GEM are from References 28, 123–125, and 164. (With permission from the American Physical society and the Oldenbourg Wissenschaftsverlag)

The discrepancy of  $\text{FWHM}_{\text{MD}}$  may be attributed to the still smaller mass range analysed by them. The calculations by the PICA3/GEM code gives a smaller  $A_p$  of  $(86 \pm 1)$  m.u. and  $\text{FWHM}_{\text{MD}}$  of  $(37 \pm 2)$  m.u. compared with the experimental  $A_p$  of  $(92 \pm 1)$  m.u. and  $\text{FWHM}_{\text{MD}}$  of  $(39 \pm 1)$  m.u. for  $^{197}\text{Au}$ . For  $^{209}\text{Bi}$ , the calculated  $A_p$  is slightly smaller,  $(94 \pm 1)$  vs  $(96 \pm 1)$ , while the calculated  $\text{FWHM}_{\text{MD}}$  agrees with the experiment. These facts indicate that there are more rooms for improvements such as the excitation energies of fissioning nuclei.

The PICA3/GEM code employs the Generalized Evaporation Model (GEM) code by Furihata,<sup>150</sup> who included the Rutherford Appleton Laboratory (RAL) model by Atchison<sup>151</sup> to describe the competition between particle evaporation and fission with use of the reevaluated parameters in the RAL model. The predicted fission yields in the energy region presently concerned do not depend strongly on the fission models and on quality of the models for the direct and preequilibrium steps that precede fission and particle evaporation. The fission is regarded as a collective process of the nucleus. After the emission of a few fast particles, the residual nucleus attains an equilibrated state, where fission competes with the particle evaporation. A large number of intermediate nuclei each with its own fission characteristics are formed. Therefore, small deviations in the cascade step may give rise a very different population of the intermediate nucleus, and contributes to different fission-fragment distributions. It will be of interest to trace precisely the calculational code for fissioning process as well as for the other competing processes mentioned before.

**6.3. Total Fission Yields: Comparison with Literature Data.** The total fission yields of  $^{197}\text{Au}$  and  $^{209}\text{Bi}$  in unit of  $\text{mb}/\text{eq. q.}$  deduced from the mass yield curves are shown as a function of  $E_0$  by open symbols in Figure 19, together with the literature data, quoted in References 26 and 28, with small

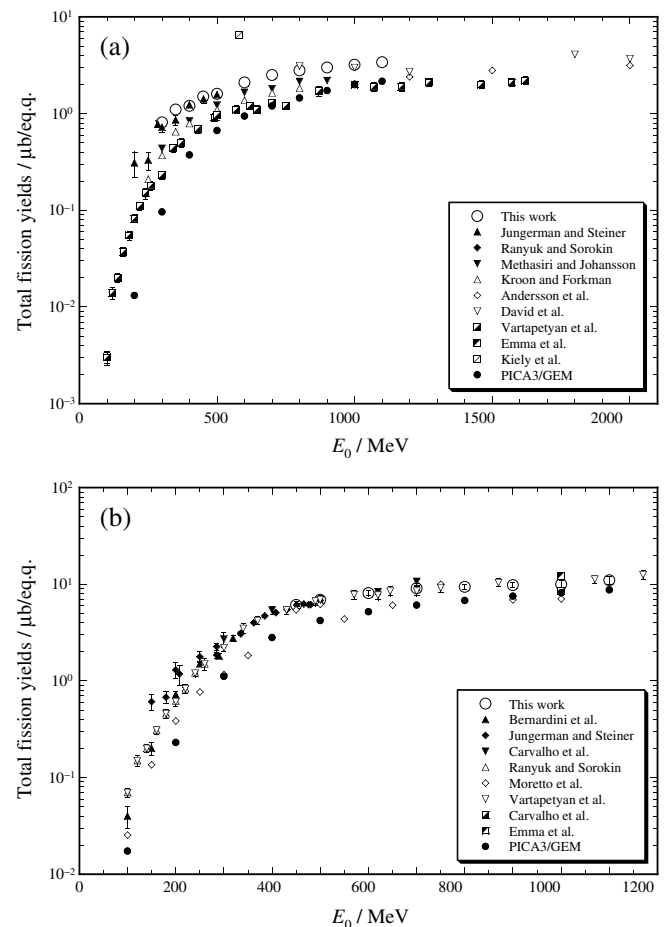


**Figure 19.** Total photofission yields of  $^{197}\text{Au}$  (a) and  $^{209}\text{Bi}$  (b) in unit of  $\mu\text{b}/\text{eq. q.}$  as a function of  $E_0$ . See text for details. (Reprinted from References 26 and 28 with permission from the Oldenbourg Wissenschaftsverlag)

symbols as indicated in the insets in the figure. The literature data were found to be in agreement with each other in the range of a factor of 2, except for the results for  $^{197}\text{Au}$  at  $E_0 = 580$  MeV by Kieley et al.<sup>152</sup> and for  $^{209}\text{Bi}$  at  $E_0 = 200\text{--}1000$  MeV by Moretto et al.<sup>153</sup> The total fission yields increase steeply by about three order of magnitude with an increase of  $E_0$  from 100 MeV to 600 MeV and increase slightly above  $E_0 = 600$  MeV. Total fission yield of  $(10 \pm 1)$  mb/eq.q. for  $^{209}\text{Bi}$  at  $E_0 = 1000$  MeV is about three times higher than the value of  $(3.2 \pm 0.1)$  mb/eq.q. for  $^{197}\text{Au}$ . This difference is well explained by a systematic trend of nuclear fissility,  $f$ , as a function of  $Z^2/A$ , i.e.  $f = \exp[0.87(Z^2/A - 35.83)]$ .<sup>154</sup> The fission yields calculated by the PICA3/GEM code, also shown in Figure 19, are smaller than the experiments for both  $^{197}\text{Au}$  and  $^{209}\text{Bi}$ , especially at lower  $E_0$ . Since 1980s, total fission cross sections have been intensively measured with glass or plastic track detectors or multi-wire spark chambers in irradiations with quasi-monochromatic photon beams of energies up to 300 MeV, produced from in-flight positron annihilation at Mainz Linac.<sup>155</sup> Laboratorio Esperienze Acceleratore Lineare Elettroni (LEALE) of Frascati ES,<sup>156, 157</sup> or from backward Compton scattering of laser light on electrons circulating in a storage ring ADONE facility of Frascati ES,<sup>158, 159</sup> Laser Electron Gamma Source (LEGS) facility of Brookhaven National Laboratory (BNL)<sup>160</sup> and at ROKK 1M<sup>161, 162</sup> and ROKK 2<sup>163</sup> of Budker Institute of Nuclear Physics, Novosibirsk, and the detailed structure of the excitation function of photofission of both  $^{197}\text{Au}$  and  $^{209}\text{Bi}$  has getting to be clear. Unfortunately these beams of  $10^5\text{--}10^6$  photons/sec are too low in intensities for our types of radiochemical study.

The fission cross sections in the energy regions for the GDR and QDR were found to be negligibly small compared with those in the  $\Delta$  resonance, as seen in Figure 19. It was concluded that the fission properties found in these works are mostly of those in the  $\Delta$  resonance, though it is obvious from Figure 19 that both the QDR and  $\Delta$ -resonance induce fission. Therefore, the measurements at  $E_0 < 300$  MeV are strongly desired, because the different contributions of the QDR and the  $\Delta$ -resonance mechanism are expected. A preliminary measurement for  $^{197}\text{Au}$  at  $E_0 = 65$  MeV have indicated a symmetric MD with  $A_p = 99 \pm 1$  and  $\text{FWHM}_{\text{MD}} = 20 \pm 1$  m.u.,<sup>164</sup> which is quite different from the results at  $E_0 \geq 300$  MeV.

A comparison of the photofission with the reported proton fission of  $^{197}\text{Au}$  has also been of interest. It was found that the shape of the MD at  $E_p = 300\text{--}400$  MeV seem to be the same as the photofission at  $E_0 = 1000$  MeV, as observed in the photofragmentation study described in 4.4. This fact may imply that the difference in the initial interactions of photon and protons with nuclei does not affect the fissioning process. Almost all the proton data were obtained by nondestructive  $\gamma$ -ray measurement of the irradiated Au target, and the number of nuclides measured were quite small and not sufficient for the same analysis as applied in our works. A few physical investigations of the mass yield curves, which were based on the coincidence measurements of the fragment pairs, were then available at  $E_p = 1000$  MeV. The  $\text{FWHM}_{\text{MD}}$  values of  $(54.5 \pm 0.6)$  m.u. reported by Kotov et al.<sup>165</sup> and 46.9 m.u. by Andronenko et al.<sup>166</sup> are discrepant with each others and both are higher than our photon result of  $(39 \pm 1)$  m.u. at  $E_0 \geq 600$  MeV. The intensive measurements of the proton fission of  $^{197}\text{Au}$ ,  $^{209}\text{Bi}$  and also other preactinides are strongly desired to determine the CD and MD and to compare them with the photofission results, as in the case of the fragmentation study.

## 7. Summary and Perspectives

(1) Almost all aspects of the yields of the final product nuclei from photonuclear reactions induced by bremsstrahlung of end-point energies of  $E_0 = 30\text{--}1200$  MeV have been investigated systematically with respect to  $k$  and/or  $E_0$ , target masses

$A_t$ , product mass and their compositions. Irradiations with bremsstrahlung of continuous spectrum ranging from photon energy of 0 to  $E_0$  induce photoreactions due to GDR, QDR and (3,3) resonance concomitantly when  $E_0$  exceeds those resonance regions, and, therefore, the irradiations have been performed in small steps of  $E_0$  of 100 MeV or less to be able to unfold the yield variations into cross sections as a function of  $k$ . Also radiochemical separation techniques were applied to the irradiated medium- and heavy-targets, in the same irradiation for nondestructive measurements, to obtain unambiguous evaluations of the reaction products. This article has restricted to descriptions of the yield measurements of photopion reactions, photospallation, fragmentation and fission of  $^{197}\text{Au}$  and  $^{209}\text{Bi}$ . A simple nuclear recoil experiment using thick-target thick-catcher method has been performed on 167 radionuclides formed from seven targets of  $^{27}\text{Al}\text{--}^{197}\text{Au}$  to obtain kinematic information, and an account on this subject has been separately published in a recent issue of this Journal by Haba.<sup>29</sup>

(2) In photopion study, irradiations were performed on 27 targets of  $^7\text{Li}$  to  $^{209}\text{Bi}$  at  $E_0 = 30\text{--}1050$  MeV in steps of 50 MeV or less. Our study started with a revisit to one of the previously most studied reactions,  $^{51}\text{V}(\gamma, \pi^+)$  and  $(\gamma, \pi^-xn)$  for  $x = 0\text{--}3$ . The yield curves exhibit clear shapes for  $\Delta(1231)$ -resonance. After the yield data were corrected for the secondary reactions by a newly devised method, the yield curves were unfolded into cross sections per photon of monochromatic energy  $k$ . Comparison with the literature data showed the discrepancies from our data both on the yield curves and excitation functions. The obtained excitation functions were then compared with theoretical calculations based on a valence nucleon model, an impulse approximation with and without final-state interaction of the outgoing pion and a combination of valence and volume production model, all of which were shown also to be discrepant from our experiment. A Monte Carlo intranuclear cascade-evaporation calculation by using the PICA code by Gabriel et al.<sup>30, 31</sup> was shown to approximate the gross feature of the experimental excitation functions, though some problems remained.

Our measurements were then extended to both the heavier and lighter nuclear targets by the same experimental methodology explored in the  $^{51}\text{V}$  study. The first one was on  $^{133}\text{Cs}(\gamma, \pi^-xn)$  reactions for  $x = 0\text{--}9$  and later on  $^{133}\text{Cs}(\gamma, \pi^+)^{133}\text{Xe}$  together with other noble gas-producing reactions, i.e.  $^{41}\text{K}(\gamma, \pi^+)^{41}\text{Ar}$ ,  $^{87}\text{Rb}(\gamma, \pi^+)^{87}\text{Kr}$ , and  $^{127}\text{I}(\gamma, \pi^-xn)^{127-x}\text{Xe}$  for  $x = 0, 2, 4, 5$ , and 6. It was surprised to find that the mass yields of  $^{133-x}\text{Ba}$  from  $^{133}\text{Cs}(\gamma, \pi^-xn)$  reactions showed high probabilities of neutron emissions of  $x$  up to 9. The same trend was observed in the measurement of  $^{127}\text{I}(\gamma, \pi^-xn)^{127-x}\text{Xe}$ . The excitation functions of  $^{133}\text{Cs}(\gamma, \pi^-xn)^{133-x}\text{Ba}$  and  $^{51}\text{V}(\gamma, \pi^-xn)^{51-x}\text{Cr}$  were found to be smooth functions of  $k$ ,  $x$ , and  $A_t$ . Also found was that all the  $(\gamma, \pi^+)$  and  $(\gamma, \pi^-)$  yields are independent of target-mass  $A_t$ . The confirmation of these findings was made by extending the targets to 23 kinds to cover from  $^7\text{Li}$  to  $^{209}\text{Bi}$  for the  $(\gamma, \pi^+)$  and/or  $(\gamma, \pi^-)$  reactions and to 12 to cover  $^{51}\text{V}$  to  $^{209}\text{Bi}$  for the  $(\gamma, \pi^-xn)$  reactions.

While the  $(\gamma, \pi^\pm)$  yields from the nuclei lighter than  $A_t = 40$  are anomalously small compared with those from the heavier ones of  $A_t = 40\text{--}209$ , the latter of which are  $A_t$ -independent, irrespective of  $E_0$ . The yield ratios of  $Y(\gamma, \pi^-)/Y(\gamma, \pi^+)$  was found to be 5–6, whereas the PICA code gave the ratio of 2. The discrepancy seemed to be explained if the neutron density in nuclear surface region is higher than the inner density of the nucleus.

On the other hand, the mass yield features of the  $(\gamma, \pi^-xn)$  reactions were found to be smooth functions of  $x$  and target composition of  $(N/Z)_t$ , and to exhibit the pronounced nuclear medium effects for  $(N/Z)_t \geq 1.3\text{--}1.4$ , i.e.  $A_t \geq 110\text{--}130$ . This has recently proved by an excellent reproduction by the calculations with use of the revised code of PICA, PICA3/GEM, by

Sato et al.,<sup>34</sup> in which an extension of photon energy, the nuclear medium effects and shadowing effects are taken into account. A search for lanthanum radioactivities in CsCl targets irradiated at  $E_0 = 600\text{--}1000$  MeV indicated no detectable effect on the reaction yields due to double pion emission.

(3) Photospallation study has been performed by paying our attentions to obtain accurate charge and mass distributions (CD and MD) to be able to systematize in a form of an empirical formula for several targets of medium-weights at  $E_0 = 100$  and  $200$  MeV. The similarity and dissimilarity of the characteristic features between photospallation and hadron-induced spallation of the same target were then investigated. Although the observed features of CD and MD appeared to be similar in photo- and hadron-spallation, the average excitation energy of the cascade residue in photospallation was found to be lower than that in hadron spallation as evidenced in the yield study of  $^{nat}\text{Cu}$  and other heavier targets. These comparisons were performed further on the kinematic properties obtained from nuclear recoil experiments by thick-target thick-catcher method, and the results supported these differences between photo- and hadron spallations.

Systematization of photospallation yields by referring to the formula by Rudstam<sup>94</sup> was successfully performed by additional measurements on  $^{51}\text{V}$ ,  $^{59}\text{Co}$ ,  $^{89}\text{Y}$ ,  $^{127}\text{I}$ ,  $^{133}\text{Cs}$ ,  $^{139}\text{I}$ , and  $^{197}\text{Au}$  at  $E_0 = 30\text{--}1000$  MeV in steps of  $100$  MeV or less with the aid of intensive radiochemical separations. And the new coefficients in the expressions for the parameters involved in the Rudstam formula for photospallation were derived as well as a separate empirical expression for the  $(\gamma, xn)$  reactions that was not included in the Rudstam formula. The PICA code was found not to be applicable in an exact way to photospallations of targets heavier than  $A_t > 100$ . It has also recently been proved that the increasing discrepancy with an increase of  $A_t$  is due to the nuclear medium effect as evidenced by an excellent reproduction by the PICA 3/GEM code, though the yield values of the products very far from targets and the kinetic energies  $T$  of the residual nucleus are underestimated systematically in the heavy target region.

(4) The light nuclear fragments, such as  $^{7,10}\text{Be}$ , and  $^{22,24}\text{Na}$ , as well as other light- and medium-weight nuclides extending to spallation and/or fission product regions formed from 23 targets ranging from  $^{nat}\text{B}$  to  $^{197}\text{Au}$  at  $E_0 = 250\text{--}1200$  MeV in steps of  $100$  MeV or less have been measured radiochemically. Here AMS technique was applied to the  $^{10}\text{Be}$  measurement and a low-level counting to the  $^{22}\text{Na}$  measurement. The reaction thresholds for  $^{7,10}\text{Be}$  and  $^{22,24}\text{Na}$  formation were found to be lower than the  $Q$  values for spallation, and the difference increases with an increase of  $\Delta A = A_t - A$ .

The  $A_t$ -dependent variations of the yields of  $^{7,10}\text{Be}$ ,  $^{22,24}\text{Na}$ , and  $^{28}\text{Mg}$  were found for the first time to have two components in a form of  $Y(A_t) = a \exp(bA_t) + c \exp(dA_t)$ ; the first term due to spallation and the second to fragmentation, and were disentangled into the respective components. The yield ratios in the fragmentation components,  $^{10}\text{Be}/^{7}\text{Be}$ ,  $^{24}\text{Na}/^{22}\text{Na}$ , and  $^{28}\text{Mg}/^{24}\text{Na}$ , are logarithmically increasing functions of target compositions,  $(N/Z)_t$ , indicating that the fragment formation is largely dependent on target properties: the neutron-rich fragments are more probable from heavier target nuclei with higher  $(N/Z)_t$ .

The literature data of proton reaction cross sections for formations of the corresponding light nuclides were analysed by the same way as above, and found that the features of the fragment productions in proton reactions at  $E_p = 600$  MeV are similar to those in photoreactions at  $E_0 = 1000$  MeV, though the proton cross section data are not sufficient enough for this type of comparison.

(5) Photofission of  $^{197}\text{Au}$  and  $^{209}\text{Bi}$  was studied by measuring radiochemically for 58 products in a mass range of  $A = 42\text{--}131$  at  $E_0 = 300\text{--}1000$  MeV and for 63 products in a mass range of  $A = 56\text{--}136$  at  $E_0 = 450\text{--}1000$  MeV, respectively, in steps of

$50\text{--}100$  MeV with use of the catcher foil technique. The characteristics of the CD, MD and the recoil properties were investigated by referring to the PICA3/GEM calculation, the results of which have been summarized recently.<sup>29</sup> The most probable mass  $A_p$  and  $\text{FWHM}_{\text{MD}}$  of the MD of the  $^{197}\text{Au}$  and  $^{209}\text{Bi}$  fission were found to be discrepant from the reported ones. Also the total fission yields as a function of  $E_0$  are presented and compared with the reported ones, too. It was found that the total fission yield of  $(10 \pm 1)$  mb/eq.q. for  $^{209}\text{Bi}$  at  $E_0 = 1000$  MeV is about 3 times higher than the value of  $(3.2 \pm 0.1)$  mb/eq.q. for  $^{197}\text{Au}$ , and the major contribution originates in  $\Delta$ -resonance. A comparison of the photofission with the reported proton fission of  $^{197}\text{Au}$  showed that the shape of the MD at  $E_p = 300\text{--}400$  MeV seemed to be the same as that of photo fission at  $E_0 = 1000$  MeV, suggesting that the difference in the initial interactions of photons and protons with nuclei does not affect the fissioning process.

(6) The present efforts in our group and the perspectives in the mentioned field of study are touched upon in each of section 3 to 5 in text, where importance of the experimental information in the QDR region has also been stressed. It is worth of mentioning that the theoretical treatment in the framework of  $\Delta$ -hole models<sup>167</sup> would be applied to the interpretations of our results.

The type of our experiments has to be extended to GeV regions, where the shadowing effect would manifest itself.<sup>87</sup> Above the  $\Delta$ -resonance region, the interaction of the incident photon with the target nucleus is reported to start to resemble a hadronic process; the incident photons mainly interact with surface nucleons leaving the interior of the nuclear volume "shadowed". This effect is an issue of current interest. Monochromatic photon sources of energies up to  $4$  GeV have recently been in use for cross section measurements of some of actinide photofission and photoreactions; up to  $800$  MeV at Mainz,<sup>168</sup> up to  $1200$  MeV at Frascati,<sup>86</sup> up to  $2600$  MeV at Yerevan<sup>169</sup> and up to  $3800$  MeV at the Thomas Jefferson National Accelerator Facility.<sup>170</sup> Photon intensity of  $\sim 3 \times 10^7/\text{s}$  is reported in the last. The SPring-8 of the Japan Synchrotron Radiation Research Institute could also be a candidate facility for such studies.

Furthermore, very interesting and important is that an application of our work on  $(\gamma, \pi^- xn)$  reactions,  $x = 0\text{--}9$ , to elucidate nuclear charge pickup ( $\Delta Z = +1$ ) of the projectiles at ultrarelativistic heavy-ion ( $158\text{A GeV Pb}$ ) collisions has recently been pointed out.<sup>171, 172</sup> The Large Hadron Collider (LHC) at European Laboratory for Particle Physics (Conseil Européen pour la Recherche Nucléaire, CERN) and the Relativistic Heavy Ion Collider (RHIC) at BNL aim the study of a possible phase transition of nuclear and hadronic matter into the so-called quark-gluon plasma at high energy densities, the conditions of which are believed to have existed in the Early Universe soon after the Big-Bang. The general picture of ultrarelativistic heavy-ion collisions requires the investigations not only of the participant zones but also of peripheral collisions where the electromagnetic interactions are considered to play important roles. The  $(\gamma, \pi^- xn)$  reactions are induced by *real* bremsstrahlung photons, but the same reactions induced by *virtual equivalent* photons are considered to be possible in peripheral collisions of ultrarelativistic heavy ions. Future experiments for this purpose are highly desired.

**Acknowledgement.** The author expresses his appreciations to the staff and crew members of the  $1.3$  GeV ES at the High Energy Accelerator Research Organization (KEK) at Tanashi (the former Institute for Nuclear Study, the University of Tokyo), of the  $600$  MeV Electron linac at the Electrotechnical Laboratory and of the  $300$  MeV Electron linac at the Laboratory of Nuclear Science, Tohoku University for their cooperations in accelerator operations. The works accounted in this article

have been performed during the period when the author was at the Department of Chemistry, Kanazawa University, by collaborations of the author's students totaling more than 78, among them, Drs. S. R. Sarkar, Y. Oura, Y. Miyamoto, H. Haba, and H. Matsumura being specially thanked, for their painstaking but fruitful efforts through their thesis works for BS, MS and Dr. Sci. Professors S. Shibata of the Research Reactor Institute of Kyoto University, M. Furukawa of Yokkaichi University and I. Fujiwara of Otomon-Gakuin University are deeply acknowledged for their pleasant collaborations in the works and for their kind guidance to the students since the earlier stage of the series of the experiments. Drs. H. Haba of RIKEN, M. Matsumura of KEK and Miss. N. Fukushima of Kanazawa University have been helpful in preparation of the figures and manuscript of this article. Thanks go also to an anonymous reviewer who has given valuable comments to improve the manuscript. The author appreciates the permissions to use the published materials (References 10–19, 24–28) from the copyright holders: the Elsevier Ltd., the American Physical Society, the Oldenbourg Wissenschaftsverlag and the Japan Society of Nuclear and Radiochemical Sciences.

## References

- (1) H. Arenhövel and D. Drechsel, ed. *Nuclear Physics with Electromagnetic Interactions, Proc. Int. Conf. on Nuclear Physics with Electromagnetic Interactions*, Mainz, 1979, Vol.108 of Lecture Notes in Physics, (Springer-Verlag, Berlin, 1979).
- (2) P. Stoler, ed. *Photopion Nuclear Physics*, (Plenum, New York, 1979).
- (3) A. Nagl, V. Devanathan, and H. Überall, *Nuclear Pion Photoproduction* (Springer-Verlag, Berlin, 1991).
- (4) I. S. Hughes and P. V. March, *Proc. Phys. Soc. (London)* **72**, 259 (1958).
- (5) E. W. Laing and R. G. Moorhouse, *Proc. Phys. Soc. (London)* **70**, 629 (1957).
- (6) E. M. McMillan, J. M. Peterson, and R. S. White, *Science* **109**, 438 and **110**, 579 (1949).
- (7) R. M. Littauer and D. Walker, *Phys. Rev.* **86**, 838 (1952).
- (8) J. Arends, P. Detemple, N. Floss, S. Huthmacher, G. Kaul, B. Mecking, G. Nöldeke, and R. Stenz, *Nucl. Phys. A* **526**, 479 (1991).
- (9) G. G. Jonsson and B. Persson, *Nucl. Phys. A* **153**, 32 (1970).
- (10) K. Sakamoto, M. Yoshida, Y. Kubota, T. Fukasawa, A. Kunugise, Y. Hamajima, S. Shibata, and I. Fujiwara, *Nucl. Phys. A* **501**, 693 (1989).
- (11) K. Sakamoto, Y. Hamajima, M. Soto, Y. Kubota, M. Yoshida, A. Kunugise, M. Masatani, S. Shibata, M. Imamura, M. Furukawa, and I. Fujiwara, *Phys. Rev. C* **42**, 1545 (1990).
- (12) Y. Oura, A. Yazawa, M. Yoshida, S. R. Sarkar, K. Sakamoto, S. Shibata, I. Fujiwara, and M. Furukawa, *Radiochim. Acta* **68**, 27 (1995).
- (13) K. Sakamoto, S. R. Sarkar, Y. Oura, H. Haba, H. Matsumura, Y. Miyamoto, S. Shibata, M. Furukawa, and I. Fujiwara, *Phys. Rev. C* **59**, 1497 (1999).
- (14) K. Sakamoto, H. Toramoto, Y. Hamajima, K. Okada, and M. Dohniwa, *Radiochim. Acta* **37**, 69 (1984).
- (15) K. Sakamoto, M. Nishio, M. Dohniwa, K. Okada, and Y. Hamajima, *Radiochim. Acta* **37**, 83 (1984).
- (16) S. Shibata, M. Imamura, T. Miyachi, M. Mutou, K. Sakamoto, Y. Hamajima, M. Soto, Y. Kubota, M. Yoshida, and I. Fujiwara, *Phys. Rev. C* **35**, 254 (1987).
- (17) S. R. Sarkar, M. Soto, Y. Kubota, M. Yoshida, T. Fukasawa, K. Matsumoto, K. Kawaguchi, K. Sakamoto, S. Shibata, M. Furukawa, and I. Fujiwara, *Radiochim. Acta* **55**, 113 (1991).
- (18) S. R. Sarkar, Y. Kubota, T. Fukasawa, K. Kawaguchi, K. Sakamoto, S. Shibata, and I. Fujiwara, *Radiochim. Acta* **55**, 139 (1991).
- (19) S. R. Sarkar, Y. Oura, K. Kawaguchi, A. Yazawa, K. Sakamoto, S. Shibata, and I. Fujiwara, *Radiochim. Acta* **62**, 7 (1993).
- (20) H. Haba, H. Matsumura, Y. Miyamoto, K. Sakamoto, Y. Oura, S. Shibata, M. Furukawa, and I. Fujiwara, *J. Radioanal. Nucl. Chem.* **239**, 133 (1999).
- (21) I. Fujiwara, H. Haba, H. Matsumura, K. Sakamoto, Y. Miyamoto, Y. Oura, S. Shibata, and M. Furukawa, *Czech. J. Phys.* **49**, 831 (1999), Suppl. S1.
- (22) H. Haba, H. Matsumura, K. Sakamoto, Y. Oura, S. Shibata, M. Furukawa, and I. Fujiwara, *Radiochim. Acta* **85**, 1 (1999).
- (23) H. Haba, H. Matsumura, K. Sakamoto, Y. Oura, S. Shibata, M. Furukawa, and I. Fujiwara, *Radiochim. Acta* **88**, 375 (2000).
- (24) S. Shibata, M. Imamura, K. Sakamoto, S. Okizaki, S. Shibutani, H. Matsumura, M. Furukawa, I. Fujiwara, H. Nagai, and K. Kobayashi, *Radiochim. Acta* **80**, 181 (1998).
- (25) H. Matsumura, K. Washiyama, H. Haba, Y. Miyamoto, Y. Oura, K. Sakamoto, S. Shibata, M. Furukawa, I. Fujiwara, H. Nagai, T. Kobayashi, and K. Kobayashi, *Radiochim. Acta* **88**, 313 (2000).
- (26) H. Haba, M. Igarashi, K. Washiyama, H. Matsumura, M. Yamashita, K. Sakamoto, Y. Oura, S. Shibata, M. Furukawa, and I. Fujiwara, *J. Nucl. Radiochem. Sci.* **1**, 53 (2000).
- (27) H. Haba, M. Igarashi, K. Washiyama, H. Matsumura, M. Yamashita, K. Sakamoto, Y. Oura, S. Shibata, M. Furukawa, and I. Fujiwara, *J. Nucl. Radiochem. Sci.* **1**, 69 (2000).
- (28) H. Haba, M. Kasaoka, M. Igarashi, K. Washiyama, H. Matsumura, Y. Oura, S. Shibata, K. Sakamoto, M. Furukawa, and I. Fujiwara, *Radiochim. Acta* **90**, 371 (2002).
- (29) H. Haba, *J. Nucl. Radiochem. Sci.* **3**, A11 (2002).
- (30) T. A. Gabriel and R. G. Alsmiller, Jr., *Phys. Rev.* **182**, 1035 (1969).
- (31) T. A. Gabriel, M. P. Guthrie, and O. W. Hermann, Oak Ridge National Laboratory Report No. ORNL-4687 (1971).
- (32) C. Y. Fu, PICA 95, *An Intra-Nuclear Cascade Code for 25-MeV to 3.5 GeV Photon-Induced Nuclear Reactions*, presented at SATIF-3, Sendai, May 12-13, 1997
- (33) T. Sato, K. Shin, S. Ban, Y. Namito, H. Nakamura, and H. Hirayama, *Nucl. Instrum. Methods A* **437**, 471 (1999).
- (34) T. Sato, K. Shin, S. Ban, T. A. Gabriel, C. Y. Fu, and H. S. Lee, *Proc. Advanced Monte Carlo on Radiation Physics, Particle Transport Simulation and Applications*, Lisbon, Oct. 23-26, 2000 (private communication).
- (35) B. Jonsson, A. Järund, and B. Forkman, *Z. Phys. A* **273**, 97 (1975).
- (36) K. Lindgren and G. G. Jonsson, *Nucl. Phys. A* **166**, 643 (1971).
- (37) K. Osada, T. Fukasawa, K. Kobayashi, Y. Hamajima, K. Sakamoto, S. Shibata, and I. Fujiwara, Research Report of Laboratory of Nuclear Science, Tohoku University **20**, 299 (1987).
- (38) U. Reus and W. Westmeier, *At. Data Nucl. Data Tables* **29**, 193 (1983).
- (39) E. Browne and R. B. Firestone, *Table of Radioactive Isotopes*, edited by V. S. Shirley (John Wiley and Sons, Inc., New York, 1986).
- (40) R. B. Firestone and V. S. Shirley, *Table of Isotopes, 8th ed.* (John Wiley and Sons, Inc., New York, 1996).
- (41) K. Komura, Technical Rept. Inst. Nucl. Study, Univ.

- Tokyo, Rept. No. INS-TCH-9 (1974).
- (42) Y. Hamajima, private communication (1998).
- (43) P. Dyal and J. P. Hummel, *Phys. Rev.* **127**, 2217 (1962).
- (44) R. A. Meyer and J. P. Hummel, *Phys. Rev.* **140**, B48 (1965).
- (45) W. B. Walters and J. P. Hummel, *Phys. Rev.* **143**, 833 (1966).
- (46) A. Masaïke, *J. Phys. Soc. Japan* **18**, 1692 (1964) and **19**, 427 (1964).
- (47) G. Nydahl and B. Forkman, *Nucl. Phys.* **B7**, 97 (1968).
- (48) I. Blomqvist, G. Nydahl, and B. Forkman, *Nucl. Phys.* **A162**, 193 (1971).
- (49) B. Friberg, I. Blomqvist, and B. Forkman, *Z. Phys.* **262**, 255 (1973).
- (50) B. Bülow, B. Johnsson, M. Nilsson, and B. Forkman, *Z. Phys.* **A278**, 89 (1976).
- (51) G. Kumbartzki and U. Kim, *Nucl. Phys.* **A176**, 23 (1971).
- (52) V. I. Noga, Yu. N. Ranyuk, P. V. Sorokin, and V. A. Tkachenko, *Sov. J. Nucl. Phys.* **14**, 506 (1972).
- (53) G. Andersson, I. Blomqvist, B. Forkman, G. G. Jonsson, A. Järund, I. Kroon, K. Lindgren, B. Schrøder, and K. Tesch, *Nucl. Phys.* **A197**, 44 (1972).
- (54) K. Min, P. Stoler, S. Trentalange, E. J. Winhold, P. F. Yergin, A. M. Bernstein, W. Turchinets, and K. S. R. Sastry, *Phys. Rev.* **C14**, 807 (1976).
- (55) I. Blomqvist, P. Janeček, G. G. Jonsson, R. Petersson, H. Dinter, and K. Tesch, *Z. Phys.* **A278**, 83 (1976).
- (56) I. Blomqvist, P. Janeček, G. G. Jonsson, H. Dinter, K. Tesch, N. Freed, and P. Ostrander, *Phys. Rev.* **C15**, 988 (1977).
- (57) V. di Napoli, F. Salvetti, M. L. Terranova, H. G. de Carvalho, J. B. Martins, and O. A. P. Tavares, *J. Inorg. Nucl. Chem.* **40**, 175 (1978).
- (58) M. Blann, *Ann. Rev. Nucl. Sci.* **25**, 123 (1975).
- (59) F. Plasil, Oak Rdge National Laboratory Report No. TM-6045 (1977).
- (60) G. Andersson, P. Dougan, and W. Stiefler, *Z. Phys.* **A272**, 265 (1975).
- (61) J. L. Matthews, W. Bertozzi, S. Kowalski, C. P. Sargent, and W. Turchinets, *Nucl. Phys.* **A112**, 654 (1968).
- (62) P. Dougan, B. Forkman, W. Stiefler, and J. L. Matthews, *Z. Phys.* **269**, 105 (1974).
- (63) N. N. Kaushal, E. J. Winhold, P. F. Yergin, H. A. Medicus, and R. H. Auguston, *Phys. Rev.* **175**, 1330 (1968).
- (64) H. J. von Eyss and G. Lührs, *Z. Phys.* **262**, 393 (1973).
- (65) Y. Oura, Ph. D. Dissertation, Kanazawa University (in Japanese, 1995).
- (66) K. Tesch, *Nucl. Instrum. Methods* **95**, 245 (1971).
- (67) J. T. Routti and J. V. Sandberg, *Comp. Phys. Comm.* **21**, 119 (1980).
- (68) L. I. Schiff, *Phys. Rev.* **83**, 252 (1951).
- (69) E. C. Booth, p.129 of ref. 2 (1979).
- (70) N. Freed and P. Ostrander, *Phys. Rev.* **C11**, 805 (1975).
- (71) N. Freed and P. Ostrander, *Phys. Rev.* **C24**, 306 (1981).
- (72) S. R. Sarkar, Ph. D. Dissertation, Kanazawa University (1991).
- (73) K. Kawaguchi, MS Thesis, Kanazawa University (1992).
- (74) V. I. Noga, Yu. N. Ranyuk, P. V. Sorokin, and V. A. Tkachenko, *Ukr. Phys. J.* **16**, 1850 (1971).
- (75) P. E. Bosted, I. Blomqvist, and A. M. Bernstein, *Phys. Rev. Lett.* **43**, 1473 (1979).
- (76) V. D. Epaneshnikov, V. M. Kuznetsov, and O. I. Stukov, *Sov. J. Nucl. Phys.* **19**, 242 (1974).
- (77) V. De Carlo, N. Freed, W. Rhodes, B. Bülow, G. G. Jonsson, K. Lindgren, and R. Petersson, *Phys. Rev.* **C21**, 1460 (1980).
- (78) P. V. March and T. G. Walker, *Proc. Phys. Soc. (London)* **77**, 293 (1961).
- (79) I. Blomqvist, B. Bülow, A. Fredrikson, B. Johnsson, G. G. Jonsson, K. Lindgren, M. Nilsson, R. Petersson, O. Glomset, N. Freed, and W. Rhodes, *Z. Phys.* **A288**, 313 (1978).
- (80) M. Nilsson, B. Schrøder, B. Bülow, J. Grintals, G. G. Jonsson, B. Lindner, K. Srinivasa Rao, and S. Susila, *Z. Phys.* **A294**, 253 (1980).
- (81) Y. Oura, K. Kawaguchi, S. R. Sarkar, H. Haba, Y. Miyamoto, K. Sakamoto, S. Shibata, I. Fujiwara, and M. Furukawa, Research Report of Laboratory of Nuclear Science, Tohoku University, **27**, 133 (1994).
- (82) H. W. Bertini, *Phys. Rev.* **131**, 1801 (1963).
- (83) R. Hofstadter, *Rev. Mod. Phys.* **28**, 214 (1956).
- (84) P. G. Hansen, A. S. Jensen, and B. Jonson, *Ann. Rev. Nucl. Part. Sci.* **45**, 591 (1995).
- (85) I. Tanihata, *J. Phys.* **G22**, 157 (1996).
- (86) N. Bianchi, V. Muccifora, E. De Sanctis, A. Fantoni, P. Levi Sandri, E. Polli, A. R. Reolon, P. Rossi, M. Anghinolfi, P. Corvisiero, M. Ripani, M. Sanzone, M. Taiuti, and A. Zucchiatti, *Phys. Rev.* **C54**, 1688 (1996).
- (87) G. Piller, W. Ratzka, and W. Weise, *Z. Phys.* **A352**, 427 (1995).
- (88) S. Furihata, *Nucl. Instrum. Methods* **B171**, 251 (2000).
- (89) R. Serber, *Phys. Rev.* **72**, 1114 (1947).
- (90) R. J. Debs, J. T. Eisinger, A. W. Fairhall, I. Halpern, and H. G. Richter, *Phys. Rev.* **97**, 1325 (1955).
- (91) I. Halpern, R. J. Debs, J. T. Eisinger, A. W. Fairhall, and H. G. Richter, *Phys. Rev.* **97**, 1327 (1955).
- (92) T. T. Sugihara and I. Halpern, *Phys. Rev.* **101**, 1768 (1956).
- (93) G. J. Kumbartzki, U. Kim, and Ch. K. Kwan, *Nucl. Phys.* **A160**, 237 (1971).
- (94) G. Rudstam, *Z. Naturforsch.* **21a**, 1027 (1966).
- (95) H. Sato, *Phys. Rev.* **C37**, 2902 (1988).
- (96) V. K. Lukyanov and A. I. Titov, *Phys. Lett.* **57B**, 10 (1975).
- (97) B. K. Gupta, S. Das, and M. M. Biswas, *Nucl. Phys.* **A155**, 49 (1970).
- (98) M. Foschina, J. B. Martins, O. A. P. Tavares, and V. di Napoli, *Radiochim. Acta* **35**, 121 (1984).
- (99) M. Foschina, J. B. Martins, O. A. P. Tavares, and V. di Napoli, *Radiochim. Acta* **46**, 57 (1989).
- (100) C. B. Fulmer, I. R. Williams, T. H. Handley, G. F. Dell, and L. N. Blumber, *Phys. Rev. Lett.* **19**, 522 (1967).
- (101) C. B. Fulmer, K. S. Toth, I. R. Williams, T. H. Handley, G. F. Dell, E. L. Callis, T. M. Jenkins, and J. M. Wyckoff, *Phys. Rev.* **C2**, 1371 (1970).
- (102) F. D. S. Butement, H. M. A. Karim, V. Myint U, and M. B. Zaman, *J. Inorg. Nucl. Chem.* **33**, 2791 (1971).
- (103) N. M. Bachschi, P. David, J. Debrus, F. Lübke, H. Hommsen, R. Schoenmackers, G. G. Jonsson, and K. Lindgren, *Nucl. Phys.* **A264**, 493 (1976).
- (104) G. A. Vartapetyan, A. S. Danagulyan, N. A. Demekhina, and A. G. Khudaverdyan, *Sov. J. Nucl. Phys.* **22**, 223 (1976).
- (105) A. S. Danagulyan, N. A. Demekhina, and G. A. Vartapetyan, *Nucl. Phys.* **A285**, 482 (1977).
- (106) V. di Napoli, F. Salvetti, and M. L. Terranova, *Phys. Rev.* **C8**, 206 (1973).
- (107) K. Lindgren and G. G. Jonsson, *Nucl. Phys.* **A197**, 71 (1972).
- (108) G. G. Jonsson and K. Lindgren, *Phys. Scripta* **7**, 49 (1973).
- (109) G. G. Jonsson and K. Lindgren, *Phys. Scripta* **15**, 308 (1977).
- (110) N. Metropolis, R. Bivins, M. Storm, J. M. Miller, G. Friedlander, and A. Turkevich, *Phys. Rev.* **110**, 204 (1958).
- (111) G. Rudstam, *Nucl. Phys.* **A126**, 401 (1969).

- (112) V. S. Barashenkov, F. G. Gereghi, A. S. Iljinov, G. G. Jonsson, and V. D. Toneev, *Nucl. Phys. A* **231**, 462 (1974).
- (113) J. B. Cumming, P. E. Haustein, R. W. Stoenner, L. Mausner, and R. A. Naumann, *Phys. Rev. C* **10**, 739 (1974).
- (114) J. B. Cumming, R. W. Stoenner, and P. E. Haustein, *Phys. Rev. C* **14**, 1554 (1976).
- (115) J. B. Cumming, P. E. Haustein, T. J. Ruth, and G. J. Virts, *Phys. Rev. C* **17**, 1632 (1978).
- (116) K. Sakamoto, Y. Hamajima, M. Soto, K. Kubota, M. Yoshida, T. Hashimoto, T. Fukasawa, I. Fujiwara, and S. Shibata, *Research Report of Laboratory of Nuclear Science, Tohoku University* **18**, 290 (1985).
- (117) S. Kaufman, *Phys. Rev.* **129**, 1866 (1963).
- (118) N. T. Porile and L. B. Church, *Phys. Rev.* **133**, B310 (1964).
- (119) T. Asano, Y. Asano, Y. Iguchi, H. Kudo, S. Mori, M. Noguchi, Y. Takada, H. Hirabayashi, H. Ikeda, K. Katoh, K. Kondo, M. Takasaki, T. Tominaka, and A. Yamamoto, *Phys. Rev. C* **28**, 1718 (1983).
- (120) T. H. Ku and P. J. Karol, *Phys. Rev. C* **16**, 1984 (1977).
- (121) P. J. Karol, *Phys. Rev. C* **10**, 150 (1974).
- (122) M. Eriksson and G. G. Jonsson, *Nucl. Phys. A* **242**, 507 (1975).
- (123) M. Yamashita, K. Yoshida, Y. Terada, A. Nagano, Y. Kawashima, D. Osada, H. Matsumura, K. Washiyama, K. Sakamoto, Y. Miyamoto, Y. Oura, S. Shibata, I. Fujiwara, and M. Furukawa, *Proc. 43rd Symp. on Radiochemistry*, Oct. 13-15, Tsukuba, Japan, Suppl. to *J. Nucl. Radiochem. Sci. Vol. 1* (1999) Abstract 3P17.
- (124) H. Matsumura, M. Yamashita, H. Haba, Y. Terada, K. Washiyama, H. Kikunaga, Y. Oura, Y. Miyamoto, K. Sakamoto, I. Fujiwara, S. Shibata, and M. Furukawa, *Proc. 44th Symp. on Radiochemistry*, Sept. 12-14, 2000, Kobe, Japan, Suppl. 2 to *J. Nucl. Radiochem. Sci. Vol. 1* (2000) Abstract 3P12.
- (125) H. Matsumura, M. Yamashita, H. Kikunaga, H. Haba, K. Washiyama, Y. Miyamoto, Y. Oura, K. Sakamoto, S. Shibata, M. Furukawa, and I. Fujiwara, *Proc. 2001 APSORC and 45th Symp. on Radiochemistry*, Oct. 30-Nov. 1, 2001, Fukuoka, Japan, Suppl. to *J. Nucl. Radiochem. Sci. Vol. 2* (2001) Abstract 2P02.
- (126) J. M. Miller and J. Hudis, *Ann. Rev. Nucl. Sci.* **9**, 159 (1959).
- (127) K. Beg and N. T. Poril, *Phys. Rev. C* **3**, 1631 (1971).
- (128) S. M. Qaim, *Radiochim. Acta* **70/71**, 163 (1995).
- (129) X. Campi, J. Desbois, and E. Lipparini, *Phys. Lett.* **138B**, 353 (1984).
- (130) J. Hüfner, *Phys. Rep.* **125**, 129 (1985).
- (131) S. Shibata, M. Imamura, H. Nagai, K. Kobayashi, K. Sakamoto, M. Furukawa, and I. Fujiwara, *Phys. Rev. C* **48**, 2617 (1993).
- (132) V. di Napoli and M. L. Terranova, *J. Inorg. Nucl. Chem.* **36**, 3633 (1974).
- (133) V. di Napoli, G. Rosa, F. Salvetti, M. L. Terranova, H. G. de Carvalho, J. B. Martins, and O. A. P. Tavares, *J. Inorg. Nucl. Chem.* **37**, 1101 (1975).
- (134) V. di Napoli, G. Rosa, F. Salvetti, M. L. Terranova, H. G. de Carvalho, J. B. Martins, and O. A. P. Tavares, *J. Inorg. Nucl. Chem.* **38**, 1 (1976).
- (135) V. di Napoli, J. B. Martins, G. Rosa, F. Salvetti, O. A. P. Tavares, M. L. Terranova, and H. G. de Carvalho, *J. Inorg. Nucl. Chem.* **40**, 1619 (1978).
- (136) R. Wolfgang, E. W. Baker, A. A. Caretto, J. B. Cumming, G. Friedlander, and J. Hudis, *Phys. Rev.* **103**, 394 (1956).
- (137) A. Järund, B. Friberg, and B. Forkman, *Z. Phys.* **262**, 15 (1973).
- (138) A. Järund and B. Forkman, *Z. Phys.* **281**, 39 (1977).
- (139) A. Järund, K. R. Lindgren, and B. Forkman, *J. Inorg. Nucl. Chem.* **43**, 1725 (1981).
- (140) K. Komura, *Proc. 1997 Int. Symp. on Environmental Radiation*, Tsuruga, Fukui, Japan (1997), edited by T. Tsujimoto and Y. Ogawa, Kansai Branch, Atomic Energy Soc. Japan, p.56 (Kansai Kosaido Co. Ltd. Osaka, 1998).
- (141) H. Matsumura, T. Aze, Y. Oura, H. Kikunaga, A. Yokoyama, K. Takamiya, S. Shibata, T. Otsuki, H. Yuki, K. Sakamoto, H. Haba, K. Washiyama, H. Nagai, and H. Matsuzaki, *Proc. Ninth Int. Conf. on Accelerator Mass Spectrometry, AMS-9 in 2002*, Nagoya, Japan, Sept. 9-13, 2002 to appear in *Nucl. Instrum. Methods B* (2003).
- (142) H. J. Rose and G. A. Jones, *Nature* **307**, 245 (1984).
- (143) E. Hourany, Carbon Decay and Fine Structure; R. Bonetti and A. Guglielmetti, Experiments on Heavy Cluster (O, F, Ne, Mg, Si). Radioactivities; D. N. Poenaru and W. Greiner, Theories of Cluster Radioactivities; R. Blendowske, T. Fliessbach, and H. Walliser, Many-body Approach to Alpha and Cluster Radioactivity, in *Nuclear Decay Modes*, edited by D. N. Poenaru (Institute of Physics Publishing, Bristol and Philadelphia, 1996).
- (144) R. Bonetti, A. Guglielmetti, D. N. Poenaru, W. Greiner, R. K. Gupta, M. Mirea, W. Scheid, A. Sandulescu, F. Carstoiu, S. Misicu, A. Florescu, I. Bulboaca, A. V. Ramayya, J. H. Hamilton, J. K. Hwang, and G. M. Ter-Akopian, New Cluster Radioactivity and the Supersymmetric Fission: Experiments and Theory, in *Heavy Elements and Related New Phenomena*, edited by W. Greiner and R. K. Gupta, (World Sci. Pub. Co., Singapore, 1999).
- (145) A. P. Komar, B. A. Bochagov, A. A. Kotov, Yu. N. Ranyuk, G. G. Semenchuk, G. E. Solyakin, and P. V. Sorokin, *Sov. J. Nucl. Phys.* **10**, 30 (1970).
- (146) B. Schröder, G. Nydahl, and B. Forkman, *Nucl. Phys. A* **143**, 449 (1970).
- (147) V. di Napoli, A. M. Laceranza, D. Margadonna, F. Salvetti, S. M. Terenzi, H. G. de Carvalho, and J. B. Martins, *Gazz. Chim. Ital.* **101**, 117 (1971).
- (148) M. Areskoug, B. Schröder, K. Lindgren, G. Andersson, and B. Forkman, *Nucl. Phys. A* **226**, 93 (1974).
- (149) M. Areskoug, B. Schröder, and K. Lindgren, *Nucl. Phys. A* **251**, 418 (1975).
- (150) S. Furihata, *Nucl. Instrum. Methods B* **171**, 251 (2000).
- (151) F. Atchison, Kernforschungsanlage Jülich, GmbH Report No. Jül-Conf-34 (1980).
- (152) F. M. Kiely, B. D. Pate, F. Hanappe, and J. Péter, *Z. Phys. A* **279**, 331 (1976).
- (153) L. G. Moretto, R. C. Gatti, S. G. Thompson, J. T. Routti, J. H. Heisenberg, L. M. Middleman, M. R. Yearian, and R. Hofstadter, *Phys. Rev.* **179**, 1176 (1969).
- (154) V. Emma, S. Lo Nigro, and C. Milone, *Nucl. Phys. A* **257**, 438 (1976).
- (155) H.-D. Lemke, B. Ziegler, M. Mutterer, J. P. Theobald, and N. Cârjan, *Nucl. Phys. A* **342**, 37 (1980).
- (156) V. Bellini, V. Emma, S. Lo Nigro, C. Milone, G. S. Pappalardo, E. De Sanctis, P. di Giacomo, C. Guaraldo, V. Lucherini, E. Polli, and A. R. Reolon, *Lett. Nuovo Cim.* **36**, 587 (1983).
- (157) C. Guaraldo, V. Lucherini, E. De Sanctis, P. Levi Sandri, E. Polli, A. R. Reolon, S. Lo Nigro, S. Aiello, V. Bellini, V. Emma, C. Milone, and G. S. Pappalardo, *Phys. Rev. C* **36**, 1027 (1987).
- (158) J. B. Martins, E. L. Moreira, O. A. P. Tavares, J. L. Vieira, J. D. Pinheiro Filho, R. Bernabei, S. D'Angelo, M. P. De Pascale, C. Schaerf, and B. Girolami, *Nuovo Cim. A* **101**, 789 (1989).
- (159) J. B. Martins, E. L. Moreira, O. A. P. Tavares, J. L. Vieira, L. Casano, A. D'Angelo, C. Schaerf, M. L. Terranova, D. Babusci, and B. Girolami, *Phys. Rev. C* **44**,

- 354 (1991).
- (160) M. L. Terranova, A. D'Angelo, J. D. Pinheiro F., E. S. De Almeida, E. Z. Bilbao, and J. B. Martins, *Nuovo Cim. A* **105**, 197 (1992).
- (161) M. L. Terranova, O. A. P. Tavares, G. Ya Kezerashvili, V. A. Kiselev, A. M. Milov, N. Yu Muchnoi, A. I. Naumenkov, V. V. Petrov, I. Ya Protopopov, E. A. Simonov, E. de Paiva, and E. L. Moreira, *J. Phys. G* **22**, 511 (1996).
- (162) M. L. Terranova, G. Ya Kezerashvili, A. M. Milov, S. I. Mishnev, N. Yu Muchnoi, A. I. Naumenkov, I. Ya Protopopov, E. A. Simonov, D. N. Shatilov, O. A. P. Tavares, E. De Paiva, and E. L. Moreira, *J. Phys. G* **24**, 205 (1998).
- (163) M. L. Terranova, G. Ya Kezerashvili, V. A. Kiselev, A. M. Milov, S. I. Mishnev, I. Ya Protopopov, V. N. Rotaev, D. N. Shatilov, and O. A. P. Tavares, *J. Phys. G* **22**, 1661 (1996).
- (164) H. Haba, M. Igarashi, M. Kasaoka, H. Kikunaga, H. Matsumura, M. Yamashita, K. Sakamoto, K. Washiyama, Y. Oura, S. Shibata, M. Furukawa, and I. Fujiwara, *Proc. 43rd Symp. on Radiochemistry*, Oct. 13-15, Tsukuba, Japan, Suppl. to *J. Nucl. Radiochem. Sci.* Vol. 1, (1999) Abstract 3P18.
- (165) A. A. Kotov, G. G. Semenchuk, L. N. Andronenko, M. N. Andronenko, B. L. Gorshkov, G. G. Kovshevnyi, V. R. Reznik, and G. E. Solyakin, *Sov. J. Nucl. Phys.* **20**, 251 (1975).
- (166) L. N. Andronenko, A. A. Kotov, M. N. Nesterov, V. F. Petrov, N. A. Tarasov, L. A. Vaishnena, and W. Neubert, *Z. Phys.* **A318**, 97 (1984).
- (167) J. H. Koch, E. J. Moniz, and N. Ohtsuka, *Ann. Phys. (N.Y.)* **154**, 99 (1984).
- (168) Th. Frommhold, F. Steiper, W. Henkel, U. Kneissl, J. Ahrens, R. Beck, J. Peise, M. Schmitz, I. Anthony, J. D. Kellie, S. J. Hall, and G. J. Miller, *Z. Phys.* **A350**, 249 (1994).
- (169) E. A. Arakelyan, A. R. Bagdarsaryan, G. L. Bayatyan, A. R. Voskenyan, N. K. Grigoryan, S. G. Knyazyan, A. T. Margaryan, G. G. Marikyan, and A. K. Papyan, *Sov. J. Nucl. Phys.* **52**, 878 (1990).
- (170) C. Cetina, P. Heimberg, B. L. Berman, W. J. Briscoe, G. Feldman, and L. Y. Murphy, *Phys. Rev.* **C65**, 044622 (2002).
- (171) K. A. Chikin, V. L. Korotkin, A. P. Kryukov, L. I. Sarycheva, I. A. Pshenichnov, J. P. Bondorf, and I. N. Mishustin, *Eur. Phys. J.* **A8**, 537 (2000).
- (172) C. Scheidenberger, I. A. Pshenichnov, T. Aumann, S. Datz, K. Sümmerer, J. P. Bondorf, D. Boutin, H. Geissel, P. Grafström, H. Knudsen, H. F. Krause, B. Lommel, S. P. Møller, G. Münzenberg, R. H. Schuch, E. Uggerhøj, U. Uggerhøj, C. R. Vane, A. Ventura, Z. Z. Vilakazi, and H. Weick, *Phys. Rev. Lett.* **88**, 042301 (2002).

